

034


**Experimental Investigation of a Novel
Finite Element Model for Southern Pine Glulam Beams**

by


Vikram Yadama

Thesis submitted to the Faculty of the
Virginia Polytechnic Institute and State University
in partial fulfillment of the requirements for the degree of
Master of Science
in
Forest Products and Wood Science

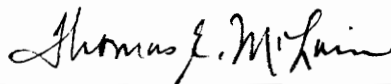
APPROVED:



J. R. Loferski, Chairman



S. M. Holzer



T. E. McLain

June, 1990

Blacksburg, Virginia

C.2

LD
5655
V855
1990
Y352
C.2

**Experimental Investigation of a Novel
Finite Element Model for Southern Pine Glulam Beams**

by

Vikram Yadama

J. R. Loferski, Chairman

Forest Products and Wood Science

(ABSTRACT)

Glued-laminated wood (Glulam) is a versatile material manufactured by gluing two or more layers of wood together with the grain of all laminae running parallel to each other. Glulam beams of many sizes, shapes, and thicknesses can be made. Innovative load-carrying structures such as lattice domes, bridges, and towers can be built using glulam members.

But, since wood is a highly variable and anisotropic material it is often difficult to accurately model the response of wood components in large structures to applied loads. Advanced computer techniques such as finite element analysis are being developed to more accurately model structure response.

The objective of this study was to evaluate the applicability of the isoparametric beam finite element to model the elastic response of straight and curved glulam beams subjected to three load conditions. Four straight and three curved southern pine glued-laminated beams were subjected to bending about their major axis, bending about their minor axis, and combined bending and compression. Strains were measured at various locations using clip-on electrical transducers; and, deflections were measured at three locations along the length. Transverse isotropy and global modulus of elasticity were assumed to determine experimentally beam material properties: longitudinal modulus of elasticity and shear modulus. The analysis was performed by using the finite element program ABAQUS.

The experimental and the analytical strain and deflection values of glulam beams in bending about the major and the minor axes agreed well for most cases. Differences of less than 10% between experimental measurements and analytical predictions were found at all locations through the depth of the beams except in the vicinity of the neutral axis. The differences between the measured and the predicted strain and deflections for beams tested in combined bending and axial compression ranged mostly between 0% and 40%.

Acknowledgements

I would like to express my sincere gratitude to Dr. Joseph Loferski for his guidance, suggestions, encouragement, and patience throughout the course of this study. I would also like to extend my sincere gratitude to Dr. S. M. Holzer for his constructive criticism, suggestions, and patience. I thank Dr. T. E. McLain for his valuable advice and suggestions. Also, thanks to Dr. Geza Ifju for providing me with financial assistance.

I also want to thank Julio Davalos and family for their encouragement and friendship and for always being there for me. I thank Julio for being patient with me and assisting me to understand many things. My sincere thanks to Sandya Gamalath for her assistance in printing this thesis and most of all for her friendship.

I would like to extend my deepest gratitude to the person who was always there to assist me with my experiments and to cheer me when I was feeling down. Thank you J.W.!(J. W. Akers). My thanks to Harold Vandivort, Kenny Albert, and Carl Price for all their assistance. I would also like to thank Mara Knott from ESM department for helping me with torsion experiments.

My sincere gratitude to Dr. P. H. Steele for his encouragement and patience. I would also like to thank all my friends and roommates at Blacksburg for their encouragement.

The following research was supported by the U.S. Department of Agriculture, Grant Administrative Management, Office of Grants and Program Systems, Agreement No. 86-FSTY-9-0178.

I thank my parents for all their support, encouragement, and love they have provided me always. I dedicate this thesis to them and my grandmother. Thanks to my brother and family members for their support and encouragement. Lastly, I am grateful to my wife, Minie, for all her moral support, encouragement, assistance, and love. Thank you all very much!

Table of Contents

CHAPTER 1 1

 1 INTRODUCTION 1

CHAPTER 2 5

 2 Literature Review 5

CHAPTER 3 54

3. EXPERIMENTAL STRAIN MEASUREMENT IN SOUTHERN PINE 54

 3.1 Introduction 54

 3.2 Objectives 55

 3.3 Background 55

 3.4 Effect of Gage Length on Strain Readings 57

 3.4.1 Procedure 57

 3.4.2 Results 59

 3.4.3 Summary and Conclusions 64

 3.5 Clip-on Displacement Transducers 65

 3.5.1 Fabrication, Operation, and Calibration 65

3.5.2 Calibration	67
3.5.3 Installation	68
3.5.4 Verification	70
3.6 Summary and Conclusions	70
CHAPTER 4	77
4. GLULAM MATERIAL PROPERTIES	77
4.1 Introduction	77
4.2 Procedure	78
4.2.1 Determination of Glulam Modulus of Elasticity	78
4.2.2 Determination of Glulam Shear Modulus	79
4.2.3 Moisture Content and Specific Gravity Measurements	87
4.3 Results and Discussion	89
4.3.1 Longitudinal Modulus of Elasticity	89
4.3.2 Shear Modulus	97
4.4 Summary and Conclusions	108
CHAPTER 5	109
5. GLULAM BEAM ANALYSIS	109
5.1 Introduction	109
5.2 Fabrication of Glulam Beams	110
5.3 Testing of Glulam Beams	114
5.3.1 In-Plane Bending	115
5.3.2 Combined Bending and Compression	115
5.4 Results and Discussion	120
5.4.1 Simple Bending About the Major Axis	124
5.4.2 Simple Bending About the Minor Axis	155
5.4.3 Combined Bending and Compression	172

5.5 Sources of Error 213

5.6 Summary and Conclusions 216

CHAPTER 6 218

6. SUMMARY, CONCLUSIONS, AND RECOMMENDATIONS FOR FUTURE RE-
SEARCH 218

6.1 Introduction 218

6.2 Summary and Conclusions 219

6.3 Recommendations for Future Work 220

BIBLIOGRAPHY 222

Appendix A. HP Data Acquisition Programs 227

Appendix B. Fortran Code To Solve Lekhnitski’s Orthotropic Torsion Solution 238

Vita 240

List of Illustrations

Figure 2.1. Degrees of freedom in a 2-D beam element	10
Figure 2.2. Degrees of freedom in a space frame or a 3-D element	11
Figure 2.3. Orthotropic material axes representing wood	13
Figure 2.4. Geometric (1,2,3) and symmetry (L,R,T) axes of a glulam specimen	15
Figure 2.5. Stress components on a differential element placed in a rectangular coordinate system	17
Figure 2.6. Effects of span-to-depth ratio (l/h) on the ratio of apparent to true modulus of elasticity under third-point loading (10)	20
Figure 2.7. Orthotropic bar subjected to torsional moment	32
Figure 2.8. Deformation of a differential element under a constant torque, T	35
Figure 2.9. Torsional deformation in a bar with non-circular cross-section	38
Figure 2.10. Distribution of stresses in a cross-section of a beam subjected to compression loads	43
Figure 2.11. Bending stresses in a beam cross-section	44
Figure 2.12. Shear stress distribution in a beam cross-section	46
Figure 2.13. Notation for bending about the two principal axes of a glulam beam cross-section	47
Figure 2.14. Distribution of bending stresses under biaxial bending loads (bending about 2- and 3- axes)	48
Figure 2.15. Possible stress distribution under compression and bending loads	50
Figure 3.1. Graphic description of locations on southern pine tension specimen where bonded strain gages were placed	58
Figure 3.2. Influence of gage length on strain readings at location A	60
Figure 3.3. Influence of gage length on strain readings at location B	61
Figure 3.4. Influence of gage length on strain readings at location C	62

Figure 3.5. Influence of gage length on strain readings at location D	63
Figure 3.6. Construction details of CET	66
Figure 3.7. Typical calibration curve of CET	69
Figure 3.8. Details about shoes used to place CET on the specimen	71
Figure 3.9. CET shoes attached to the glulam beam	72
Figure 3.10. Glulam beam instrumented with CETs to measure strain	73
Figure 3.11. Comparison of strain induced in aluminum compression block	74
Figure 3.12. Comparison of strain in aluminum tension block	75
Figure 4.1. Loading end of the tension set-up for determining lamina modulus of elasticity ..	80
Figure 4.2. Pinned end of the tension set-up of determining lamina modulus of elasticity ...	81
Figure 4.3. CET installed on a lamina at the center of a 30-inch segment to measure strain in tension	82
Figure 4.4. Torsion specimen cross section showing the growth ring orientation of a pair of samples to determine shear moduli	85
Figure 4.5. Torsion set-up to determine shear modulus	88
Figure 4.6. Placement of laminae and their E-values at three sections along the length of beam B1S	90
Figure 4.7. Placement of laminae and their E-values at three sections along the length of beam B2S	91
Figure 4.8. Arrangement of laminae and their E-values at three sections along the length of beam B3S	92
Figure 4.9. Arrangement of laminae and their E-modulus at three sections along the length of beam B4S	93
Figure 4.10. Arrangement of laminae and their E-values at three sections along the length of beam B1C	94
Figure 4.11. Arrangement of laminae and their E-modulus at three sections along the length of beam B2C	95
Figure 4.12. Arrangement of laminae and their E-modulus at three sections along the length of beam B3C	96
Figure 5.1. Flow chart of the experimental testing procedure	111
Figure 5.2. Displacement transducer used to measure beam deflections	116
Figure 5.3. Bending set-up to test glulam beams in simple bending about 2- or 3- axis	117
Figure 5.4. End support in the beam bending set-up	118

Figure 5.5. Experimental set-up to test glulam beams under combined bending and and compression loads	121
Figure 5.6. Combined bending and compression set-up for beams -- boundary condition on the side from where axial loads were applied	122
Figure 5.7. Combined bending and compression set-up -- boundary condition on the side where load cell was placed	123
Figure 5.8. Finite element mesh used to analyze all beams in bending about the major and the minor axes	125
Figure 5.9. Comparison of the experimental and the analytical normal strain in beam B1S83 under bending in the direction of 2-axis	142
Figure 5.10. Comparison of the experimental and the analytical normal strain in beam B1S114 under bending in the direction of 2-axis	143
Figure 5.11. Comparison of the experimental and the analytical normal strain in beam B4S132 under bending in the direction of 2-axis	144
Figure 5.12. Comparison of the experimental and the analytical normal strain in beam B1C83 under bending in the direction of 2-axis	145
Figure 5.13. Comparison of the experimental and the analytical normal strain in beam B2C83 under bending in the direction of 2-axis	146
Figure 5.14. Comparison of the experimental and the analytical normal strain in beam B2C114 under bending in the direction of 2-axis	147
Figure 5.15. Comparison of the experimental and the analytical deflections for beam B1S83 under bending in the direction of 2-axis	148
Figure 5.16. Comparison of the experimental and the analytical deflections for beam B1S114 under bending in the direction of 2-axis	149
Figure 5.17. Comparison of the experimental and the analytical deflections for beam B4S132 under bending in the direction of 2-axis	150
Figure 5.18. Comparison of the experimental and the analytical deflections for beam B1C83 under bending in the direction of 2-axis	151
Figure 5.19. Comparison of the experimental and the analytical deflections for beam B2C83 under bending in the direction of 2-axis	152
Figure 5.20. Comparison of the experimental and the analytical deflections for beam B2C114 under bending in the direction of 2-axis	153
Figure 5.21. Beam B2S83 -- comparison of strain distribution between faces 1 and 2 under bending in the direction of 2-axis	170
Figure 5.22. Beam B3C83 -- comparison of strain distribution between faces 1 and 2 under bending in the direction of 2-axis	171
Figure 5.23. Comparison of the experimental and the analytical normal strain in beam B3S83 under bending in the direction of 3-axis	179

Figure 5.24. Comparison of the experimental and the analytical deflections for beam B3S83 under bending in the direction of 3-axis	186
Figure 5.25. Finite element mesh used to analyze beams in combined bending and compression (table shows where load, P, was applied)	188
Figure 5.26. Comparison of strain distribution in beam B2S108 under combined bending in 2-direction and axial compression	199
Figure 5.27. Comparison of strain distribution in beam B2S108 under combined bending in 3-direction and axial compression	200
Figure 5.28. Comparison of strain distribution in beam B3S130 under combined bending in 2-direction and axial compression	201
Figure 5.29. Comparison of strain distribution in beam B3S130 under combined bending in 3-direction and axial compression	202
Figure 5.30. Comparison of strain distribution in beam B2C114 under combined bending in 2-direction and axial compression	203
Figure 5.31. Comparison of deflections for beam B3S130 under combined bending in 2-direction and axial compression	214
Figure 5.32. Comparison of deflections for beam B2C114 under combined bending in 2-direction and axial compression	215

List of Tables

Table 4.1. Longitudinal modulus of elasticity of glulam beams	84
Table 4.2. Torsion test samples with three planes of material symmetry	98
Table 4.3. Aspect ratio and measured torsional stiffness of orthotropic southern pine torsion specimens	100
Table 4.4. Combinations of orthotropic samples within each aspect ratio group	101
Table 4.5. Mean values of orthotropic shear moduli for the three cross section sizes	102
Table 4.6. Measured and computed torsional stiffness of the orthotropic circular samples (diameter = 1-inch)	103
Table 4.7. Cross section size, measured torsional stiffness, and computed shear modulus of glulam torsion bars	105
Table 4.8. Torsional stiffness and shear modulus of glulam bars with circular cross-section	106
Table 4.9. Mean values of G for the rectangular and circular glulam samples	107
Table 5.1. Geometry of glulam beams and their allowable stresses	112
Table 5.2. Details of tests performed on each beam and the effective spans for each test	119
Table 5.3. Beam B1S83: Comparison of the experimental and the analytical strain in bending about the 3-axis	126
Table 5.4. Beam B1S114: Comparison of the experimental and the analytical strain in bending about 3-axis	127
Table 5.5. Beam B2S83: Comparison of the experimental and the analytical strain in bending about 3-axis	128
Table 5.6. Beam B2S114: Comparison of the experimental and the analytical strain in bending about 3-axis	129
Table 5.7. B3S83: Comparison of the experimental and the analytical strain in bending about 3-axis	130

Table 5.8. Beam B3S132: Comparison of the experimental and the analytical strain in bending about 3-axis	131
Table 5.9. Beam B4S83: Comparison of the experimental and the analytical strain in bending about 3-axis	132
Table 5.10. Beam B4S114: Comparison of the experimental and the analytical strain in bending about 3-axis	133
Table 5.11. Beam B4S132: Comparison of the experimental and the analytical strain in bending about 3-axis	134
Table 5.12. Beam B1C83: Comparison of the experimental and the analytical strain in bending about 3-axis	135
Table 5.13. Beam B2C83: Comparison of the experimental and the analytical strain in bending about 3-axis	136
Table 5.14. Beam B2C114: Comparison of the experimental and the analytical strain in bending about 3-axis	137
Table 5.15. Beam B3C83: Comparison of the experimental and the analytical strain in bending about 3-axis	138
Table 5.16. Beam B3C114: Comparison of the experimental and the analytical strain in bending about 3-axis	139
Table 5.17. Beam B3C132: Comparison of the experimental and the analytical strain in bending about 3-axis	140
Table 5.18. Beam B1S83: Comparison of the experimental and the analytical deflections in bending about 3-axis	154
Table 5.19. Beam B1S114: Comparison of the experimental and the analytical deflections in bending about 3-axis	156
Table 5.20. Beam B2S83: Comparison of the experimental and the analytical deflections in bending about 3-axis	157
Table 5.21. Beam B2S114: Comparison of the experimental and the analytical deflections in bending about 3-axis	158
Table 5.22. Beam B3S83: Comparison of the experimental and the analytical deflections in bending about 3-axis	159
Table 5.23. Beam B3S132: Comparison of the experimental and the analytical deflections in bending about 3-axis	160
Table 5.24. Beam B4S83: Comparison of the experimental and the analytical deflections in bending about 3-axis	161
Table 5.25. Beam B4S114: Comparison of the experimental and the analytical deflections in bending about 3-axis	162
Table 5.26. Beam B4S132: Comparison of the experimental and the analytical deflections in bending about 3-axis	163

Table 5.27. Beam B1C83: Comparison of the experimental and the analytical deflections in bending about 3-axis	164
Table 5.28. Beam B2C83: Comparison of the experimental and the analytical deflections in bending about 3-axis	165
Table 5.29. Beam B2C114: Comparison of the experimental and the analytical deflections in bending about 3-axis	166
Table 5.30. Beam B3C83: Comparison of the experimental and the analytical deflections in bending about 3-axis	167
Table 5.31. Beam B3C114: Comparison of the experimental and the analytical deflections in bending about 3-axis	168
Table 5.32. Beam B3C132: Comparison of the experimental and the analytical deflections in bending about 3-axis	169
Table 5.33. Beam B1S83: Comparison of the experimental and the analytical strain in bending about 2-axis	173
Table 5.34. Beam B1S114: Comparison of the experimental and the analytical strain in bending about 2-axis	174
Table 5.35. Beam B2S83: Comparison of the experimental and the analytical strain in bending about 2-axis	175
Table 5.36. Beam B2S114: Comparison of the experimental and the analytical strain in bending about 2-axis	176
Table 5.37. Beam B3S83: Comparison of the experimental and the analytical strain in bending about 2-axis	177
Table 5.38. Beam B3S132: Comparison of the experimental and the analytical strain in bending about 2-axis	178
Table 5.39. Beam B1S83: Comparison of the experimental and the analytical deflections in bending about 2-axis	180
Table 5.40. Beam B1S114: Comparison of the experimental and the analytical deflections in bending about 2-axis	181
Table 5.41. Beam B2S83: Comparison of the experimental and the analytical deflections in bending about 2-axis	182
Table 5.42. Beam B2S114: Comparison of the experimental and the analytical deflections in bending about 2-axis	183
Table 5.43. Beam B3S83: Comparison of the experimental and the analytical deflections in bending about 2-axis	184
Table 5.44. Beam B3S132: Comparison of the experimental and the analytical deflections in bending about 2-axis	185
Table 5.45. Beam B1S108: Comparison of the experimental and the analytical strain in combined bending about 3-axis and compression	189

Table 5.46. Beam B1S108: Comparison of the experimental and the analytical strain in combined bending about 2-axis and compression	190
Table 5.47. Beam B2S108: Comparison of the experimental and the analytical strain in combined bending about 3-axis and compression	191
Table 5.48. Beam B2S108: Comparison of the experimental and the analytical strain in combined bending about 2-axis and compression	192
Table 5.49. Beam B3S130: Comparison of the experimental and the analytical strain in combined bending about 3-axis and compression	193
Table 5.50. Beam B2S130: Comparison of the experimental and the analytical strain in combined bending about 2-axis and compression	194
Table 5.51. Beam B1C81: Comparison of the experimental and the analytical strain in combined bending about 3-axis and compression	195
Table 5.52. Beam B2C109: Comparison of the experimental and the analytical strain in combined bending about 3-axis and compression	196
Table 5.53. Beam B3C130: Comparison of the experimental and the analytical strain in combined bending about 3-axis and compression	197
Table 5.54. Beam B1S108: Comparison of the experimental and the analytical deflections in bending about 3-axis and compression	204
Table 5.55. Beam B1S108: Comparison of the experimental and the analytical deflections in bending about 2-axis and compression	205
Table 5.56. Beam B2S108: Comparison of the experimental and the analytical deflections in bending about 3-axis and compression	206
Table 5.57. Beam B2S108: Comparison of the experimental and the analytical deflections in bending about 2-axis and compression	207
Table 5.58. Beam B3S130: Comparison of the experimental and the analytical deflections in bending about 3-axis and compression	208
Table 5.59. Beam B3S130: Comparison of the experimental and the analytical deflections in bending about 2-axis and compression	209
Table 5.60. Beam B1C81: Comparison of the experimental and the analytical deflections in bending about 3-axis and compression	210
Table 5.61. Beam B2C109: Comparison of the experimental and the analytical deflections in bending about 3-axis and compression	211
Table 5.62. Beam B3C130: Comparison of the experimental and the analytical deflections in bending about 3-axis and compression	212

CHAPTER 1

1 INTRODUCTION

Wood is one of the oldest materials used to construct structures. It is a renewable resource; ironically, the world today is faced with dwindling forests and a shortage of clear solid wood. Therefore, research is being conducted worldwide to develop new wood composites, made of smaller lower quality trees, to compete with other construction materials. Technological advances have made wood a valuable engineering material. Many of the wood products used for construction are highly engineered composites such as laminated wood, plywood, waferboard, fiberboards, and particleboards. These composites are replacing sawn wood for structural use.

Glued-laminated timber, or 'glulam', is a composite used to construct large wood structures and is manufactured by bonding lumber laminae with structural adhesives to produce straight or curved members with large cross-sections. The grain of all laminations is oriented approximately parallel to long axis of the member. Aesthetic beauty, good thermal and fire resistance properties, excellent acoustical properties, and low construction costs are some of the attractive benefits of glulam compared to steel or aluminum (75). Recently, curved glulam beams have been used to construct large-span lattice domes and space frames.

1.1 The Problem

Since wood is highly variable and anisotropic, it is difficult to predict its response to applied loads. Presently there is no standard method of predicting the complete structural behavior, including the ultimate load capacity, of glulam space frames and lattice domes (17,36). Advanced techniques, such as finite element analysis, are being developed to accurately model the structural behavior of wood. However, these analytical models must be verified experimentally.

This study is part of a project designed to formulate a finite element method of analysis to predict the complete structural response of glulam space frames and lattice domes up to collapse (17,36). A finite element model is being developed to predict the linear and nonlinear response of straight and curved glulam space beams in three load conditions: bending, bending and compression, and biaxial bending (19). Geometric nonlinearity due to large displacements and large rotations should be considered in timber design since the ultimate load capacity of single-layer timber space frames may be governed by elastic instability (18). Material nonlinearity is not being considered because the constitutive matrix relating stresses and strains for nonlinear response is not available. However, it could be included in the finite element model following the procedure described by Connors (15,18). The model incorporates the effect of shear and torsional deformations. When the effect of shearing deformation is negligible (i.e. length-to-depth ratio is usually greater than (21), the deformed state of the element is characterized by axial deformation, flexural deformations about the two principal axes, and torsional deformation. In non-circular cross sections, torsional moments cause plane sections to deform out of their planes or warp (35). In linear small displacement theory, if the cross sections are free to warp then the deformations are uncoupled (35). However, in a space structure, such as a glulam lattice dome, the deformations are not independent. The centroid of the cross section may not coincide with the shear center and the center of the twist thus causing coupling of deformations (12,35). The significance of warping displacements on torsional stiffness of glulam beams should be investigated and, if significant, should be included in the finite element model.

The variation in material properties along the length and throughout the cross-section of the glulam beams complicates the formulation of the finite element model. Unlike solid sawn wood, glulam beams do not exhibit material symmetry. Due to the random growth ring orientation, it would be convenient to consider a glulam cross-section transversely isotropic in its plane (18,50).

1.2 Objectives

The objective of the study is to evaluate the applicability of the isoparametric beam finite element to model the elastic response of straight and curved glulam beams subjected to three load conditions: bending about the major axis, bending about the minor axis, and combined bending and compression.

To accomplish the objective, it was necessary to experimentally evaluate the constitutive matrix to model a 3-D glulam beam. For solid sawn wood beams, the required parameters are the longitudinal Young's modulus (E_L) and transverse shear moduli (G_{LR} and G_{LT}). For simplicity, it would be convenient to model glulam beams using a reduced constitutive matrix that incorporates transverse isotropy. This study investigated the suitability of using a three-noded isoparametric element for modeling glulam beams with the above assumptions regarding material properties of the beams.

1.3 Overview

This thesis contains six chapters. In Chapter 2, a literature review is presented on glulam beam manufacturing standards, lumber grades, and design stresses. Also, included is a review on space structures, orthotropic characterization of wood, the constitutive matrix of wood and glulam beams, determination of material properties of glulam beams, stress analysis in glulam beams, and finite element analysis of wood systems.

Chapters 3,4,and 5 are written in journal format to simplify the presentation. Chapter 3 contains details of the strain measuring device constructed for this study. It also discusses a small scale investigation conducted to gain insight into the effect of bonded gage lengths on strain measurements in southern pine. A laboratory built clip-on transducer developed to measure strains in wood is presented with the details of its fabrication, calibration, validation, and applications.

In chapter 4, the procedures used to determine the required material properties are discussed. Longitudinal modulus of elasticity and shear modulus were determined experimentally.

Chapter 5 contains details of the experimental materials and testing procedures, and the experimental and analytical results of glulam beams tested in bending about major and minor axes, and combined compression and bending. The analytical and the experimental results are compared and discussed. A discussion on sources of errors is also provided in Chapter 5.

Finally, in Chapter 6, a summary of results is presented along with the conclusions. In addition, recommendations for future work are provided.

CHAPTER 2

2 Literature Review

2.1 Introduction

In this chapter, a brief background on manufacturing specifications of glulam beams is presented. Commercial dimensions of glulam beams, type of adhesives used, the effect of selective placement of laminae, and advantages of glulam members over solid wood beams are also discussed (sections 2.2 & 2.3). Structural analysis of space frames is briefly presented in section 2.4. Section 2.5 discusses the orthotropic elasticity of wood and the formulation of Hooke's law for orthotropic material. Then, determination of material properties of glulam beams (longitudinal Young's modulus and shear modulus) is presented in section 2.6. Different methods of predicting lamina longitudinal modulus of elasticity and shear modulus are presented. Stress analysis in glulam beams is discussed briefly followed by a discussion on Finite Element Method (FEM) to model the response of a structure or its elements. Finally, a summary of existing FE-models for glulam beams and the FE-model in this study are provided.

2.2 Manufacturing Specifications, Sizes, Species, and Grades

In the U.S.A. the manufacture of structural glued-laminated timber must be in accordance with the ANSI/AITC A190.1 specification (2,3,23). It contains specifications for the production, testing, and certification of structural glulam timber. Canadian Standards Association (CSA) standard O 122 contains the requirements for the manufacture of structural glulam members in Canada. American Institute of Timber Construction (AITC) 117-84 MANUFACTURING also has the standard manufacturing specifications for structural glued-laminated timber of softwood species. AITC 117--DESIGN gives the design specification for glued-laminated timber. The National Design Specification for Wood Construction and Supplement also provides the glulam design specifications (53). The design values for glued-laminated timber are established by following the procedures given in Standard Method of Establishing Stresses for Structural Glued Laminated Timber (Glulam), ASTM D 3737 (3).

Many of the glulam beams produced in the U.S. are for custom products. They are manufactured according to the specifications for a specific use. Lumber that qualifies for laminating purposes is selected and planed so that the adhesive has intimate contact with the laminae. Phenol-resorcinol and melamine adhesives are the most widely used wet-use adhesives in structural glued-laminated members. Casein adhesives are the standard dry-use adhesives used to manufacture glulam members (31). Today, however, wet-use adhesives are most common. A uniform application of a predetermined amount of adhesive is achieved using special glue spreading equipment.

Adhesive is spread uniformly on one or both faces of each lamina. Then the laminae are placed on a clamping form that has been set to the required shape of the finished member. Clamping pressure is applied to bring the surfaces of the laminae into intimate contact, to pull the member into shape, to force out excessive adhesive, and to hold the pieces firmly together until the adhesive has developed sufficient bond strength. The clamps have to be uniformly spaced and tightened to maintain a uniform pressure throughout the adhesive curing period. After the beams are removed from the clamps, they are planed to the required sizes and cut to length. The finished

members are usually wrapped in water-resistant paper for protection during transit, storage, and erection (31,75).

Industry standards permit the use of several widths and depths of glulam members. Most Southern Pine glulam beams have widths of 3", 5", 6 3/4", 8 1/2", or 10 1/2". Nominal sizes of glulam beams produced commercially are given in table form by AITC (2). Other sizes are readily available for custom orders. The nominal thickness of each lamina may not exceed two inches nominal for straight beams and one inch nominal for curved beams (2,23).

The arrangement of laminae by stiffness during the manufacturing process is advantageous (43,44). It not only makes the beam stiffer, but also increases the strength of the beam. Stiffer and stronger laminae are placed on the outer edges where maximum tension and compression stresses occur. Moody (52) concluded in his studies that the stiffness of the outer laminae play an important role in determining the strength of a beam. Koch and Bohannon (44) compared the strength of beams with laminae arranged according to specific gravity, stiffness, appearance, and random selection. The beams with laminae arranged by stiffness were stronger than other arrangements. It was discovered that lay-up of beams by stiffness not only increased the average strength, but also decreased the variability between beams.

Several softwood and hardwood species are used for glulam members. The most commonly used species groups for glulam members in the United States are Douglas-fir-larch, southern pine, and hem-fir (23,31). Many studies have been conducted to evaluate the strength properties of glued-laminated beams composed of more than one species (21,27,52,60). All the studies found that the ultimate strength in bending was influenced by the grade and strength of the face boards because the maximum bending stresses are induced in the outer laminae. Lumber, used for glulam beams, is either visually graded or "E-rated" as required for the laminating combinations. Visual grading of lumber is performed on the basis of knots and slope of grain. Many non-destructive testing methods are available to evaluate the stiffness ("E-rating") of laminae (9,23,28,61,74).

Clear-wood strength, knots, slope of grain, and other grade characteristics are the principal determinants of bending strength of glulam beams (2). The number, size, and position (with respect to the neutral axis) of the knots affect the bending strength and stiffness of the beams (31). For axially loaded beams, the total area of knots in the cross section affects strength and stiffness. So, if knots are present in the critical regions, such as in the tension zone, the strength of the beam will be reduced considerably. More information on the effect of knots on glulam strength and stiffness properties is in the literature (5,23,31). Also, the slope of grain in the outer edges of the beam will considerably reduce the stiffness and the strength of the beam. In addition, the size of the beam cross section can also affect the strength of the beam because of Weibull's weak link theory (49), which states that there is higher probability of finding a critical flaw in the material with increased volume.

2.3. Advantages of Using Glulam Members

Glulam is often preferred over solid wood because glulam members of any length, size, or structural shape can be fabricated. Laminae can be end-joined, glued edge to edge, or bent to a curved form during gluing. Also, lower quality lumber can be utilized with high grade lumber to manufacture structural members of required standards. This allows for controlled dispersal of lumber characteristics, such as knots, to produce glulam members with the required structural properties. Since knotty lumber has high shear strength it is often placed close to the neutral axis of the beam where maximum horizontal shear stresses occur. In addition, the finished members have a high degree of dimensional stability under dry-use conditions. Also, checking is minimized since glulam is made from kiln dried lumber (23,70,75).

2.4 Structural Analysis of Space Structures

Structural analysis is used to predict the behavior or performance of a structure from mathematical models that approximate the behavior of the structure (35,48). Since a structure is an as-

sembly of elements, the properties of the system are determined from the properties of the elements and connections. The performance of the structure is then predicted from the way the elements interact with each other (35,48). Therefore, to analyze the behavior of a structure, one has to evaluate the internal characteristics of the elements including forces, strains, and stresses, and the external characteristics of the elements which include the interactions at the element boundaries.

To formulate a mathematical model of a structure, an idealization model that defines the deformed configuration of the structure at any given point is necessary. The number of independent parameters needed to define the configuration represents the degrees of freedom of the model (35,48). In engineering analysis, the deformed configuration of a model is defined by the displacements at each point from its initial state (3).

In a two dimensional analysis of a beam element each node has three degrees of freedom as shown in Figure 2.1 (35). A space frame element is characterized by six degrees of freedom at each node (Figure 2.2) (35). The deformed state of an element is characterized by axial deformation, flexural deformations about the two principal axes, and torsional deformation.

2.5 Orthotropic Elasticity

Wood is a highly variable cellular material made up of various types of cells which vary in size, cell wall thickness, and in the physical structure of the cell wall. It can be classified as an anisotropic material. The evaluation of the mechanical behavior of wood is complex since the compliance matrix for an anisotropic material in a generalized Hooke's law has 21 independent constants (10,40). However, on a pointwise basis in perfectly formed trees wood can be classified as an orthotropic material with three mutually orthogonal planes of symmetry (10).

2.5.1 Orthotropic Characteristics of Wood

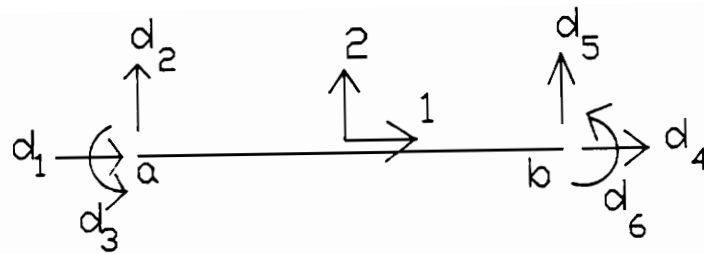


Figure 2.1 Degrees of freedom in a 2-D beam element

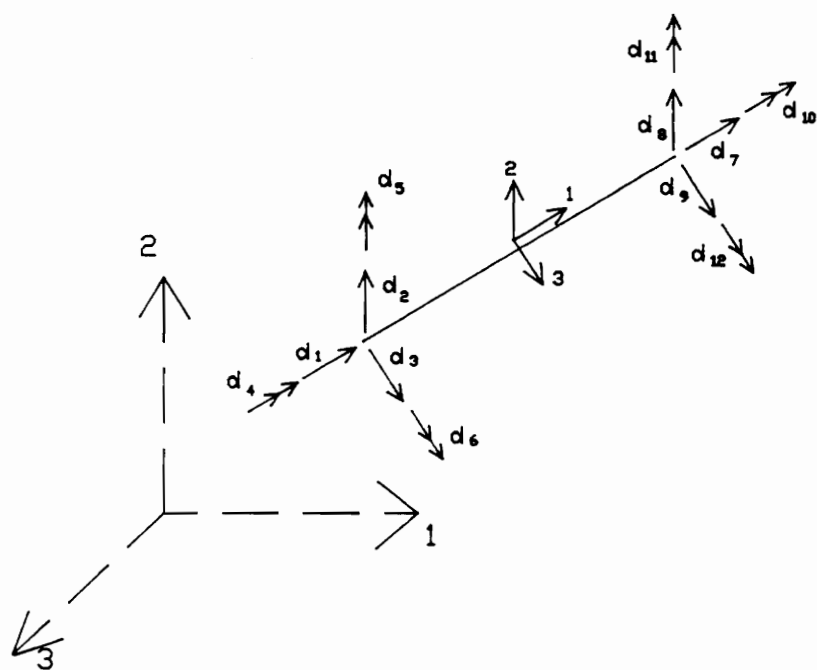


Figure 2.2 Degrees of freedom in a space frame or a 3-D element

Figure 2.3 shows the orthotropic material axes representing wood. The longitudinal axis, L, runs parallel to the fiber length; the radial axis, R, is normal to the growth rings; and, the tangential axis, T, runs tangent to the growth rings. It is convenient to neglect the curvature of growth rings and assume that wood has three orthogonal planes of symmetry. Therefore, the constitutive equation for wood takes the following form (10,40):

$$\begin{bmatrix} \gamma_L \\ \gamma_R \\ \gamma_T \\ \gamma_{RT} \\ \gamma_{LT} \\ \gamma_{LR} \end{bmatrix} = \begin{bmatrix} \frac{1}{E_L} & \frac{-\nu_{RL}}{E_R} & \frac{-\nu_{TL}}{E_T} & 0 & 0 & 0 \\ \frac{-\nu_{LR}}{E_L} & \frac{1}{E_R} & \frac{-\nu_{TR}}{E_T} & 0 & 0 & 0 \\ \frac{-\nu_{LT}}{E_L} & \frac{-\nu_{RT}}{E_R} & \frac{1}{E_T} & 0 & 0 & 0 \\ 0 & 0 & 0 & \frac{1}{G_{RT}} & 0 & 0 \\ 0 & 0 & 0 & 0 & \frac{1}{G_{LT}} & 0 \\ 0 & 0 & 0 & 0 & 0 & \frac{1}{G_{LR}} \end{bmatrix} \begin{bmatrix} \sigma_L \\ \sigma_R \\ \sigma_T \\ \sigma_{RT} \\ \sigma_{LT} \\ \sigma_{LR} \end{bmatrix} \quad [2.1]$$

where,

$\gamma_L, \gamma_R, \gamma_T$ = normal strain in L, R, and T directions

γ_{LR}, γ_{LT} , and γ_{RT} = shear strain in LR, LT, and RT planes

E_L, E_R , and E_T = Young's modulus in L, T, and R directions

ν_{ij} = Poisson's ratio for transverse strain in j-direction when stressed in the i-direction

G_{LR}, G_{LT} , and G_{RT} = shear moduli in the LR, LT, and RT planes

σ_L, σ_R , and σ_T = normal stresses in the L, R, and T directions

σ_{LR}, σ_{LT} , and σ_{RT} = shear stresses in LR, LT, and RT planes, respectively.

The 6 X 6 matrix in the equation is termed the compliance matrix. Twelve compliance coefficients are required to specify the elastic character of an orthotropic material as indicated by the compliance matrix. However, the compliance matrix can be simplified to characterize an

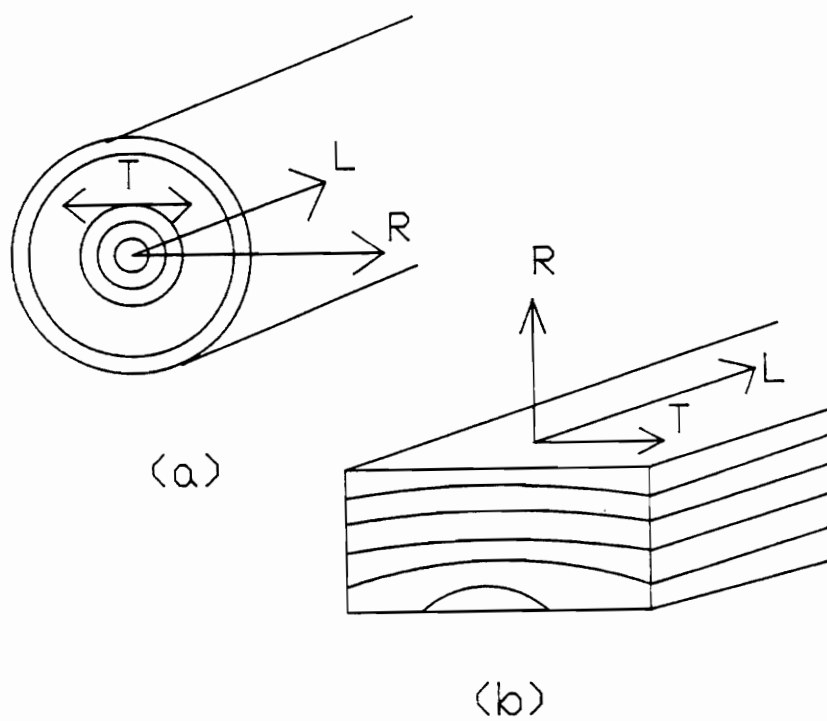


Figure 2.3 Orthotropic material axes representing wood

orthotropic material by introducing the concept of strain energy stored in the orthotropic body when acted on by a simple system of stresses (38). Therefore, due to the orthotropy assumption and symmetry of the matrix, the following relations hold (10,38,40):

$$\frac{\nu_{LR}}{E_L} = \frac{\nu_{RL}}{E_R}$$

$$\frac{\nu_{LT}}{E_L} = \frac{\nu_{TL}}{E_T} \quad [2.2]$$

$$\frac{\nu_{RT}}{E_R} = \frac{\nu_{TR}}{E_T}$$

Thus, only nine independent constants need to be evaluated to characterize stress-strain relationship in wood (9,10,40):

$$E_L, E_R, E_T, G_{RT}, G_{LT}, G_{LR}, \nu_{LR}, \nu_{LT}, \nu_{RT}$$

However, due to random orientation of growth rings across the cross section in glulam beams, it is normally accepted to specify the elastic character of a glulam beam in terms of the beam's geometric axes instead of symmetry axes. Geometric axes are the axes defining the physical shape of the material; whereas, symmetry axes define the material properties. Figure 2.4 shows the geometric and symmetry axes of a glulam beam. The symmetry axes and the geometric axes are generally not exactly coincident except for the L- and l- axes. The compliance matrix components in terms of the geometric axes of a glulam beam is written as (10,40):

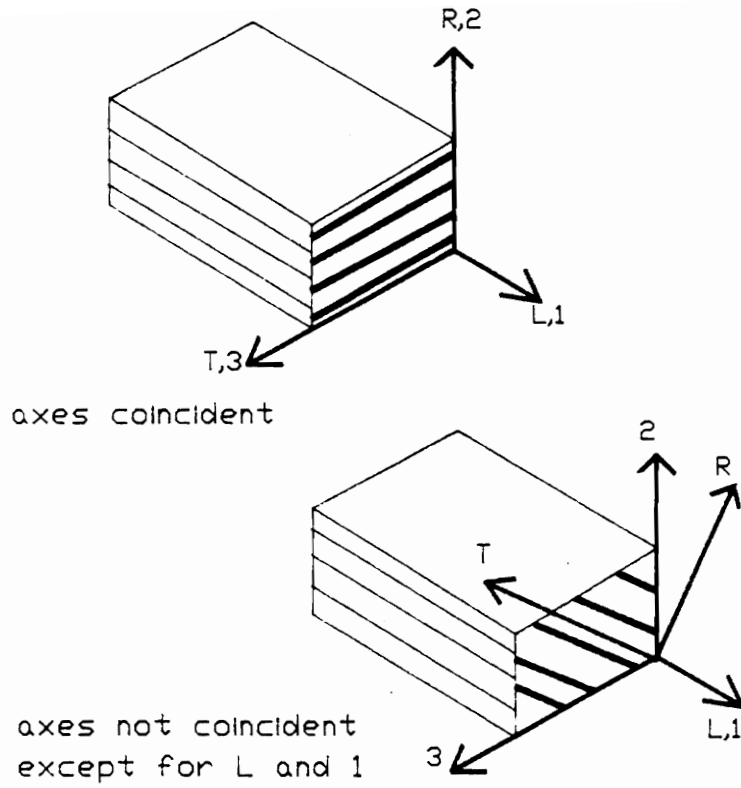


Figure 2.4 Geometric (1,2,3) and symmetry (L,R,T) axes of a glulam specimen

$$[S_{ij}] = \begin{bmatrix} \frac{1}{E_1} & \frac{-\nu_{21}}{E_2} & \frac{-\nu_{31}}{E_3} & 0 & 0 & 0 \\ \frac{-\nu_{12}}{E_1} & \frac{1}{E_2} & \frac{-\nu_{32}}{E_3} & 0 & 0 & 0 \\ \frac{-\nu_{13}}{E_1} & \frac{-\nu_{23}}{E_2} & \frac{1}{E_3} & 0 & 0 & 0 \\ 0 & 0 & 0 & \frac{1}{G_{23}} & 0 & 0 \\ 0 & 0 & 0 & 0 & \frac{1}{G_{31}} & 0 \\ 0 & 0 & 0 & 0 & 0 & \frac{1}{G_{21}} \end{bmatrix} \quad [2.3]$$

where,

E_1, E_2, E_3 = Young's moduli in 1,2, and 3 directions

ν_{ij} = Poisson's ratio for transverse strain in j-direction when stressed in the i-direction

G_{23}, G_{31}, G_{12} = shear moduli in the 2-3, 3-1, and 1-2 planes, respectively.

Figure 2.5 shows the nine components of stress acting in a small rectangular parallelepiped. Note that $\sigma_{ij} = \sigma_{ji}$ for $i, j = 1, 2, 3$. The stiffness matrix relating stresses to strains takes the form:

$$\sigma = S^{-1}\gamma \quad [2.4]$$

Knowing this relationship and the compliance matrix, the components of the stiffness matrix, C , can be written as (10,40):

$$C_{11} = \frac{S_{22}S_{33} - (S_{23})^2}{|S|} = \frac{1 - \nu_{23}\nu_{32}}{E_2E_3|\Delta|}$$

$$C_{22} = \frac{S_{11}S_{33} - (S_{13})^2}{|S|} = \frac{1 - \nu_{31}\nu_{13}}{E_1E_3|\Delta|}$$

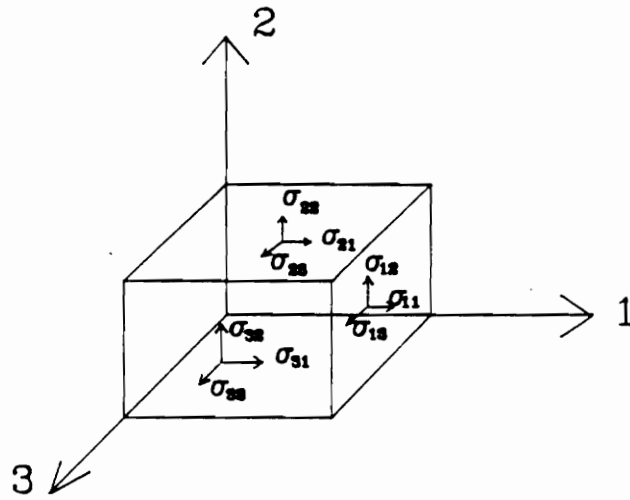


Figure 2.5 Stress components on a differential element placed in a rectangular coordinate system

$$C_{33} = \frac{S_{11}S_{22} - (S_{12})^2}{|S|} = \frac{1 - \nu_{21}\nu_{12}}{E_1E_2|\Delta|} \quad [2.5]$$

$$C_{12} = C_{21} = \frac{S_{21}S_{23} - S_{23}S_{31}}{|S|} = \frac{\nu_{21} + \nu_{23}\nu_{31}}{E_2E_3|\Delta|}$$

$$C_{13} = C_{31} = \frac{S_{31}S_{22} - S_{21}S_{32}}{|S|} = \frac{\nu_{31} + \nu_{21}\nu_{32}}{E_2E_3|\Delta|}$$

$$C_{23} = C_{32} = \frac{S_{31}S_{12} - S_{11}S_{32}}{|S|} = \frac{\nu_{23} + \nu_{21}\nu_{13}}{E_1E_2|\Delta|}$$

$$C_{44} = \frac{1}{S_{44}} = G_{23}$$

$$C_{55} = \frac{1}{S_{55}} = G_{13}$$

$$C_{66} = \frac{1}{S_{66}} = G_{12}$$

where

$$|S| = S_{11}S_{22}S_{33} + 2S_{12}S_{23}S_{31} - S_{11}(S_{23})^2 - S_{22}(S_{13})^2 - S_{33}(S_{12})^2$$

$$\Delta = \frac{1 - 2\nu_{21}\nu_{32}\nu_{13} - \nu_{13}\nu_{31} - \nu_{23}\nu_{32} - \nu_{12}\nu_{21}}{E_1E_2E_3}$$

Therefore, to formulate the stiffness matrix, nine independent parameters are needed.

2.5.2 Basic Assumptions

The elementary bending theory (Bernoulli-Euler beam theory) makes the following assumptions (12,31,35,48,67):

1. Small displacements.
2. Plane sections remain plane.
3. Direct stresses normal to the center-line of the element (stresses perpendicular to the grain) are ignored.
4. Shear strains are ignored.

However, for wood shear strain may be important ,especially, when the length-to-depth ratio is less than 20 (7,10,23,31,37). In short deep beams, shear stresses contribute significantly to the total stress and deflection. The effect of span-depth ratio (l/d) for wood beams on the ratio of apparent to true modulus of elasticity is shown in Figure 2.6 (10).

Therefore, in this study, the FE-model incorporated the Mindlin-Reissner beam theory (Timoshenko beam-bending theory) to analyze the behavior of a beam subjected to combined loading where axial, biaxial bending, torsion, and shearing deformations are possible (17,18,19). This theory incorporates the effect of shear deformations. A plane section originally normal to the midsurface does not necessarily remain normal to the midsurface in the deformed state (67,68). The Mindlin-Reissner theory accomadates geometric nonlinearities by allowing large displacements and rotations, but small strains. These features are common to space frame elements (18,19).

To carry out the analysis of glulam beams, the following additional assumptions were made:

1. Gluelines between laminae were of infinitesimal thickness with no interlaminar slippage. This assumption is commonly made by many researchers (10,31).
2. The longitudinal axis of the laminae coincides with the longitudinal axis of the beam. Thus, it was assumed that the longitudinal fibers were parallel to the axis of the beam.
3. The beam cross-section was transversely isotropic due to the random orientation of the laminae growth rings. In this study, tests were conducted on small glulam samples to justify the assumption of transverse isotropy for southern pine glulam beams.

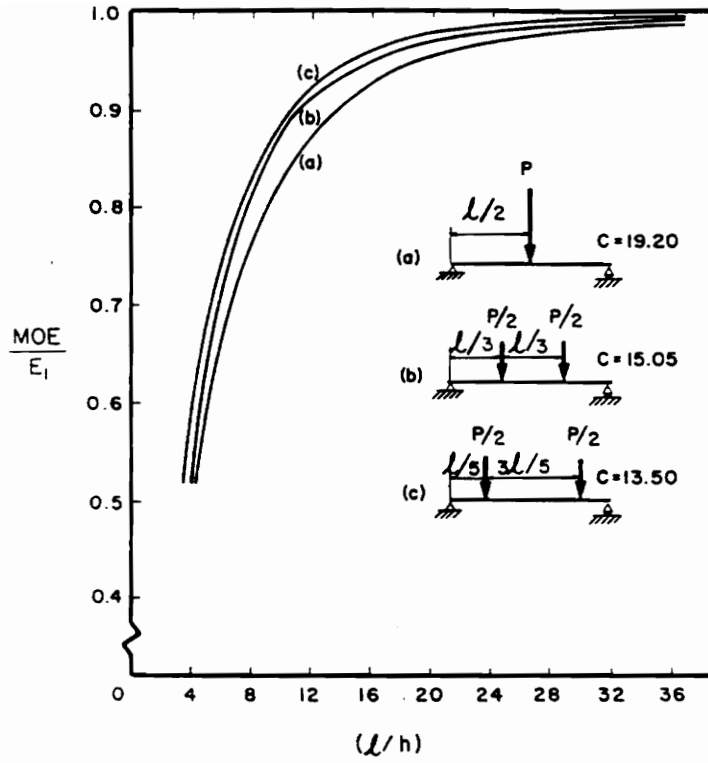


Figure 2.6 Effects of span-to-depth ratio (l/h) on the ratio of apparent to true modulus of elasticity under third-point loading (10)

2.5.3 Reduction of the Constitutive Matrix

The principal stresses considered in this study are normal stresses (along 1-axis) and shear stresses in 1-2 and 1-3 planes. Therefore, it is assumed that three of the six stress components -- σ_2 , σ_3 , and σ_{23} -- are zero. Thus, the constitutive matrix for an orthotropic beam can be reduced by eliminating the following components: $\frac{-\nu_{21}}{E_2}$; $\frac{-\nu_{31}}{E_3}$; $\frac{1}{E_2}$; $\frac{-\nu_{32}}{E_3}$; $\frac{-\nu_{23}}{E_2}$; $\frac{1}{E_3}$; and $\frac{1}{G_{23}}$.

Moreover, under the Mindlin-Reisner theory, the cross section of the beam does not deform in its plane, but undergoes a rigid body movement (that is, plane sections remain plane). Due to this assumption, the remaining two Poisson's coefficients, ν_{12} and ν_{13} , are very small and can be considered to be zero.

2.5.4 Specialized Constitutive Matrix for Glulam Beams

The elastic constants required to model glulam beams, using the Mindlin-Reissner beam theory, are the longitudinal elastic modulus E_1 , and the two shear moduli G_{12} and G_{13} . The constitutive law can be expressed as follows (19):

$$\begin{bmatrix} \sigma_{11} \\ \sigma_{12} \\ \sigma_{13} \end{bmatrix} = \begin{bmatrix} E_1 & 0 & 0 \\ 0 & KG_{12} & 0 \\ 0 & 0 & KG_{13} \end{bmatrix} \begin{bmatrix} \epsilon_{11} \\ \gamma_{12} \\ \gamma_{13} \end{bmatrix} \quad [2.6]$$

where K is the shear correction factor which is constant over the cross section (12,17,67). According to the Mindlin-Reissner beam theory, the shear strain is constant across the section. Therefore, assuming that E does not vary pointwise, the shear stress should also be constant across the section (17,67). However, according to the elementary beam theory, shear stress varies parabolically for a rectangular cross section. The shear stress can be expressed as an equivalent constant stress by applying the shear correction factor, K , which can be evaluated using the prin-

cipal of virtual work (17). For a rectangular cross section, K calculated by the elastic strain energy method is $5/6$ (17,67).

2.6 Determination of Material Properties of Glulam Beams

To apply equation [2.6], the material properties E , G_{12} , G_{13} , must be known or estimated. This section discusses methods to measure those properties for glulam beams. The longitudinal modulus of elasticity of a glulam beam can be estimated by applying a bending moment to the beam and measuring the deflection at the center of the span (43,44,51,52,60). This method, however, yields deflection that is due to normal, as well as, shear stress. Consequently, the true modulus of elasticity is underestimated yielding an apparent modulus of elasticity commonly referred to as MOE (10). Errors become larger as the depth of the beams increases. Moreover, in a beam subjected to bending, stress distribution in the cross section of the beam is not uniformly distributed. Therefore, it is not necessarily true that the estimated elastic modulus reflects the influence of defects located in slightly stressed areas. Jones (40) states that bending test is a structural element test and not a material property test. To achieve a uniform stress distribution across the section, the member must be subjected to axial loads which is a difficult task to perform on full-size samples such as glulam beams. In addition, a sensitive strain measuring system is needed to record tensile strains. Due to these difficulties, the bending method to determine modulus of elasticity is used.

Other researchers (25,26) have cut small bending and compression samples from glulam beams to determine the longitudinal modulus of elasticity and Young's modulus perpendicular to grain. Another alternative is to estimate the longitudinal modulus of elasticity of glulam beams from individual laminae properties using a suitable composite theory. However, to measure the shear modulus, it is better to test smaller glulam samples than larger ones because smaller samples are easier to handle and they are more homogeneous than the larger specimens. In this study, I was interested in accurate material property estimates for each beam. These properties were measured by conducting non-destructive tension tests on the lumber laminae to determine E_1 before beam

manufacturing, and small torsion samples to determine shear modulus, G . Small samples were used because there were no means of testing large scale samples, such as beams, in torsion.

2.6.1 Determination of Longitudinal Young's Modulus, E_1

There are many composite theories for calculating the laminate stiffness from the individual laminae stiffnesses (40). Some theories work well for composites such as graphite- epoxy composites (40). Generally, composite theories are effective only for plane stress analysis (40). In addition, the complexity of these theories increases for unsymmetric composite laminates (40). One of the underlying assumptions of some composite theories is that the laminate is thin and its thickness is small compared to its length or width (40). In glulam beams the nominal thickness of the individual laminae is either one or two inches and the laminate (beam) is relatively thick or deep.

Another alternative to estimate beam's longitudinal modulus of elasticity is to calculate the effective modulus of elasticity, $E_{L \text{ eff}}$, for beams based on the laminae stiffness (10). The effective modulus is calculated from:

$$E_{L \text{ eff}} = \frac{2}{I} \sum_{i=1}^n E_L^i [I_o^i + A^i (d^i)^2] \quad [2.7]$$

where

E_L^i = modulus of elasticity of the i th lamina in longitudinal direction

I^i = moment of inertia of the i th lamina about the neutral plane of the beam

I = moment of inertia of the entire beam

n = one-half the total number of laminae

I_o^i = moment of inertia of the i th lamina about its neutral plane

A^i = cross-sectional area of the i th lamina

d_i = distance between the centroidal plane of the laminated beam and the i th lamina

In transformed section analysis method, the outside laminae contribute more toward the effective modulus of elasticity in bending than those close to the neutral plane (10). Therefore, E_L can be greater in bending than in uniaxial tension. Calculating the effective modulus of elasticity is appropriate when beam is fabricated with laminae of high stiffness placed near the upper and lower surfaces of the beam where bending stresses are maximum. Bodig and Jayne suggest using E_{Leff} only to calculate the deflection of a laminated beam. However, the transformed section method neglects shear deformation in predicting stiffness (6). It was found that using the transformed section method, the average error between predicted and actual values of modulus of elasticity was 7 percent (41).

Foschi and Barrett (24) and Davalos (17) used the harmonic and the arithmetic means of laminae stiffness to estimate the beam's longitudinal Young's modulus. These mean values were assumed to be the global longitudinal modulus of elasticity, E_1 , of the glulam beams. Therefore, the longitudinal modulus of elasticity of the lumber used to manufacture the beams must be measured by a non-destructive method. Several methods for determining the elastic properties of individual lamina are discussed next.

Stress-wave timing

This method measures the time required for an induced stress wave to travel between two accelerometers placed on the specimen. The modulus of elasticity of lumber can be estimated from the velocity of the stress wave. The dynamic modulus of elasticity is calculated (28,10) from:

$$E_d^{sw} = V \frac{g}{\rho} \quad [2.8]$$

where:

E_d^w = dynamic modulus of elasticity from longitudinal stress wave propagation (psi)

V = velocity of the stress wave (in/sec)

ρ = mass density of the material (lb/in³), and

g = gravitational constant (386 in/sec²)

The dynamic modulus of elasticity computed from equation [2.8] is approximately 10 percent greater than the static MOE. Also defects such as knots influence the wave velocity. Therefore this method is most useful for developing rough estimates of the E .

Vibration method

In this method, a lumber specimen is supported at its ends as plank. A rapidly applied force causes the piece to vibrate. The free vibration displacement-time curve is obtained and the dynamic modulus of elasticity, E_d , is calculated using the following formula (10,61):

$$E_d = \frac{f^2 WL^3}{2.46Ig} \quad [2.9]$$

where

f = resonant frequency (cycle/sec)

W = weight of the beam (lb)

L = span (in)

I = moment of inertia (in⁴)

g = acceleration due to gravity (386 in/sec²)

Another resonance method used in wood testing is presented by by Sinclair and Farshad (61). This method consists of subjecting a cantilever beam specimen to harmonic support excitation and measuring the excitation frequency at which the beam specimen resonates. Then, using a theore-

tical model the Young's modulus in the longitudinal direction is calculated. The authors used two formulas derived from beam theory. One of the formula ignores shear deflection ; whereas, the other considers shear deflection to calculate the Young's modulus. Vibration methods were used by some investigators to measure the longitudinal modulus of elasticity of lumber (11).

Static (flexure) test

This method is widely used by researchers to evaluate the modulus of elasticity of wood beams (5,10,11,17,21,23,24,25,27,29,32,37,39,41,42,43,44,51,52). The test involves subjecting a simply supported lumber specimen to a mid-span concentrated load and measuring the deflection at the mid-point. Euler-Bernoulli beam theory is used to calculate E_1 :

$$E_1 = \frac{P L^3}{48 I \Delta} \quad [2.10]$$

where

P = applied load (lbs)

L = test span (inches)

I = second moment of inertia (in^4)

Δ = measured mid-span deflection (inches)

Static bending method ignores the effects of shear deformation and is often referred to as an effective modulus of elasticity. If shear is taken into account, the mid-point deflection can be calculated using

$$\Delta = \frac{PL^3}{48EI} \left[1 + \frac{3}{10} \left(\frac{h}{1/2} L \right)^2 \frac{E}{G} \right] \quad [2.11]$$

where, h is depth of the specimen and G is the shear modulus.

The static bending test is an easy method of estimating the longitudinal modulus of elasticity experimentally. However, the stress in the cross section of the beam is not uniformly distributed. Therefore, the flaws in the material may not be highly stressed (40). Obtaining Young's modulus using the static bending test is also complex because the total flexural deformation comprises deformations caused by tension, compression, and shear (22).

Tension Young's modulus

The tensile test is a material property characterization test. Using the theory of deformable bodies, the longitudinal Young's modulus can be determined by:

$$E_1 = \frac{\sigma_1}{\varepsilon_1} \quad [2.12]$$

where, σ_1 is the longitudinal stress and ε_1 is the strain in the 1-direction. From Saint-Venant's theory, stress in the tensile specimen is uniformly distributed at a sufficient distance from the ends. This gives a better approximation of the material property, E_1 than a bending test. In timber engineering this method has not been used by many investigators because it is difficult to measure strain, expensive to use bonded strain gages, and difficult to minimize the grip effects.

2.6.2 Determination of the Shear Modulus, G

The shear modulus is another material property required in equation [2.6] to analyze glulam beams using the Mindlin-Reissner beam theory. However, shear modulus is difficult to measure in wood materials because of the problems associated with producing and measuring pure shear strain in a specimen. Wood has three principal shear moduli: G_{LR} , G_{LT} , and G_{RT} . These correspond to shearing strains in the three orthogonal planes: LR plane, LT plane, and RT plane. The shear

modulus of a beam depends on the grain orientation and ring angles. If a beam is flat sawn and stressed in bending, then shear modulus, G_{LR} , will be the governing elastic shear constant. Likewise, if the beam is quarter sawn and stressed in bending, then shear modulus, G_{LT} , will be the governing modulus.

However, glulam beams do not conform to orthotropic symmetry because the laminae are randomly selected from quarter sawn and flat sawn stock. Thus, as an approximation, the composite may be considered a transversely isotropic material (19,40,50,69), and an average shear modulus for a glulam cross-section can be computed from the average of G_{LR} and G_{LT} or by using an engineering torsion solution. In the following sections, a few methods of determining shear moduli will be briefly discussed. In this study, torsion tests were conducted on small glulam samples to compute an average shear modulus to be applied to southern pine glulam beams. The experimental procedure is presented in Chapter 3. But, details on torsion theories are discussed in the following section.

Flexure Method

The shear moduli, G_{12} and G_{13} , for glulam beams can be obtained by ASTM D 198 (3,6,17,67). In this method, simply supported beam samples of different length to depth ratios (l/d) are centrally loaded and the midspan deflections are measured. Then, the shear modulus is computed from Timoshenko beam theory (which includes shear deflection) by solving simultaneous equations for two l/d ratios (3,6,17,67). But, the shear modulus computed by the shear-deflection method is not exact because the simplifying assumption of the beam-bending theory that shear strain is constant across the section. Also, it is very sensitive to experimental errors.

Plate Tests

Many researchers developed methods to determine the shear moduli of wood by testing square flat plates of wood (9,10,30,66,72). The method was based on the theory of bending of thin plates developed by Nadai and Timoshenko (6,67,68). The planes of the faces and edges of the plate are cut parallel to the planes of symmetry in the wood. According to the theory, the deflection of the plate at a point (x,y) has the form (66):

$$\delta = \frac{6M_t}{h^3} S_{ii}xy + ax + by + c \quad (i = 4,5,6) \quad [2.13]$$

where a, b, and c are constants, h is the plate thickness, M_t is the twisting couple equal in magnitude to $P/2$, and S_{ii} is equal to $\frac{1}{G_{xy}}$. The constants are determined from the boundary conditions of the test arrangement. According to van Wyk and Gerischer (73), the problem with plate tests is that the stresses which occur in the specimen are not pure shear stresses. Also the sample preparation is difficult. Bodig and Goodman (9,29) conducted plate tests to determine the shear modulus of several commercially important hardwoods and softwoods in the United States. They estimated an average value of 134,100 psi for G_{LR} and 121,800 psi for G_{LT} for southern yellow pine. Ebrahimi and Sliker (20) state that it is difficult to determine the shear modulus using plate tests because of the large plate size required at specified grain orientations. The plates must be prepared so that the orthotropic and geometric axis coincide (9,20,29). Therefore, for glulam beam cross sections, this test is not appropriate since the growth rings are randomly oriented.

Tension and Compression Tests

It is also possible to use tension test specimens to determine the shear modulus (20). Tension tests were conducted on wood specimens in which the angle between the load axis and the fiber axis varied between 15 degrees and 75 degrees. Strain gages were used to measure strain. Then using engineering theory the shear modulus was calculated. However, the problem with this procedure is the difficulty in preparing the test specimens with the desired fiber and grain angles.

Radcliffe (56) described another method of determining the shear-modulus. He bonded electrical resistance strain gages to a wood compression specimen with the orthotropic axis offset by 45° from the geometric axis. However, this method is very sensitive to the specimen alignment with the loading head and the specimen manufacturing tolerance.

Torsion Test

The torsion test can be used to determine the shear modulus of isotropic materials, and had been applied to wood since it is relatively simple to conduct (66). Torsional stiffness is the resistance of a body to twisting about its longitudinal axis.

There are several torsion theories developed for circular and non-circular sections for isotropic materials. Coulomb (1784) was the first person to develop an analytical expression for torsion (18). Then in 1826, Navier published the first rigorous solution for torsion of an elastic circular shaft. He also derived expressions for rectangular sections assuming that torsional stresses are proportional to the distance from the axis of twist. However, his solution for rectangular sections overestimated the torsional stiffness of the bar. The torsion problem for homogeneous, elastic, isotropic non-circular cross sections was solved by Saint-Venant in a memoir to the French Academy in 1853 (16). His solution showed that when non-circular prismatic members are subjected to torsional moments, the cross sections warp and distort out of their plane (16,18). Lekhnitskii applied Saint-Venant's solution to anisotropic materials and obtained solutions for circular and rectangular orthotropic bars (47).

In a wooden bar subjected to torsional moment, two types of shearing strains are present (69). One strain is due to the sliding of the elements of one cross section over those of an adjoining section, and the other is due to the relative sliding of different longitudinal elements in the direction of the length of the member (69). The shearing strains in the plane of the cross section are expressed in terms of the angle through which the plane of the section has been rotated. This angle is assumed to be proportional to the distance from one end. The second type of strain produces

displacement of the fibers of a section in the direction of the length of the member. This strain causes the cross sections to deform out of their plane or warp (69,72).

Lekhnitskii (47) derived the solution for torsion of an orthotropic bar with a rectangular cross-section. The solution relates the applied torque to the dimensions of the cross-section, the two shear moduli, and the angle of twist. The following Hooke's law shear relations for orthotropic materials hold (47):

$$\gamma_{LR} = \frac{\tau_{LR}}{G_{LR}} \quad \gamma_{LT} = \frac{\tau_{LT}}{G_{LT}} \quad [2.14]$$

where,

γ_{LR}, γ_{LT} = shear strains in LR and LT planes

τ_{LR}, τ_{LT} = shear stresses in LR and LT planes

G_{LR}, G_{LT} = shear modulus in LR and LT planes

Consider a homogeneous rectilinear orthotropic bar of rectangular cross section with sides a , b and length l with the principal shear moduli G_{LR} and G_{LT} (Figure 2.7). One end of the bar is restrained from rotation and the other is subjected to a moment with no other forces applied externally. Warping deformations are not restrained in the bar. Let the T-axis be directed along the shorter side and the R-axis parallel to the longer side. The L axis is oriented in the longitudinal direction. According to the orthotropic theory developed by Lekhnitskii, the torsional stiffness in L-T and L-R planes can be expressed as:

$$K1 = ab^3 G_{LT} \frac{\beta_1}{L} \quad K2 = ab^3 G_{LR} \frac{\beta_2}{L} \quad [2.15]$$

where,

$K1$ = torsional stiffness in L-T plane

$K2$ = torsional stiffness in L-R plane

a = width of the bar, inches

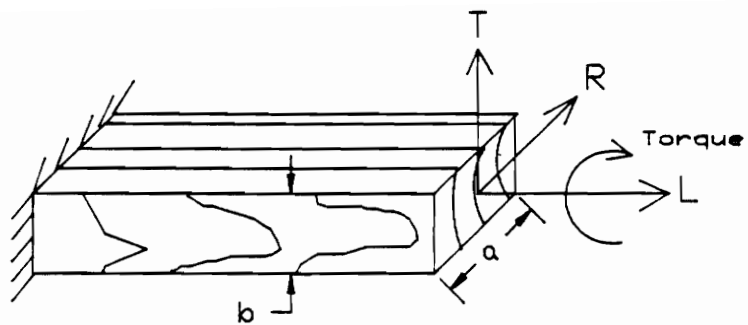


Figure 2.7 Orthotropic bar subjected to torsional moment

b = depth of the bar, inches

L = length of the bar, inches

$$\beta_1 = \frac{32}{\pi^4} \frac{a^2}{b^2} \frac{G_{LR}}{G_{LT}} \sum_{k=1,3,5,\dots}^n \frac{1}{k^4} \left[1 - \frac{2}{k} \pi \frac{a}{b} \sqrt{\frac{G_{LR}}{G_{LT}}} \tanh\left(k \frac{\pi}{2} \frac{b}{a} \sqrt{\frac{G_{LT}}{G_{LR}}}\right) \right] \quad [2.16]$$

$$\beta_2 = \frac{32}{\pi^4} \frac{a^2}{b^2} \frac{G_{LT}}{G_{LR}} \sum_{k=1,3,5,\dots}^n \frac{1}{k^4} \left[1 - \frac{2}{k} \pi \frac{a}{b} \sqrt{\frac{G_{LT}}{G_{LR}}} \tanh\left(k \frac{\pi}{2} \frac{b}{a} \sqrt{\frac{G_{LR}}{G_{LT}}}\right) \right] \quad [2.17]$$

Therefore, from torsion about the L axis, values of G_{LR} and G_{LT} can be obtained by solving two simultaneous equations. The torsional stiffness, K1 and K2, can be experimentally obtained by testing rectangular bars that are quarter sawn and flat sawn. K1 and K2 are the slopes of the linear portion of the Torque-rotation curve. For detailed explanations on torsion tests to determine the principal shear moduli for wood and wood base composite materials see references 50, 58, 59, 66, 69, and 72.

Lekhnitskii's orthotropic theory, however, applies only to orthotropic materials. In glulam beams, there is a random tangential and radial growth ring angle orientation of the laminae. A tensor transformation of the axes for each lamina is required to apply this theory. Consequently, it is not a practical approach. Hypothetically, the cross section can be considered as transversely isotropic and a single shear modulus could be measured to characterize the beams. Trayer and March (69) have done studies on the difference between the radial modulus of rigidity (shear modulus) and the tangential modulus of rigidity for Sitka spruce. They concluded that no great error occurs if the mean modulus as obtained through the test of a circular section used in calculating the modulus of rigidity of Sitka spruce for application to beams.

Bodig and Jayne (10) suggest a formula to calculate effective shear modulus by combining two shear moduli:

$$G = \frac{2G_{LR}G_{LT}}{G_{LR} + G_{LT}} \quad [2.18]$$

But, this requires that the orthotropic and geometric axes of the composite coincide. Therefore, it is not applicable to glulam beams. However, some of the torsion theories for isotropic materials could be applied to glulam beam to compute its shear modulus assuming that it is transversely isotropic. Navier's and Saint-Venant's torsion solutions are discussed briefly next.

Navier's solution for elastic circular sections

The deformation of the differential bar shown in Figure 2.8, when subjected to a constant torque, T , is described by two assumptions of compatibility:

1. The shape of the cross section remains unchanged after twisting, and
2. A plane section must remain plane after twisting (no warping).

θ is the angle of twist per unit length of the shaft and is represented as:

$$\theta = \frac{d\phi}{dz} \quad [2.19]$$

where, $\frac{d\phi}{dz}$ = the rate of twist. Then, the shear strain can be defined as:

$$\gamma = r\theta \quad [2.20]$$

where, γ is shear strain at an arbitrary radius, r ., and

$$\gamma_{\max} = R\theta \quad [2.21]$$

where, R is the radius of cross section of the circular bar. Therefore, the shear stress will be

$$\tau = rGj\theta \quad [2.22]$$

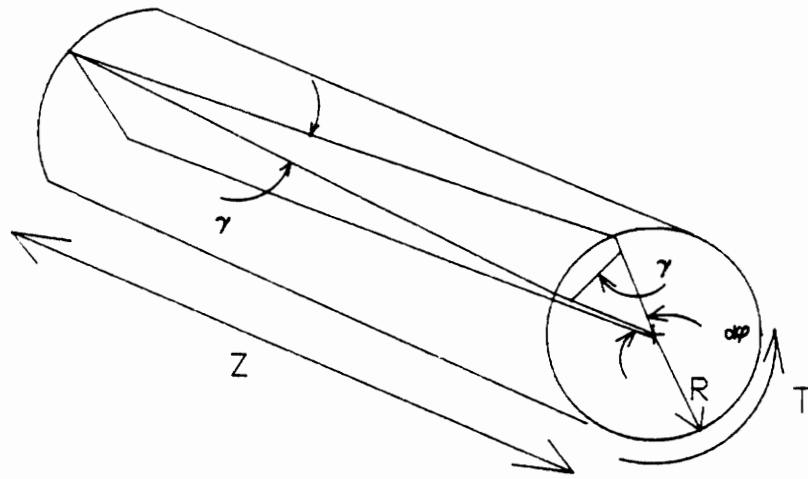


Figure 2.8 Deformation of a differential element under a constant torque, T

and,

$$\tau_{\max} = RG\theta \quad [2.23]$$

From conditions of equilibrium, it can be shown that:

$$T = \int_A (\tau dA)r \quad [2.24]$$

Where substituting equation [2.22] into equation [2.24] and rearranging terms:

$$T = G\theta \int_A r^2 dA \quad [2.25]$$

where the integral term is the polar moment of inertia of a circular section:

$$I_p = 2\pi \frac{r^4}{4} = \pi \frac{d^4}{32} \quad [2.26]$$

where d is the diameter of the cross section. Therefore, the shear stress can be rewritten as:

$$\tau = \frac{Tr}{I_p} \quad [2.27]$$

and,

$$\tau_{\max} = \frac{TR}{I_p} \quad [2.28]$$

Substituting equation [2.26] in [2.27] and rewriting equation [2.27] in terms of torsional moment (9,18,23):

$$T = \frac{\pi}{32} G \frac{d^4}{l} \theta \quad [2.29]$$

where,

T = torque, in-lbs

G = shear modulus, psi

d = diameter of the circular section, inches

l = length of the bar, inches

θ = angle of twist, radians

Equation [2.29] is the Navier's equation for torsion of a homogeneous, isotropic circular section.

Saint-Venant's solution for elastic, isotropic non-circular sections

Navier derived the expressions for rectangular sections assuming that torsional stresses are proportional to the distance from the axis of twist. The polar moment of inertia for a rectangular section is (10,12,67):

$$I_p = ab \frac{(a^2 + b^2)}{12} \quad [2.30]$$

However, extrapolation of Navier's solution for torsion of circular section to square sections was found to give values of shear modulus that were 20% less than that from circular sections. The following assumptions are made to describe the displacement components for non-circular sections:

1. The shape of the cross-section remains unchanged after twisting.
2. Warping of the cross-section is identical throughout the length of the non-circular member.

Let u and v be the displacements in the x and y axes in the plane of the generalized non-circular section (Figure 2.9). Let w be the deformation along the z -axis due to warping. Then, the three displacement functions can be defined as (47,68,69):

$$u = -\theta zy \quad v = +\theta zx \quad w = \theta \phi(x,y) \quad [2.31]$$

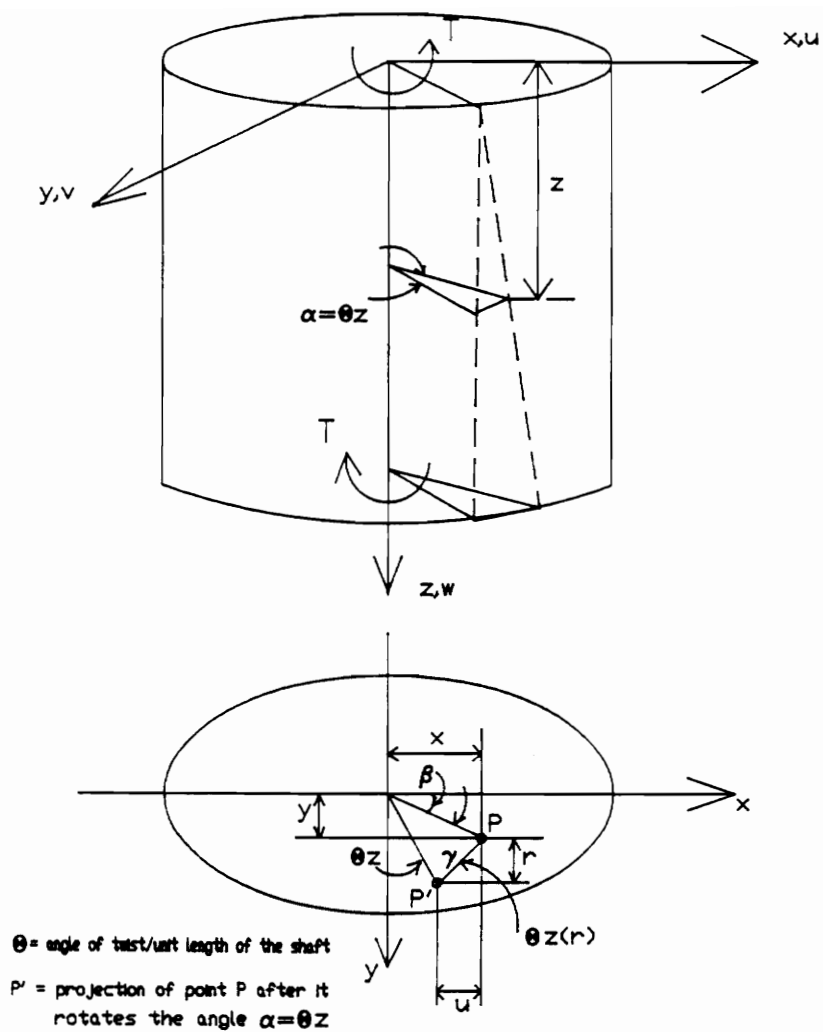


Figure 2.9 Torsional deformation in a bar with non-circular cross-section

where $\phi(x,y)$ is the warping function. Using u,v , and w , the strain-displacement relations, and the stress-strain relations, the equation for torsional moment is: written as:

$$T = GJ\theta \quad [2.32]$$

where,

$$J = \text{torsional constant} = \iint_R (x^2 + y^2 + x \frac{\partial \phi}{\partial y} - y \frac{\partial \phi}{\partial x}) dx dy \quad [2.33]$$

where,

R = the cross-sectional area of the bar

T = torque (in-lbs)

θ = angle of twist (radians)

T is proportional to the angle of twist per unit length.

The product of GJ provides a measure of the torsional stiffness of the bar. The torsional constant, J , incorporates the out-of-plane deformation (i.e. warping). For a rectangular cross section, the torsional moment can be expressed as (18,66,68):

$$T = \frac{ka^3bG\theta}{L} \quad [2.34]$$

where,

a = length of the shorter side, inches

b = length of the longer side, inches

k = constant depending on the ratio b/a of the cross-section dimensions

(given in tabulated form by Timoshenko) (67,68)

L = length of the bar

For a circular cross-section Saint-Venant's solution coincides with Navier's solution.

2.6.3 Young's Modulus Perpendicular to the Grain

Curved glued-laminated beams are used in frames, arches, and domes. For example, members of a glulam lattice dome are all slightly curved. In curved beams, radial stresses are induced due to the initial curvature introduced during beam manufacture. In a sharply curved beam, the flexural stresses induced by applied moments vary significantly from those in a straight beam. When a curved linearly elastic beam of rectangular section is subjected to bending moment, the strain and stress reach their maximum values at the extreme fiber closest to the center of the curvature (31,27). Therefore, the strain in the shortest fiber (one closest to the center of the curvature) will be the greatest. If a sharply curved beam is bent so that its radius of curvature increases, tensile stresses will be induced perpendicular to the grain (2,25,26). This is an important factor to consider when designing curved glulam beams because wood is weak in tension perpendicular to grain.

The American Institute of Timber Construction (2) specifies that, for curved beams, the design value in bending should be modified by multiplying it by the curvature factor.

$$C_c = 1 - 2000\left(\frac{t}{R}\right)^2 \quad [2.35]$$

where,

C_c = curvature factor

t = thickness of lamina (inches)

R = radius of curvature of beam (inches)

This curvature factor is applied only to the curved portion of the beam. The AITC also specifies that t/R ratio should not exceed 1/100 for southern pine.

If an applied bending moment in a curved beam causes tensile stresses in the perpendicular to grain direction, the design stress is limited to 1/3 the allowable stress in horizontal shear for southern pine (2,3). The Young's modulus perpendicular to the grain is needed to compute the radial stresses

in curved beams. Young's modulus perpendicular to the grain is found from the measured strain in samples loaded in compression or tension perpendicular to the grain and the corresponding calculated stress (9,26). However, the effect of radial stresses in not so sharply curved glulam beams has been found to be negligible (17,23). By definition (2), a sharply curved beam has a radius of curvature of 9ft 4 inches. In this study, the radius of curvature of all curved beams was 50 ft. Therefore, the radial stresses were considered to insignificant.

2.7 Stress Analysis in Glulam Beams

In this study, beams were subjected to bending and combined bending and axial loads. The response of a glulam beam under these loads is briefly discussed in the following sections.

2.7.1 Axial Load

In theory, concentric axial load produces a uniform stress (13,23):

$$f_c = \frac{P}{A} \quad [2.36]$$

where f_c is axial stress, P is axial load, and A is cross-sectional area. This is valid for solid wood columns that are classified as short columns. Short, rectangular columns are those whose length is less than 11 times the least cross-sectional dimension of the column (53). Compression perpendicular is the assumed common failure mode in short columns. Intermediate columns are columns with l_e/d ratio between 11 and K, where (53):

$$K = 0.671 \sqrt{\frac{E}{F_c}} \quad [2.37]$$

where,

E = modulus of elasticity, psi

F_c = design value in compression parallel to grain, psi

The failure mode for intermediate columns is generally a combination of compression perpendicular and buckling. When l_e/d ratio is K or greater, the column is classified as a long column or Euler column. Buckling is the assumed failure mode in long columns. The National Design Specification (53) states that the slenderness ratio shall not exceed 50. The allowable compression stress for long columns is computed from the following equation.

$$F'_c = \frac{0.30E}{(l_e/d)^2} \quad [2.38]$$

For intermediate columns, the allowable compression stress is:

$$F'_c = F_c \left[1 - \frac{1}{3} \left(\frac{l_e/d}{K} \right)^4 \right] \quad [2.39]$$

Figure 2.10 shows compression stresses in the cross-section of a beam in compression.

2.7.2 Bending Load

For straight and curved beams with large radius of curvature, bending moments produce maximum normal stresses at the extreme fibers of the beam. In a straight beam, the concave edge of the beam is in compression and the convex edge is in tension (Figure 2.11). In a curved beam, the concave edge is in tension and the convex edge is in compression. Bending stress at an arbitrary point is given by:

$$f_b = \frac{My}{I} \quad [2.40]$$

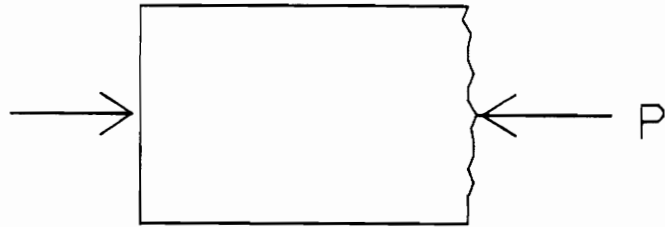
where

f_b = bending stress (psi)

M = bending moment (in-lbs)

y = distance from the neutral axis (inches)

I = moment of inertia (*inches*⁴)



Stress Distribution



$$f_c = P/A$$

Figure 2.10 Distribution of stresses in a cross-section of a beam subjected to compression loads

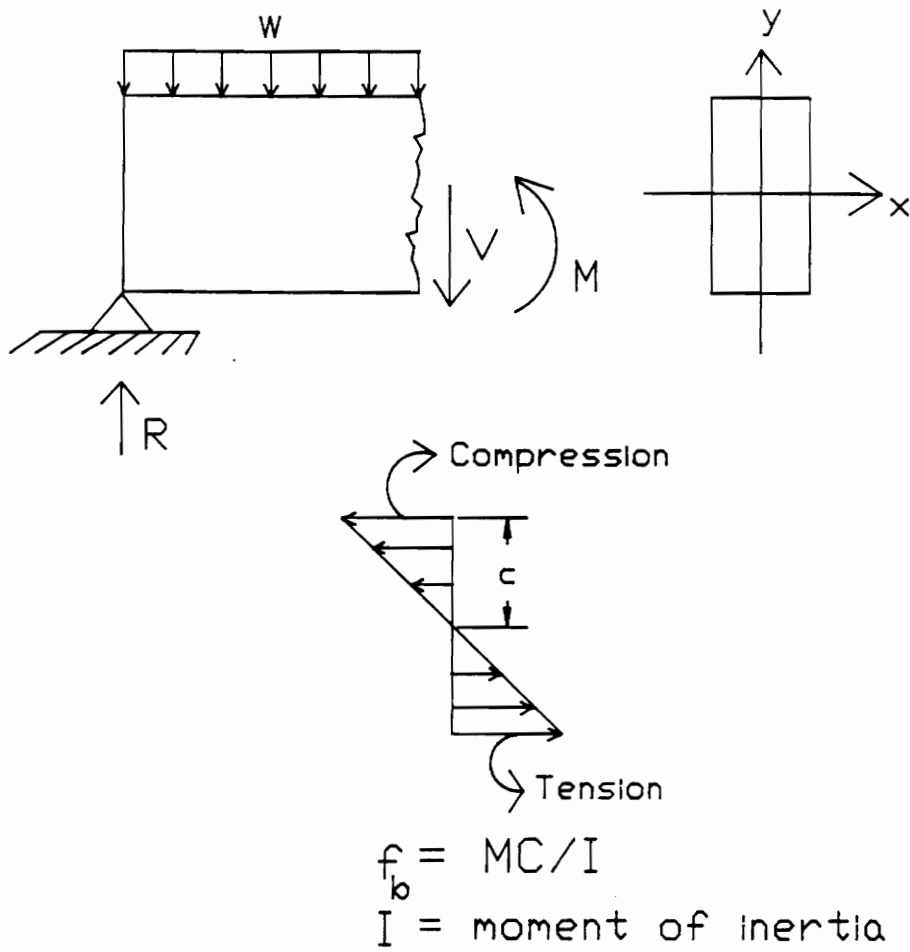


Figure 2.11 Bending stresses in a beam cross-section

Since wood is weak in shear parallel to grain, it is important to evaluate the shearing stresses. Shear is of special concern in beams with small length to depth ratios (10). Relatively short, deep beams are subject to shear failures. The shear stress at any point in the cross section of a beam can be computed by the formula

$$f_v = \frac{VQ}{Ib} \quad [2.41]$$

where,

f_v = horizontal shear stress (psi)

V = vertical shear force on cross section (lbs)

Q = the first area moment (*inches*³)

I = moment of inertia (*inches*⁴)

b = width of the beam (inches)

Figure 2.12 shows typical shear distributions in beams with rectangular cross-sections. Derivations of the beam bending formulas can be found in any strength of materials book.

2.7.3 Biaxial Bending

Bending can occur about either of the principal axes of a glulam beam. Figure 2.13 shows the notation used to refer to bending about the two principal axes of a glulam beam in this study. The distribution of bending stresses under biaxial bending loads is shown in Figure 2.14. Superposition of the bending stresses about both the axes is used to determine the total stress. This is possible only if the strains induced are within the linear range. In Figure 2.14, the two compression bending stresses at point A and the two tensile stresses at point C are additive. The stresses at points B and D are combined algebraically (13).

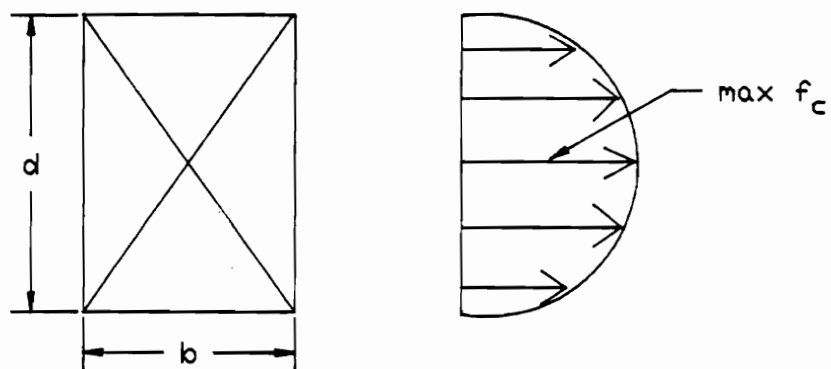


Figure 2.12 Shear stress distribution in a beam cross-section

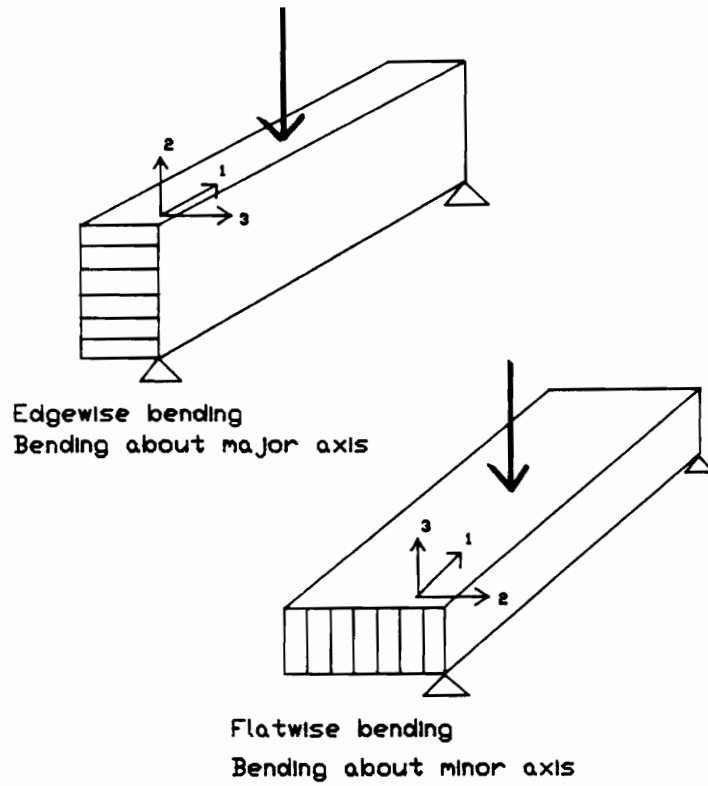


Figure 2.13 Notation for bending about the two principal axes of a glulam beam cross-section

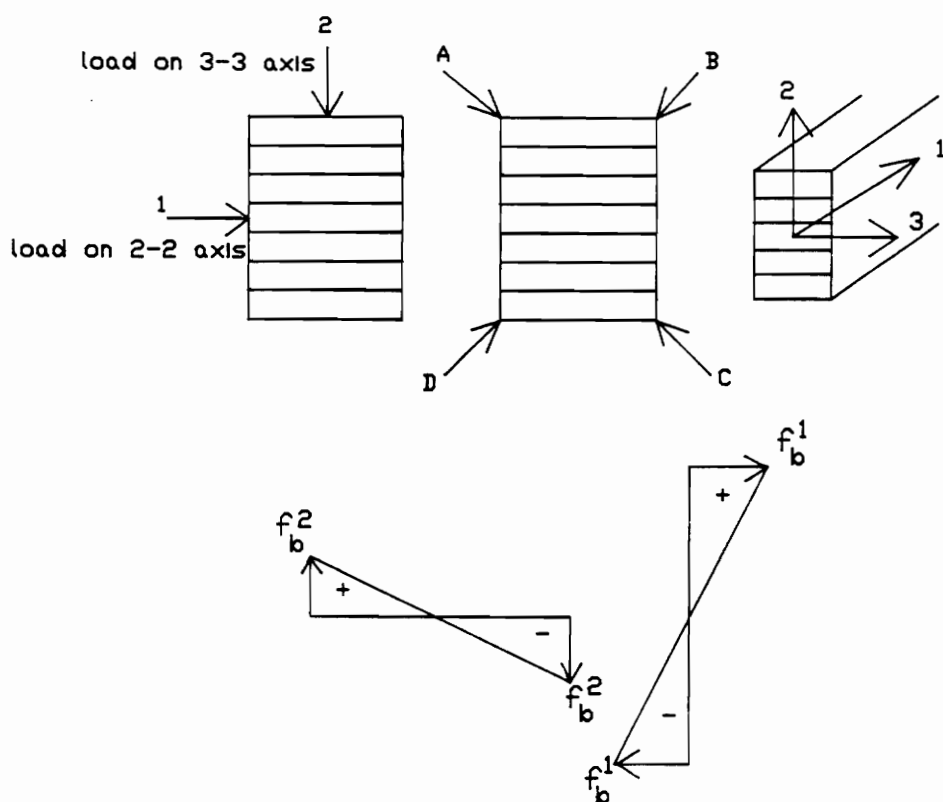


Figure 2.14 Distribution of bending stresses under biaxial bending loads (bending about 2- and 3- axes)

2.7.4 Combined Bending and Compression Load

The glulam members in a lattice dome are subjected simultaneously to axial and bending loads (17,19,36). The interaction formula to handle the combination of these stresses is an expansion of the basic straight-line interaction formula (13). Under combined bending and compression loading a stress, called the P-Δ effect (13,2), is produced from the additional bending moment when axial loads are applied to curved columns or eccentrically loaded beams. The axial force, P, causes an additional bending moment of $P \times \Delta$ (16,23).

The Wood Handbook (23) gives a formula to calculate the bending stresses under combined bending and compression loads:

$$f_b = \frac{f_{bo}}{1 \pm \frac{P}{P_{cr}}} \quad [2.42]$$

where,

f_b = net bending stress from combined bending and axial load (psi)

f_{bo} = bending stress without axial load (psi)

P = axial load (lbs)

P_{cr} = buckling load of the beam under axial compressive load only

The total stress under combined bending and compression is calculated by superposition of the stresses given by equations [2.41] and [2.42] (13). It should be noted, however, that superposition of the stresses does not work when the initial bending deflection (Δ) is large. Figure 2.15 shows the possible stress distributions in a beam under combined loading.

2.8 Finite Element Analysis

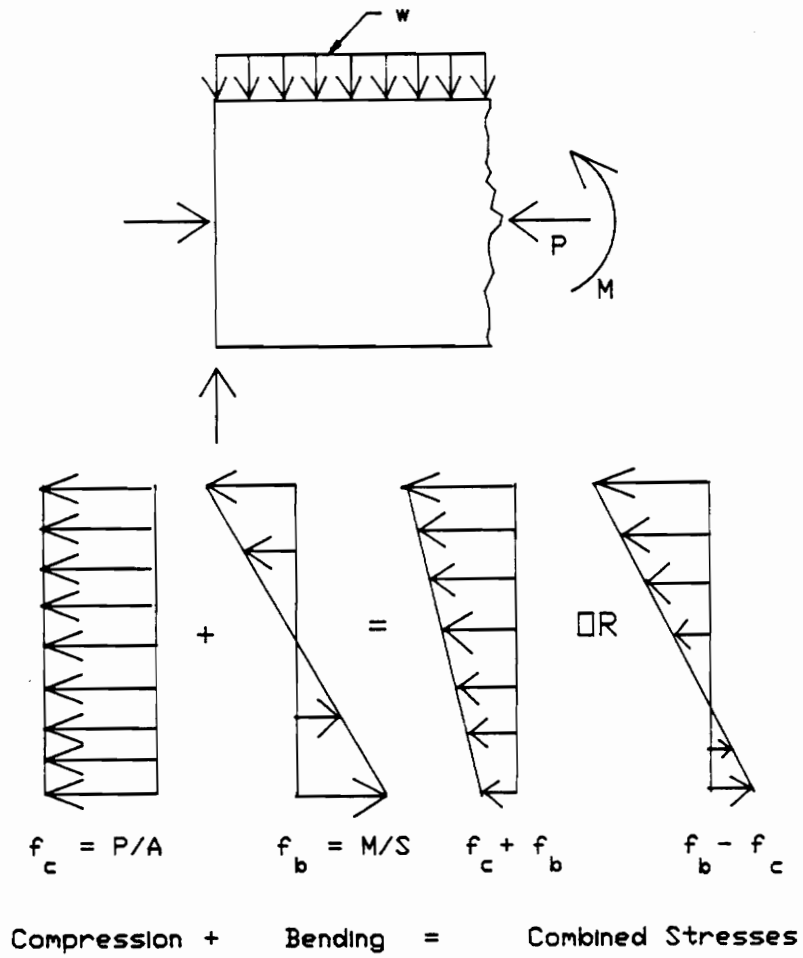


Figure 2.15 Possible stress distribution under compression and bending loads

The finite element method (FEM) is a general technique for approximating the behavior of a physical continuous medium by an assemblage of discrete elements and localized interpolation functions (4,35,57). Finite element methods have been widely applied to solve structural problems. The finite element approach analyzes a structure in two parts: first, it looks at the behavior of each individual member of the structure; and second it models the behavior of the complete structure using the external relationships of individual elements of the structure (4,35,57). The material properties and geometry of the elements and structure are input parameters to the FEM.

The finite elements are joined at the nodes to form a structure. At these nodes the conditions of displacement, compatibility, and equilibrium are imposed. The properties of the individual elements are characterized by relations between nodal loads and nodal displacements. External loads are replaced by statically equivalent concentrated loads at the nodes (4,35,57). Finally, all the element force-displacement equations are assembled, corresponding to the manner in which they are interconnected, to form the stiffness equations for the entire assemblage of elements. These equations are called the structural stiffness equations (4).

The stresses in glulam beams have been analyzed using the finite element technique (17,18,24,32). Finite element analysis is especially useful when modelling a composite beam, such as a glulam beam, or a space frame, such as a glulam lattice dome, that consists of hundreds of members subjected to various kinds of loads. The finite element model verified in this study models the 3-D response characteristics of a space structure. It is based on engineering theory, rather than on continuum theory (19).

Foschi and Barrett (24) have developed a finite element simulation model that allows one to evaluate several different lamina configurations of beams and to estimate the population statistics for similar beams. They used a five-node finite element. Their model uses the data of the laminae properties for computer simulations to estimate variability in beam strength and stiffness and the corresponding statistics for design. The model was developed using data on Douglas-fir beams. They hypothesized that the bending strength of glulam beams depends on the pattern in which the

laminae are glued, the strength-reducing characteristics, the strength and location of end-joints, the thickness of the laminae, and the size of the beam. Their simulated strength results compare well with their experimental results. The coefficients of variation of the experimental bending test results ranged from 14 to 25%. The coefficients of variation of the simulated results ranged from 18 to 26% (24).

Gutkowski, Dewey, and Goodman (32) did experimental tests on Douglas-fir and southern pine glulam beams to evaluate stresses under bending and perpendicular-to-grain tensile loads. They (32) evaluated the applicability of the finite element method for theoretical analysis. Analytical and experimental studies were performed on double-tapered glulam beams. The authors conclude that the FEM predictions reasonably confirm the measured response quantities. The FEM model they have used incorporated an isoparametric, plane stress, quadrilateral element with orthotropic material properties (24,32).

However, using continuum elements to analyze glulam systems is uneconomical and impractical in terms of computer memory (19). Continuum elements require a fine mesh. The finite element mesh used by Gutkowski, Dewey, and Goodman had 360 elements, which was found to be necessary to produce sufficiently accurate results (32). Alternatively, in the following study, one dimensional structural isoparametric beam elements based on engineering theory was used to characterize the response of 3-D beams (19). The finite element was formulated with the following characteristics (19):

1. Timoshenko beam theory incorporating shear deformations
2. Cross sections do not deform in their planes, but out of plane deformations due to torsional warping is allowed.
3. Coordinate interpolations permit the representation of straight and curved elements by the same formulation.
4. Accurate modeling of large displacements, large rotations, but small strains.
5. Complete generality in material properties at an integration point.

2.9 Summary of Literature

In this chapter, some general characteristics of glulam beams were presented. The reduced constitutive matrix for glulam beams used in this study was derived. Different methods of obtaining the two essential material properties, modulus of elasticity and shear modulus, were discussed with their corresponding advantages and disadvantages. Following that, a brief description on stress analysis in glulam beams was presented with discussions on in-plane bending, biaxial bending, and combined bending and compression. Finally, a brief background on FEM was presented along with the characteristics of the finite element that was used for this study.

For this study, modulus of elasticity was determined using a nondestructive tension test of laminae. The two principal shear moduli were replaced by a single shear modulus obtained by conducting torsion tests on glulam specimens and applying Saint-Venant's torsion solution for homogeneous, isotropic material. And biaxial bending of glulam beams was checked by comparing the experimental and the analytical results from bending about the principal axes of the cross-section.

CHAPTER 3

3. EXPERIMENTAL STRAIN MEASUREMENT IN SOUTHERN PINE

3.1 Introduction

Investigation of the stress distribution in beams requires accurate strain measurements. Electrical strain gages are widely used for strain measurements. However, testing of many specimens requires taking multiple strain measurements and using many bonded strain gages. This is not an economical and efficient method for timber engineering applications. It is possible to use displacement measuring transducers, such as LVDT, to measure the displacements and convert them to strains. But, these devices are large, heavy, and difficult to attach to the specimen. In addition, their sensitivity may not be adequate to measure very small strains. Therefore, a reusable Clip-on Electrical Transducer (CET) was developed to measure strain for this study.

3.2 Objectives

The primary objective of this study was to develop a Clip-on Electrical Transducer (CET) to measure strain in southern pine. To gain a better understanding of the performance and use characteristics of clip-on electrical transducers, the following sub-objectives were necessary:

1. To determine a suitable gage length for strain measurements in southern pine.
2. To compare the performance of the CET against the bonded strain gages on wood specimens and verify the performance of the CET.

3.3 Background

Today there is a variety of electronic strain measuring devices. Electronic measuring systems range from small to very large sizes, and their operation can be simple to very complex (1,54). A single, small package can contain the sensing device as well as the display device. On the other hand, a system might have a number of subsystems, including data storage, and display equipment (1,54). An example of a measuring system would be an electrical resistance strain gage connected to a strain gage indicator.

A device that converts energy from one form to another is known as a transducer. For example, a transducer might convert a physical quantity, property, or condition into an electrical signal that is proportional to the physical condition of a specimen. The choice of the transducer for a particular application depends on the following considerations (1,54,55):

- The type quantity, property, or condition being measured or evaluated.
- The nature of the transducers operation
- Special features of the transducer that might be required
- The magnitude of the measurand quantity (reading high strains vs low strains)

- The required accuracy
- The limitations of the transducer
- Amount of money available

An ideal strain gage has the following characteristics (17,55):

- Small size and insignificant mass
- Easy to install onto the member
- Characterized by an infinitesimal gage length
- High sensitivity to minute displacements
- Unaffected by temperature, vibration, humidity, etc.
- Capable of sensing both static and dynamic strains
- Inexpensive

Measuring strain in wood is not an easy task because wood is an inhomogeneous, hygroscopic, anisotropic material. It is important to consider the variability in wood so that the strain measurement reflects the actual deformation of a structural member, and not just a localized strain at a particular point. Variations in specific gravity at small intervals through the length of a clear specimen are significant (65); since specific gravity is correlated to the strength and stiffness of the material, an improper consideration of this variability causes misleading strain measurements. Thus, when measuring strain in wood, careful attention must be given to gage placement so that the distribution of springwood and summerwood, as well as the characteristics of defects, such as cross-grain, pitch pockets, knots, and other growth characteristics are properly represented.

In addition to gage placement, it is also important to use the appropriate gage length to measure strain in wood. In this study, to investigate the effect of the gage length on strain readings in southern pine, the following experiment was conducted.

3.4 Effect of Gage Length on Strain Readings

Bonded, electrical resistance strain gages are widely used to measure strain in isotropic, homogeneous materials (17,21,22,24,25,26,56,64). They have been also used on wood, but the anisotropic nature of wood can cause localized strain in the specimen that is not representative of the strain under the gage, particularly in coarse-grained species, such as southern pine, which has large earlywood-latewood anatomical differences. For example, under uniform stress a strain gage bonded to an earlywood zone may detect a different magnitude of strain than a gage bonded to an adjacent latewood zone. To minimize the error due to material property variation and to measure strain that is representative of the strain in the specimen, long gage lengths may be used. But, long, bonded gages are expensive and are difficult to align with the specimen axes. Therefore an experiment was conducted to determine a suitable gage length for measuring the average strain over a region of the specimen. The objectives of this study were to:

1. Determine a suitable gage length for strain measurements in southern pine.
2. Compare the performance of the CET and the bonded strain gages on wood specimens.

3.4.1 Procedure

The following tests were conducted on a 2" by 6" by 14ft (nominal) southern pine specimen. The sample's moisture content was 7.7% and its specific gravity was 0.60. Strain was measured at four locations on the specimen. The locations were selected so that the strain gage was applied to (a) a latewood zone, (b) an earlywood zone, and (c) and (d) combinations of latewood and earlywood zones. Figure 3.1 gives a graphic description of each location.

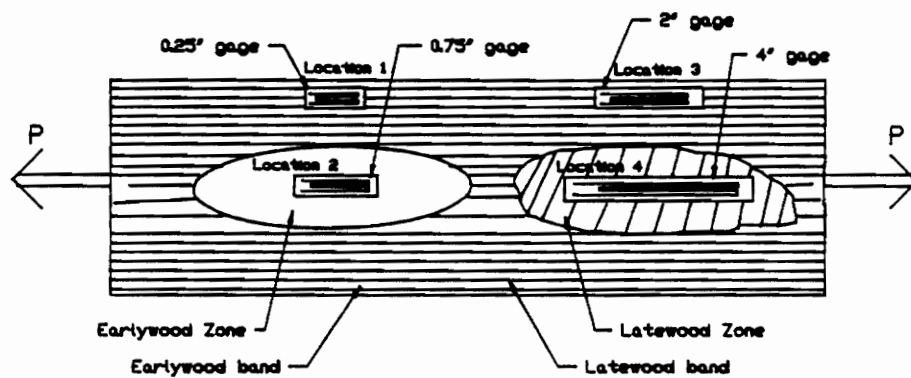


Figure 3.1 Graphic description of locations on southern pine tension specimen where bonded strain gages were placed

Bonded foil gages (120 Ohms) were used to measure strain at the chosen locations on the specimen. Gage lengths of the foil gages were carefully chosen to cover a wide range. Four different gage lengths were tested in each location: 0.25 inch, 0.75 inch, 2.00 inches, and 4.00 inches. A randomized block design was used to randomize the order in which the gages were placed at each location. This was necessary to determine the influence of the gage application sequence at each location since a finely tuned cabinet scraper was used to remove the gage, the adhesive, and a thin layer of wood after each test. Care was taken to remove minimum amount of wood and to produce a clean, fresh surface for bonding the next gage.

The test specimen was subjected to tension parallel to the grain and strain was read from the gages using the HP-data acquisition system. The maximum applied load was 3000 lbs (48% of the design load obtained from NDS, 1986). After each test, the strain gage and adhesive at each location was removed with the scraper. Then, the next randomly selected gage from each group was bonded to each location and the specimen was retested. Thus, each gage length was tested in each location resulting in four independent strain readings for each location. To minimize test-to-test variations, care was taken to bond the gages at the same location everytime. Thus, the effect of gage length was observed with minimal effect of property variation in the test specimen. After all the bonded strain gages were tested, the CET was placed at each location on the test specimen to measure strain. Strain readings were recorded at the same load levels as those used for the bonded strain gages.

3.4.2 Results

The strain readings from all gages are plotted against the gage lengths in Figures 3.2, 3.3, 3.4, and 3.5 for locations 1, 2, 3, and 4 respectively. Each point on the plot represents the average of six replications for each gage.

At locations 1, 2, and 3, there was an upward trend in strain as the gage length was increased from 0.25 to 2.18 inches (CET gage length). However, strain measured by the 4 inch gage was ei-

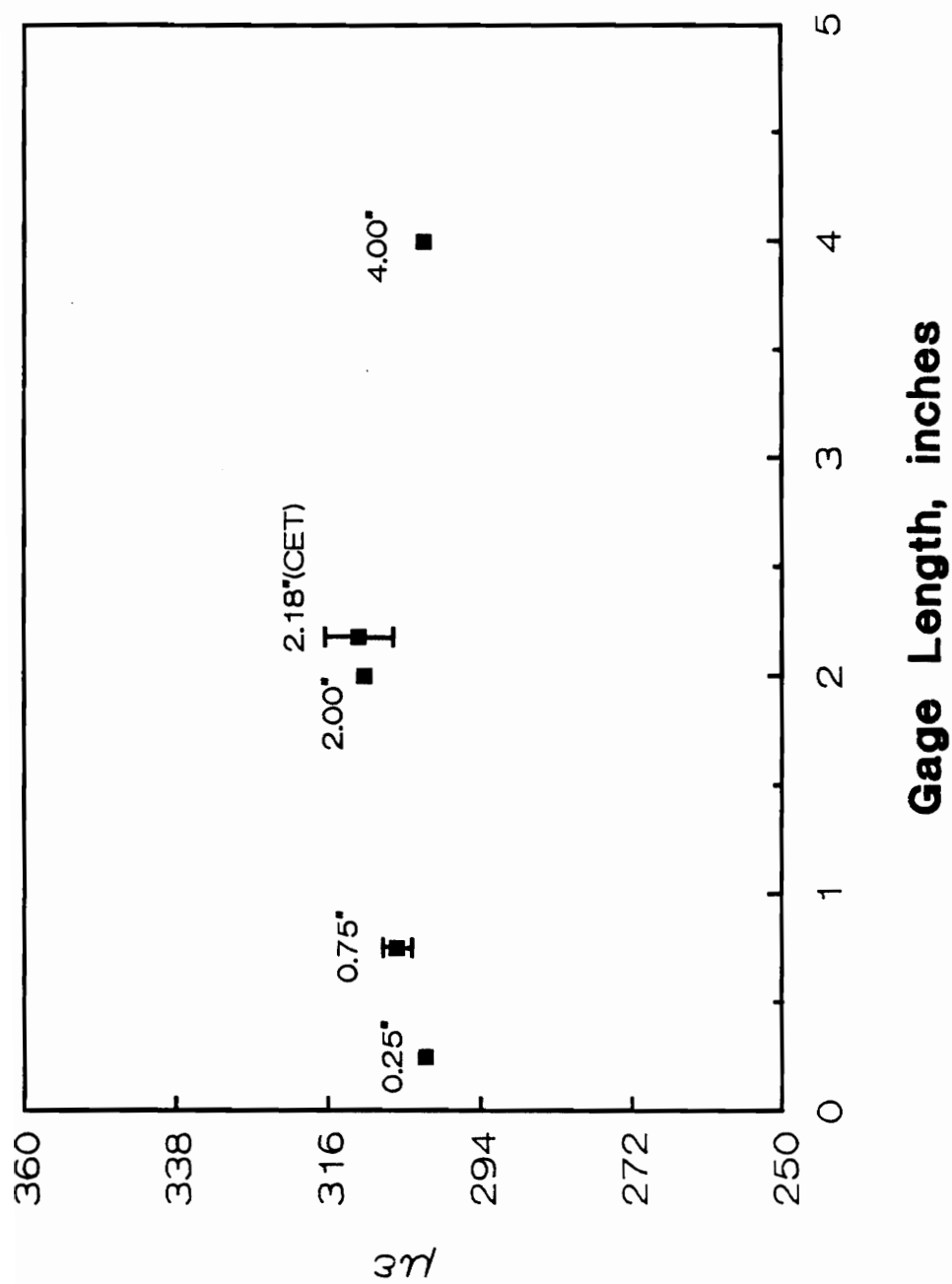


Figure 3.2 Influence of gage length on strain readings at location A

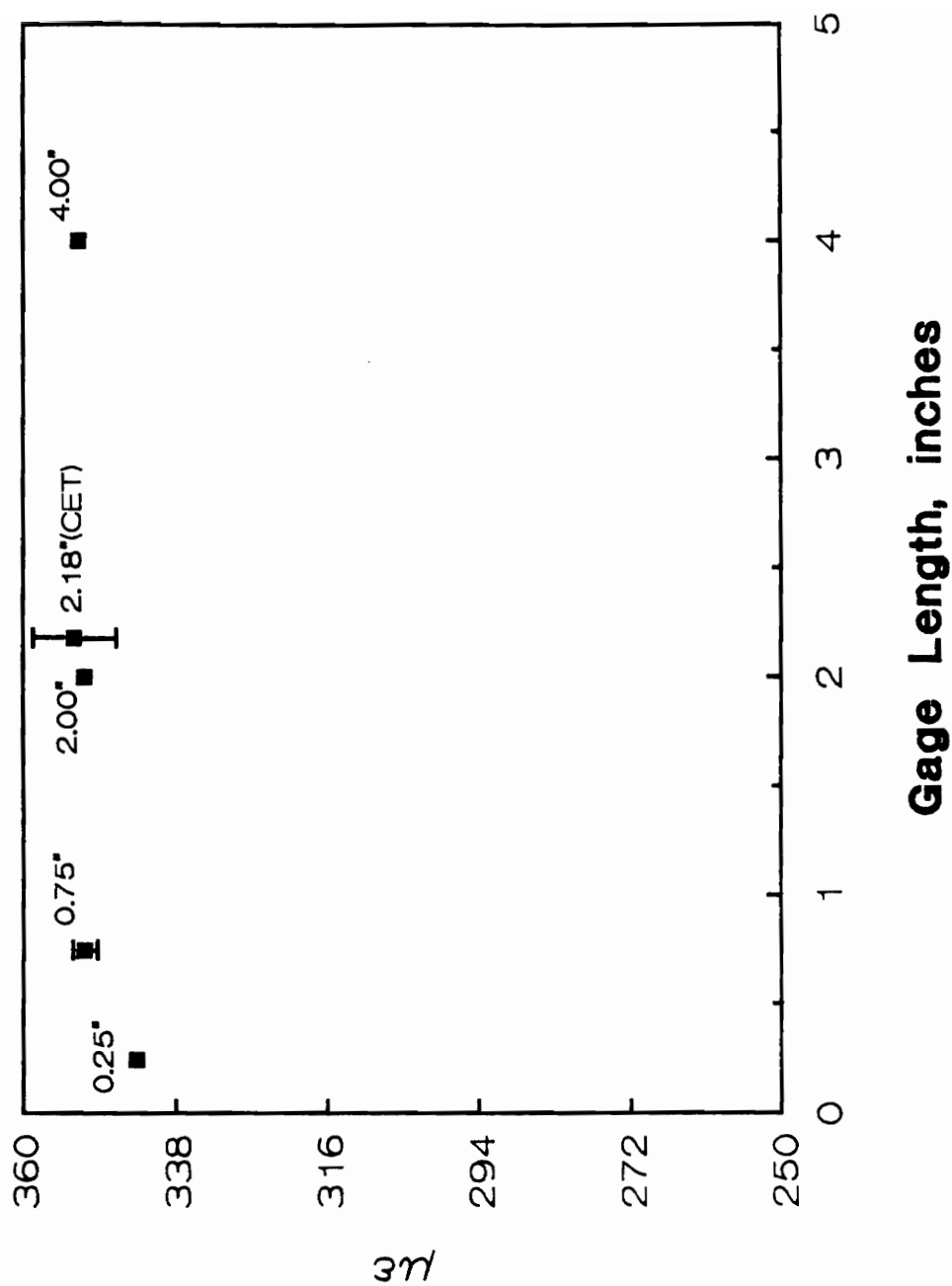


Figure 3.3 Influence of gage length on strain readings at location B

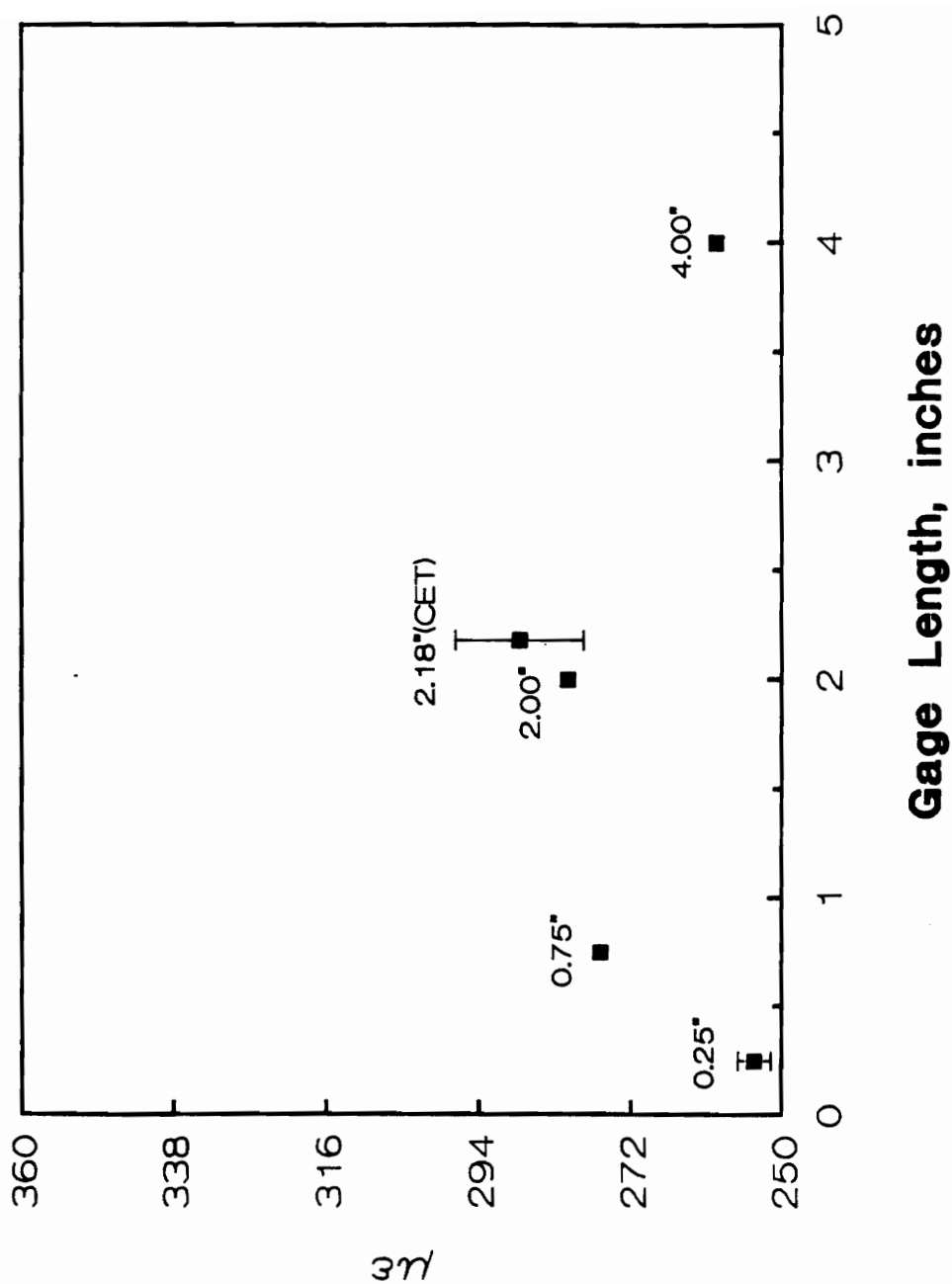


Figure 3.4 Influence of gage length on strain readings at location C

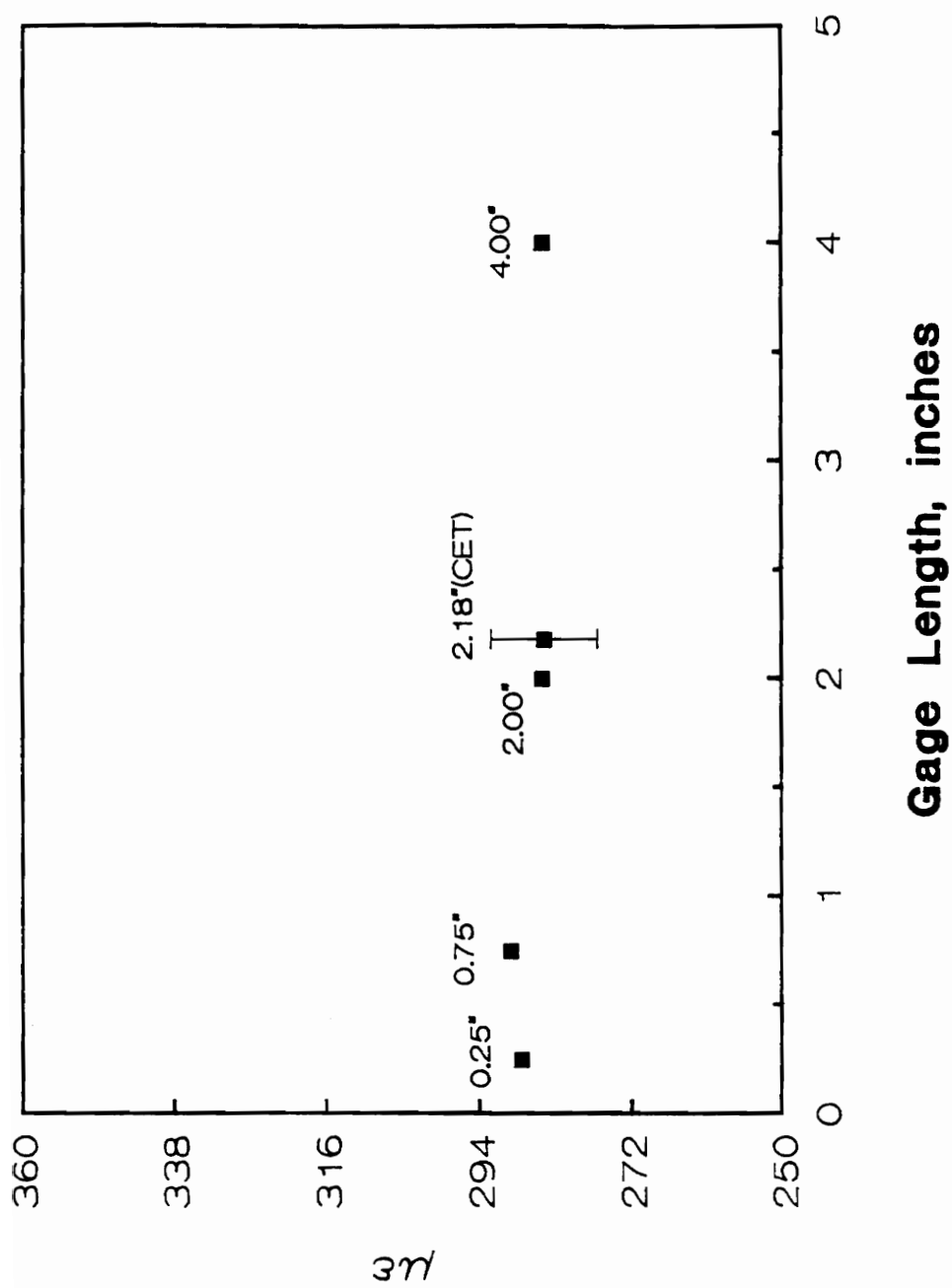


Figure 3.5 Influence of gage length on strain readings at location D

ther very close to or less than the 2 inch gage readings. The Least Significant Difference (LSD) test at an α -level of 0.05 was performed to compare the means at each location. At location 1, strain recorded by the 2 inch gage and the CET were not significantly different. There was a significant difference between the 2 inch gages and of other gages. At location 2, the average strain read by the 0.75 inch, 2 inch, and 4 inch gages, and the CET were not significantly different. Strain recorded by the 0.25 inch gage was significantly different from other means. At location 3, two inch and 0.75 inch gages recorded strains that were not significantly different. However, strain recorded by the CET was significantly different from others. But, the CET reading was closer to the reading recorded by 2 inch gage. Gages with 4 inch and 0.25 inch lengths read strains that were not statistically different.

At all four locations the CET (2.18 inches) measured the largest strain followed by the 2 inch strain gage. At three locations, 0.25 inch gage recorded the lowest strain. This was expected since shorter gage lengths cover smaller areas, and thus fewer defects. At location 4, the average strain recorded by all gage lengths were not statistically different. As shown in Figure 3.1, location 4 was completely in a latewood zone. At this location, there was a slight decrease in strain readings as the gage length increased. In the latewood zone, longer gage lengths cover more latewood area and record lower strain.

3.4.3 Summary and Conclusions

From this study, it seems that 2 inch gage lengths are suitable for strain measurements in southern pine. There was good agreement between the strain readings recorded by the 2 inch gage and the CET. It is also preferable not to have too long a gage length because it would be harder to mount the CET on the specimen and to align it with the axes of the specimen. A full field strain measuring method, such as digital correlation or holography, would eliminate the gage length problem. However, such a method was not available for this study.

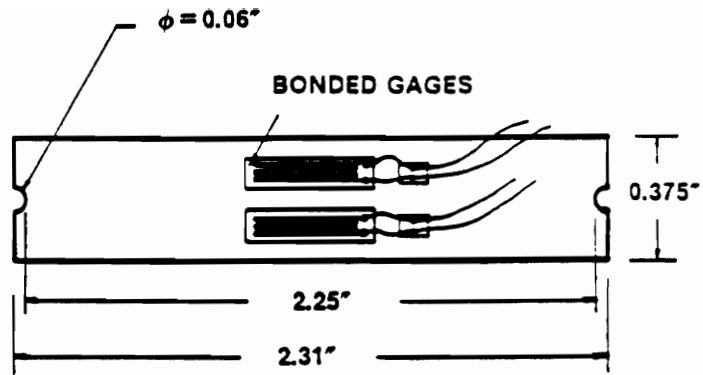
3.5 Clip-on Displacement Transducers

Laboratory-built clip-on electrical transducers are an attractive alternative for strain measurements in wood. They can be manufactured to satisfy the requirements of an experiment because they can be built to measure either large or small strains. They are reusable, light weight, and inexpensive and can be used to measure strain in wet or dry specimens (17).

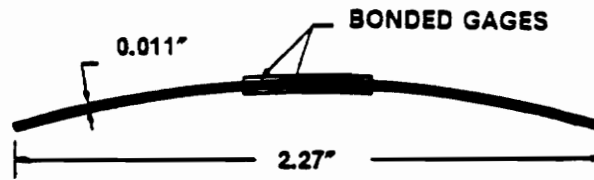
Many researchers have used variations of clip-on displacement transducers (9,17,29). A Delta-Element Strain Transducer (46) and a portal-frame clip gage are a few examples of clip-on transducers that have been used successfully in the past. However, the design and operation of these transducers is complicated. The clip-on transducer used in this study is accurate and relatively simple to build, calibrate, install, and use.

3.5.1 *Fabrication, Operation, and Calibration*

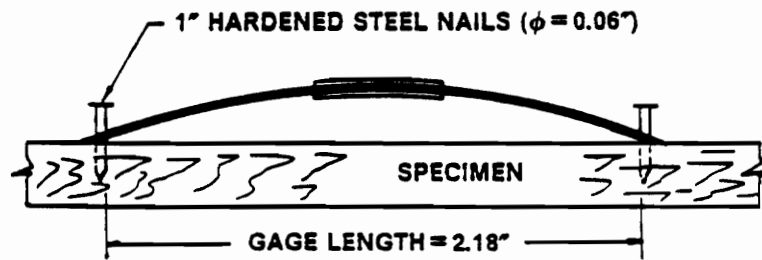
The clip-on electrical transducer (CET) was constructed using a thin, flexible, hardened spring-steel obtained from a clock mainspring. The advantage of using spring-steel is that it is flexible and resilient. It is capable of deforming and returning to its initial shape. The cross-section of the transducer used in this study was 0.375 by 0.011 inches. The construction details, including the dimensions and lengths, are shown in Figure 3.6 (17). For calibration and installation purposes, the CET was built with two semicircular notches at the ends. The CET was clipped between two nails located at a desired gage length, which is same as calibration gage length. When mounted on the specimen, the CET was prestressed with a slight amount of additional curvature. This enables the gage to elongate and contract, thus measuring both tensile and compressive strains. The pre-stressing allows the gage to measure strain reversals when testing samples under combined or cyclic loads (17).



(a) PLAN (WHEN FLAT)



ORIGINAL SHAPE



ON TEST-SPECIMEN

(b) ELEVATION

Figure 3.6 Construction details of CET

Four quarter inch resistance strain gages were bonded to the spring-steel as shown in Figure 3.6. The gages were wired in a full Wheatstone bridge circuit to a strain gage card in a 9000 series HP-data acquisition system. Shielded, braided lead wires were used to reduce the influence of electrical noise. The bridge measured the change in voltage due to the change in electrical resistance of the bonded gages. The differential voltage was then converted into strain induced in the CET using the following equation:

$$\varepsilon_{cg} = \frac{-V_r}{GF} \quad [3.1]$$

where,

ε_{cg} = Strain recorded by the CET

V_r = Differential voltage ratio

GF = Gage factor

The gage factor is the strain sensitivity of a strain gage. It is the ratio of the relative change of resistance, $\frac{\Delta R}{R}$, to the relative change in length, $\frac{\Delta L}{L}$, of the grid wires on the foil gages. The gage factor is provided by the manufacturer of the bonded foil gages.

3.5.2 Calibration

The clip-on transducer was calibrated using an INSTRON micrometer with a one inch range and an accuracy of ± 0.00002 inch. The CET was calibrated at gage length of 2.180 inches. A known displacement of the CET ends was induced, and the corresponding differential-voltage was read using the data acquisition system. The CET was calibrated in both tension and compression (± 0.003 inch). This range was chosen to cover the expected strain in the gage length in the glulam beam specimens. Then, a calibration equation was fit to the displacement versus differential-voltage relationship. Figure 3.7 shows a typical calibration curve for a CET. From the calibration curve the differential-voltage is correlated to displacement in the specimen through the regression

equation. The following relationship was used to calculate the relative displacement between the two end points of the CET:

$$\Delta_e = \epsilon_{cg} \frac{\Delta_{cc}}{\epsilon_{cc}} \quad [3.2]$$

where,

Δ_e = Relative displacement between the CET end points

Δ_{cc} = Displacement from calibration curve

ϵ_{cc} = Strain corresponding to Δ_{cc} ϵ_{cg} = Strain recorded by the clip gage

Then the strain in the specimen can be calculated using:

$$\epsilon_s = \frac{\Delta_e}{\text{Gage Length}} \quad [3.3]$$

Each CET had its own calibration curve. Therefore, for each CET, a calibration constant was determined from its calibration curve at a Δ_{cc} of 0.001 inch. To evaluate the strain in the test specimen, the output voltage was multiplied by its calibration constant.

3.5.3 Installation

The transducer must be firmly attached to the specimen. The CET in this study was clipped onto specially built aluminum base plates or shoes. These shoes are attached to the specimen with screws as shown in Figures 3.8 and 3.9. A metal template with predrilled holes at a specified gage length was used to position the base plate screw holes to achieve the target gage length of 2.180 inches. The advantage of using base plates was two-fold: it allowed alignment of the gage with the direction in which strain was being measured, and it allowed for adjusting the gage length to a desired value by rotating and sliding the slotted upper plate (Figure 3.8). Moreover, the shoes help

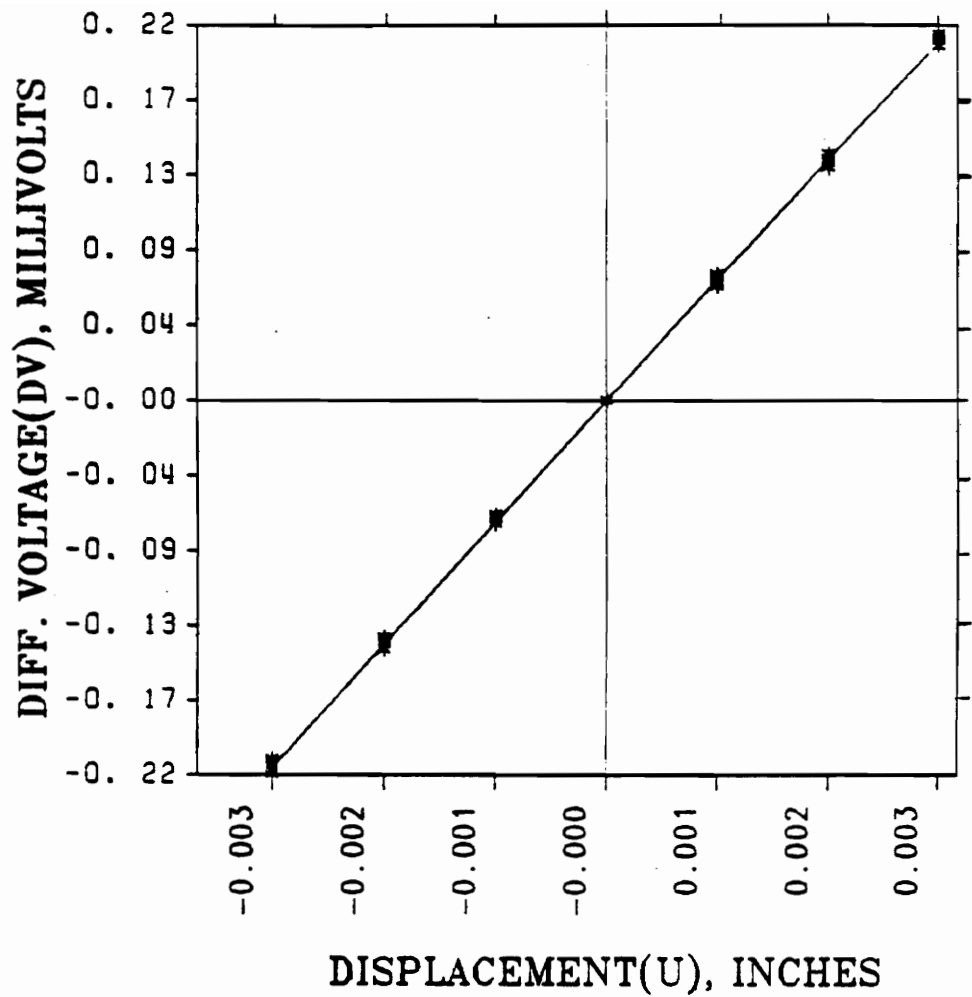


Figure 3.7 Typical calibration curve of CET

in stabilizing the CET and eliminate lateral movement. Care was taken not to overstrain the gages during mounting and dismounting. A beam instrumented with CET is shown in Figure 3.10.

3.5.4 Verification

To verify the performance of the CET, two tests were carried out on aluminum specimens. Aluminum was chosen because it is an isotropic and homogeneous material with low property variation. Thus, the variations in strain readings were influenced by CET's performance and not the variability within the specimen. The two verification tests were as follows:

1. A T6061 aluminum block ($E = 10^7 \text{ psi}$) was loaded in compression, and the compressive strains were read with CET and bonded gages. Strains were recorded at different load levels. Figure 3.11 shows very good agreement between the strain measurements of the CET and the bonded gage. The measured strains also agree very well with the strength of materials theory.

2. A T6061 aluminum bar ($E = 10^7 \text{ psi}$) was loaded at different levels in tension, and the strains were measured using the CET. Figure 3.12 shows excellent agreement between the strains read by CET and the strain based on strength of materials theory.

3.6 Summary and Conclusions

From the above experiments, the following can be summarized and concluded:

1. Experiments conducted on the effect of strain gage size on strain measurements in southern pine showed that two inch gage length was suitable to record strain. Therefore, all the CET's used in this study were constructed with approximately a two inch gage length (to be exact 2.18 inches).

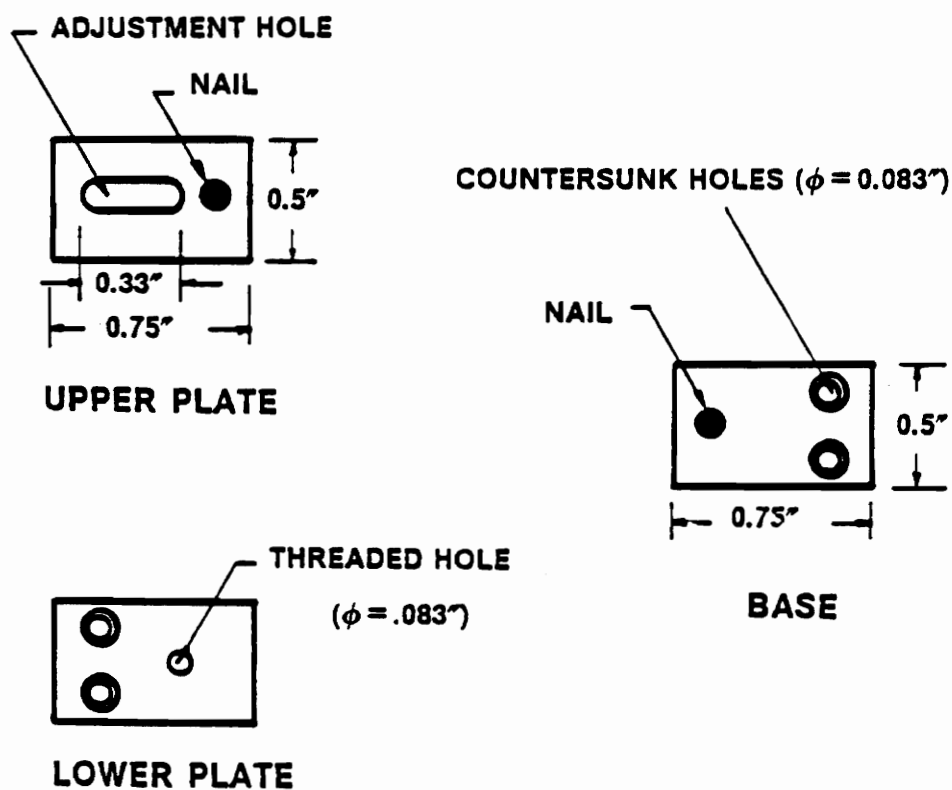
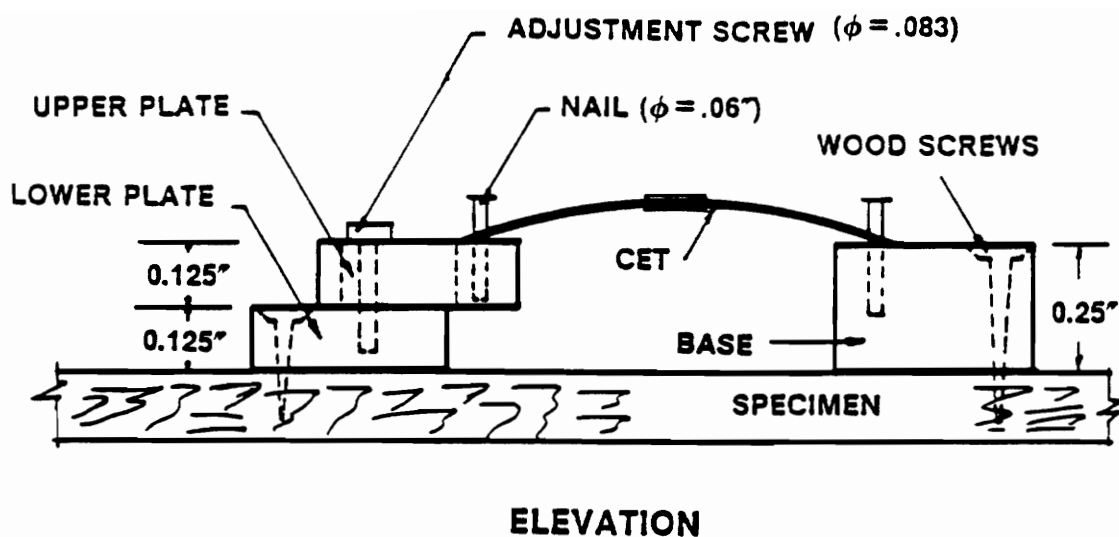


Figure 3.8 Details about shoes used to place CET on the specimen



Figure 3.9 CET shoes attached to the glulam beam

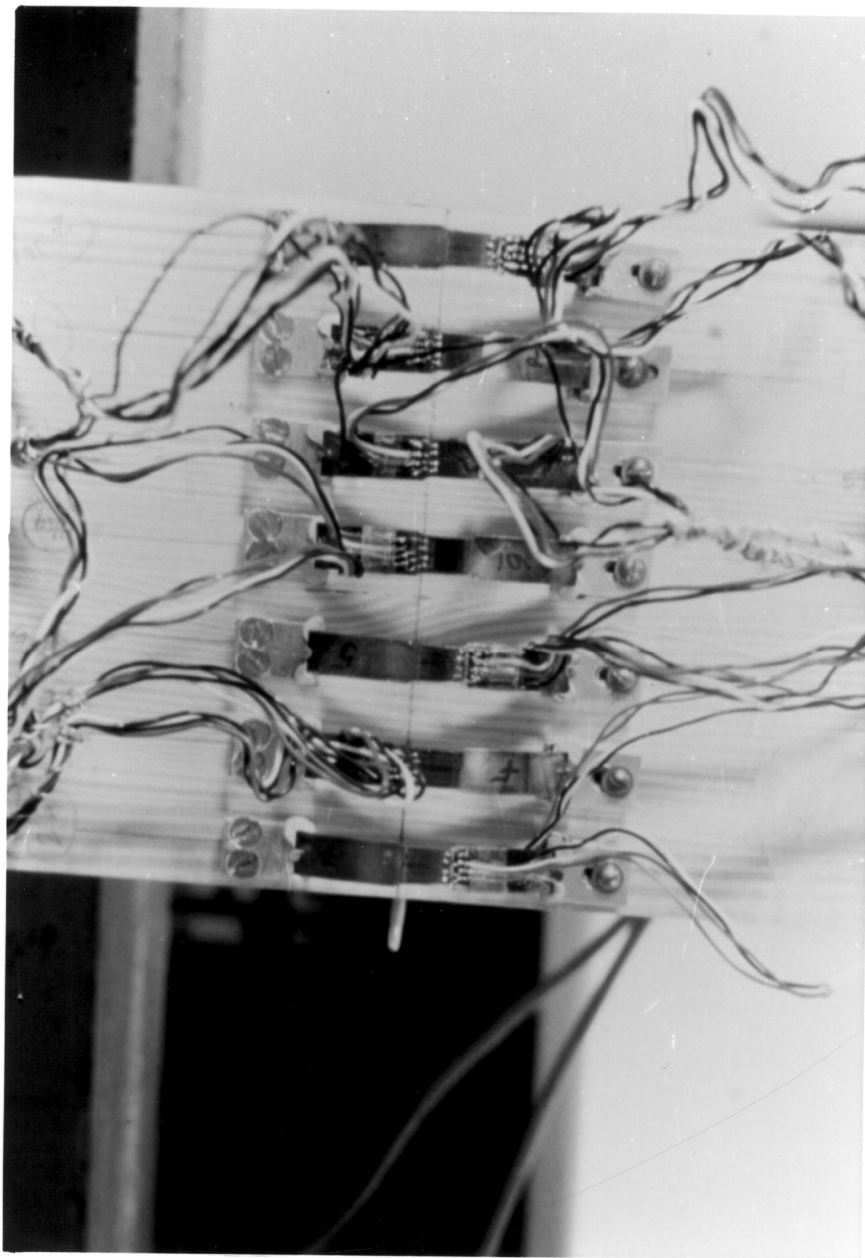


Figure 3.10 Glulam beam instrumented with CETs to measure strain

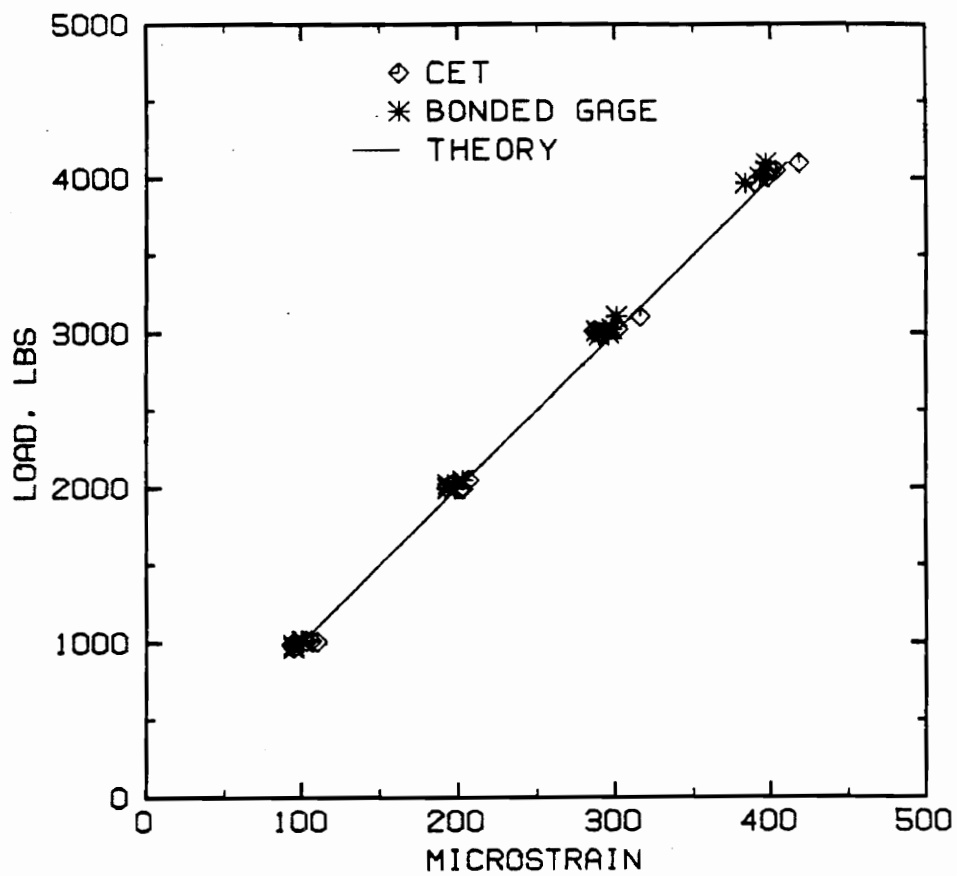


Figure 3.11 Comparison of strain induced in aluminum compression block

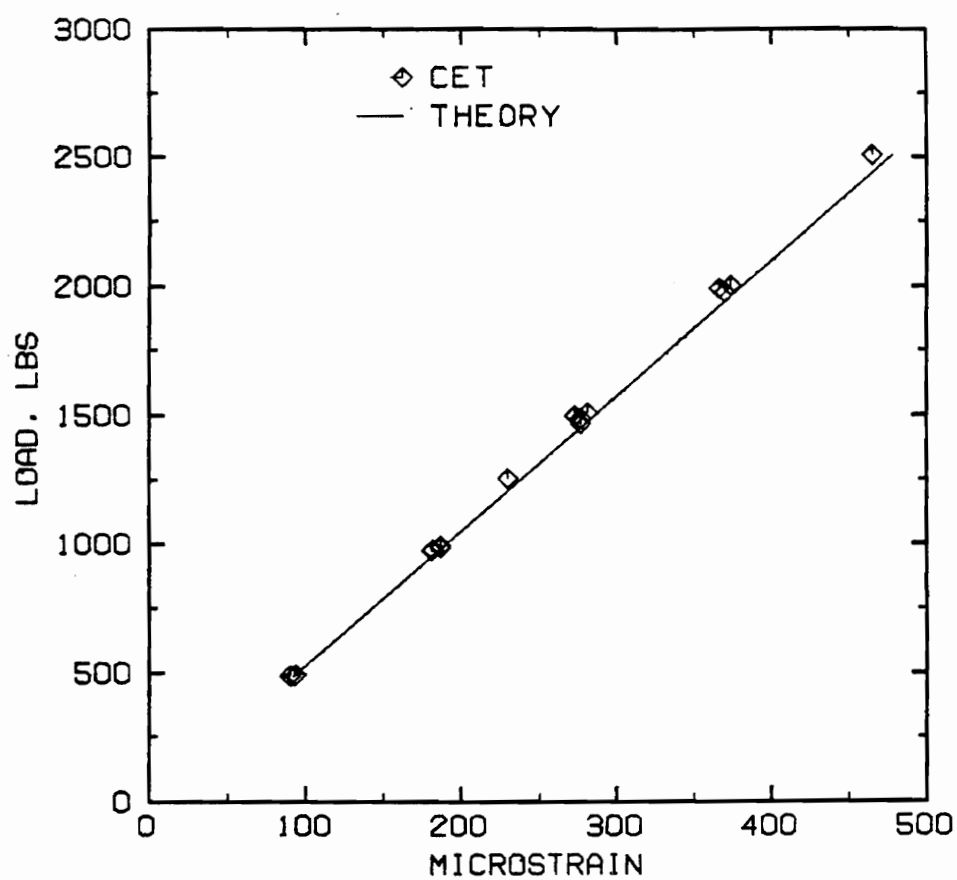


Figure 3.12 Comparison of strain in aluminum tension block

DATE DUE

JAN 10 1982

VOL. 8 NO. 1 JAN 1982
200-10-10

clip-on Electrical Transducer (CET) was fabricated, calibrated, and agreement between the strains read by CET and the strain recorded

urate, and reliable strain measuring device for southern pine. In this s were built. They were reused for strain readings at various lo- ae and glulam beams subjected to various loading conditions. The changed throughout the testing period.

CHAPTER 4

4. *GLULAM MATERIAL PROPERTIES*

4.1 Introduction

The longitudinal Young's modulus of the glulam beams were determined from individual laminae properties of each beam. The shear modulus of the beams was determined using small glulam torsion specimens. This chapter contains details of material property determination. It also includes the torsion test procedures for measuring the two principal shear moduli (G_{LR} , G_{LT}) of southern pine and the shear modulus of small glulam samples. The torsion test was conducted to show that there was not a significant difference between the two principal shear moduli of southern pine, and that the cross section of a glulam member could be considered to be transversely isotropic.

4.2 Procedure

Clear select structural southern pine boards, that were used to manufacture the beams, were tested to determine the material properties. The laminae were classified as No.1 Dense (N1D) or higher grade (Select Structural or SS) according to AITC 117-84 Design Standard Specifications (2). The average moisture content of the laminae was 8.5%. The average specific gravity was 0.58. All laminae were planed and tested nondestructively in tension to determine their modulus of elasticity; and the corresponding E-Rated grade was determined using AITC 117-84 Design Standard Specifications (2). Over 50% of the laminae were categorized as 1/6-2.0E or higher and the remaining were 1/6-1.8E.

4.2.1 Determination of Glulam Modulus of Elasticity

Prior to beam fabrication, each lamina was nondestructively tested to measure the longitudinal elastic modulus. The laminate or beam modulus of elasticity in the longitudinal direction, E_L , was predicted from the longitudinal modulus of elasticity (E_L) of the individual laminae. E_L of each lamina was measured from the tensile tests. The test set-up is shown in Figures 4.1 and 4.2. Pinned end conditions were used to allow for rotation. To avoid damage in the laminae, less than 50% of the allowable stress specified by the National Design Specification was applied (53). Strains were measured simultaneously at three locations using clip-on electrical transducers. The gages were located in the center of three 30-inch segments along the length of each specimen (Figure 4.3). Data was collected using the HP-data acquisition system. A 10,000 lbs Baldwin-Lima-Hamilton load cell was used to read the applied load. It had an accuracy of $\pm 0.25\%$ of the full-scale load. The load cell was calibrated using a TINIUS OLSEN universal testing machine. Voltage readings were recorded at increasing load increments, and a calibration curve and its equation was obtained statistically. During testing voltage was read directly by the HP-data acquisition system. The load

cell calibration equations, incorporated into the computer code, automatically converted the measured voltage into load.

Young's modulus was computed at each gage location. Then E_1 of each beam was computed by taking an average of E_L of each lamina used to fabricate the beam. An average of laminae longitudinal modulus of elasticity was taken instead of transformed section analysis because preliminary comparison of the experimental and the analytical strain readings of beams produced better agreement with an estimate of E_1 for the beams derived from the average of laminae Young's modulus.

4.2.2 Determination of Glulam Shear Modulus

The analysis of a beam composed of a homogeneous material with three clearly defined planes of elastic symmetry requires two shear moduli (G_{LR} and G_{LT}) to evaluate the longitudinal stress. However, in a glulam beam each lamina has different ring angles, thus the material and geometric axes do not coincide. In addition, it is not practical to apply tensor transformation since the ring angle in each lamina must be known. Therefore, researchers often consider a glulam cross-section to be transversely isotropic (i.e. having the same shear modulus in both tangential and radial directions) (18,50). Using a single shear modulus for southern pine glulam beams would also be justified if the two principal shear moduli of an orthotropic southern pine cross-section do not differ significantly. Predicting the behavior of glulam beams with reasonable accuracy using fewer material properties would be more economical and efficient. To show that the two principal shear moduli of a southern pine cross-section do not vary much from each other, and to estimate an appropriate value for a single representative shear modulus of a southern pine glulam cross-section, an experiment was conducted using torsion tests to measure the shear modulus of small clear orthotropic specimens and small glued-laminated specimens.

The objectives of the experiment were:

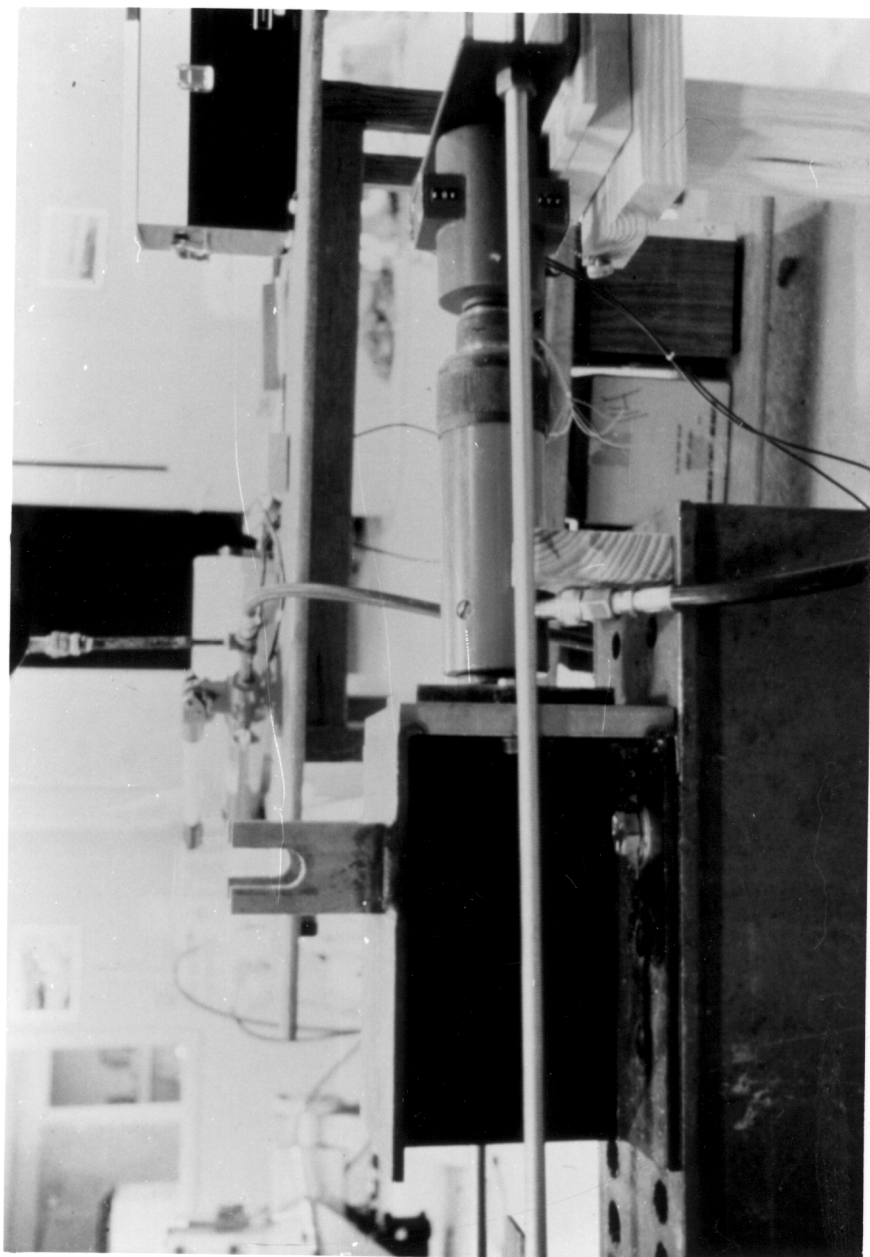


Figure 4.1 Loading end of the tension set-up for determining lamina modulus of elasticity

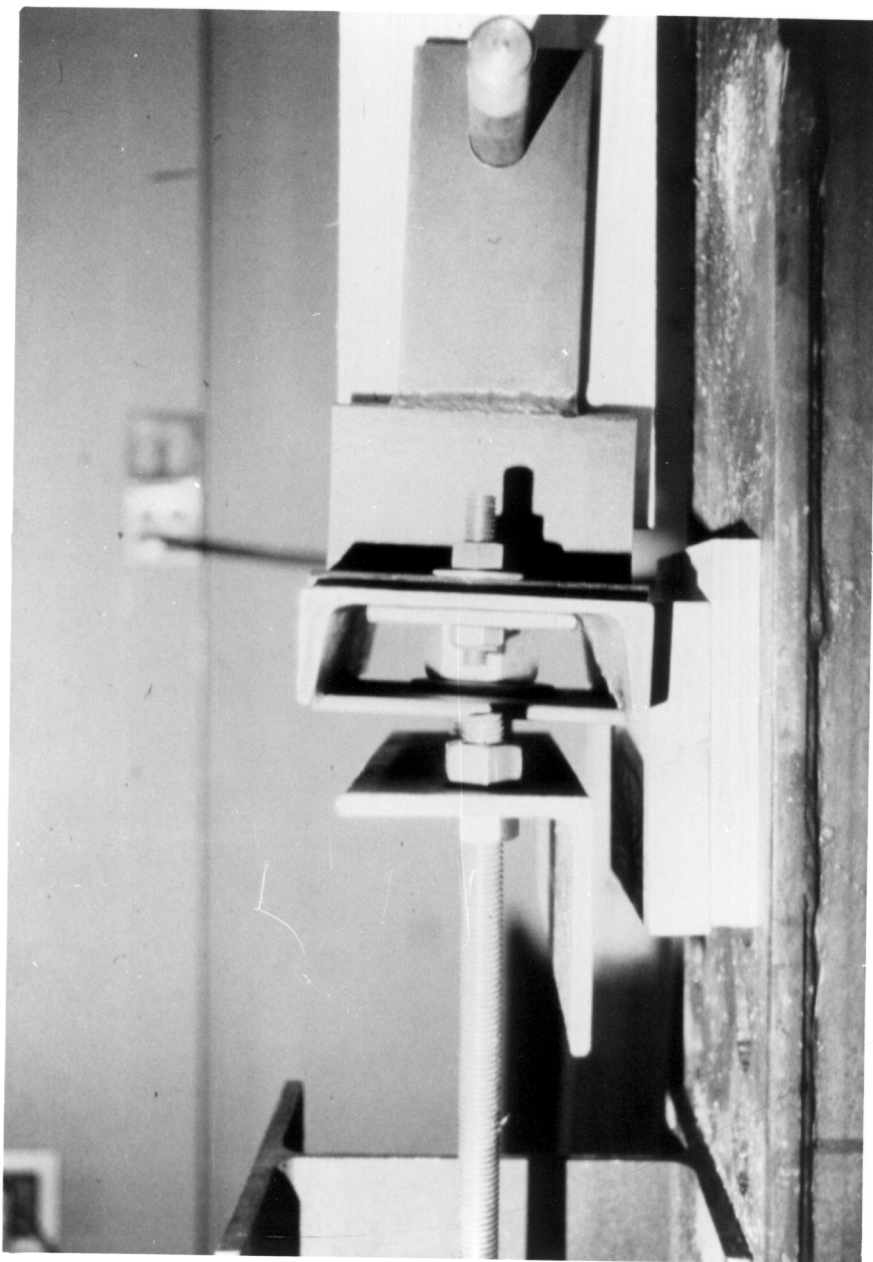


Figure 4.2 Pinned end of the tension set-up of determining lamina modulus of elasticity

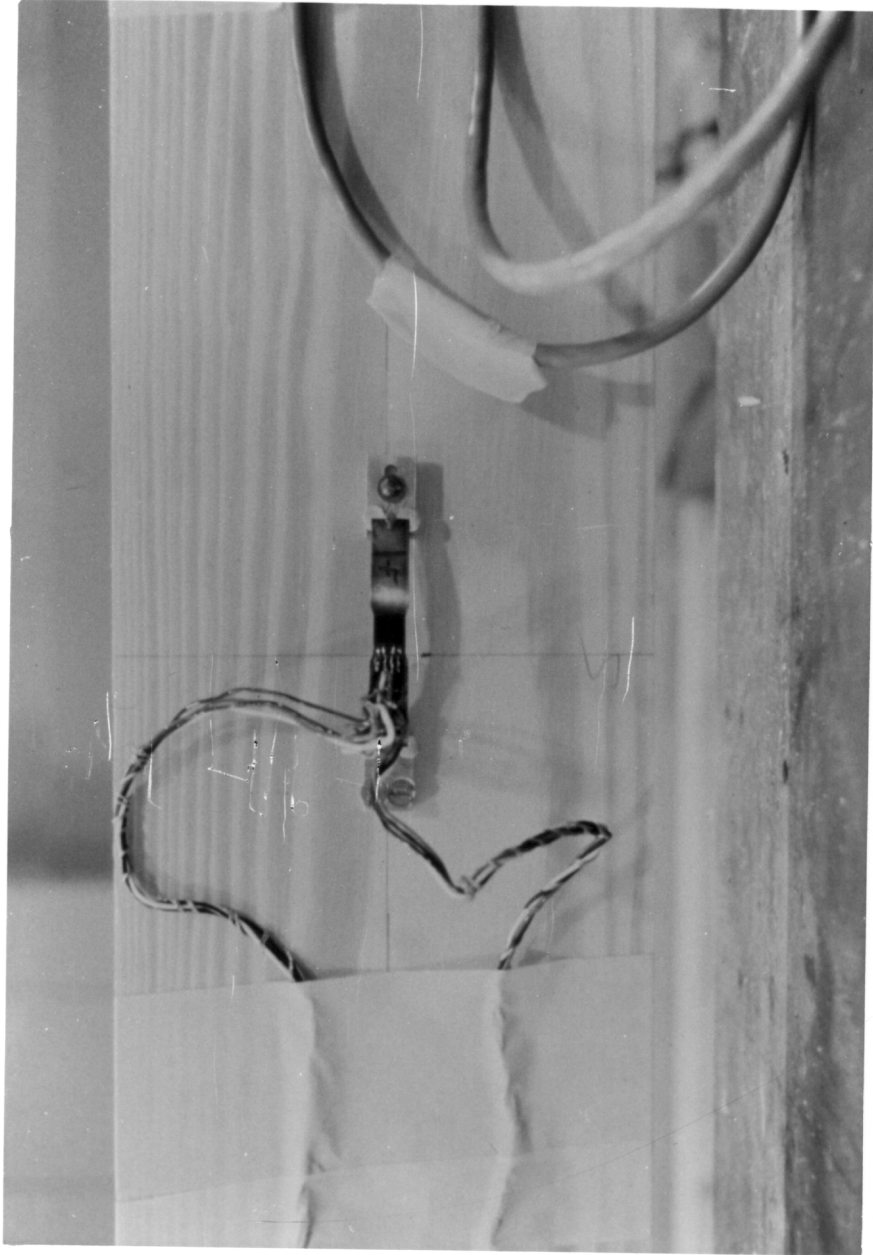


Figure 4.3 CET installed on a lamina at the center of a 30-inch segment to measure strain in tension

1. To measure the two principal shear moduli, G_{LR} and G_{LT} , from torsion tests for orthotropic southern pine specimens, and to determine if these moduli are approximately equal.
2. To estimate the average shear modulus for southern pine glulam beams from torsion tests of glulam specimens.

The testing program was divided in two parts:

1. In the first part, the principal shear moduli, G_{LR} and G_{LT} , of orthotropic southern pine samples were measured by testing orthotropic rectangular southern pine specimens in torsion. For each sample, a torsional stiffness was obtained from the slope of the applied torque vs. angle of twist curve, and the two principal shear moduli were computed from Lekhnitskii's (47) orthotropic solution (Chapter 2, equations [2.15], [2.16], and [2.17]). The values of G_{LR} and G_{LT} were compared to determine if they were significantly different. The principal shear moduli were computed from 12 inch long southern pine specimens of rectangular cross-sections that were carefully machined with three planes of material symmetry and geometric symmetry coincident. A total of 18 rectangular samples, divided in three shape-groups, were tested in torsion to determine G_{LR} and G_{LT} (Table 4.1). Aspect ratio, in this case, indicates the depth-to-width (a/b) ratio of the specimens. The three ratios were 2, 3, and 4. The corresponding cross-section sizes were 0.5" by 1.0", 0.5" by 1.5", and 0.5" by 2.0" respectively. This was carried out to determine the influence of shape ratio on the value of elastic shear constant.

Six samples were used for each shape ratio. Three of the six samples had the growth rings oriented parallel to the longer side (flatsawn), and the other three had the growth rings oriented perpendicular to the longer side (quartersawn). Figure 4.4 shows growth ring orientation of a pair of samples to determine the shear moduli. For each sample, a torsional stiffness was obtained from the slope of the applied torque vs. angle of twist, and the two principal shear moduli were computed from Lekhnitskii's orthotropic solution (47). By combining the samples within each shape-group, a total of nine sets of values of G_{LR} and G_{LT} were obtained. The torsional stiffnesses of all the samples tested were calculated from the linear region of the torque vs. angle of twist curve.

Table 4.1 Longitudinal modulus of elasticity of glulam beams

Beam ID	# of Laminae	Calculated Average E (10 ⁶ psi)	COV(%)	Minimum Lamina E (10 ⁶ psi)	Maximum Lamina E (10 ⁶ psi)
B1S	6	1.80	27	1.08	2.60
B2S	4	1.81	21	1.28	2.60
B3S	5	1.98	22	1.25	2.84
B4S	10	1.85	24	1.06	2.71
B1C	9	1.87	22	1.05	2.66
B2C	4	2.22	20	1.56	2.83
B3C	11	2.11	23	1.09	2.98

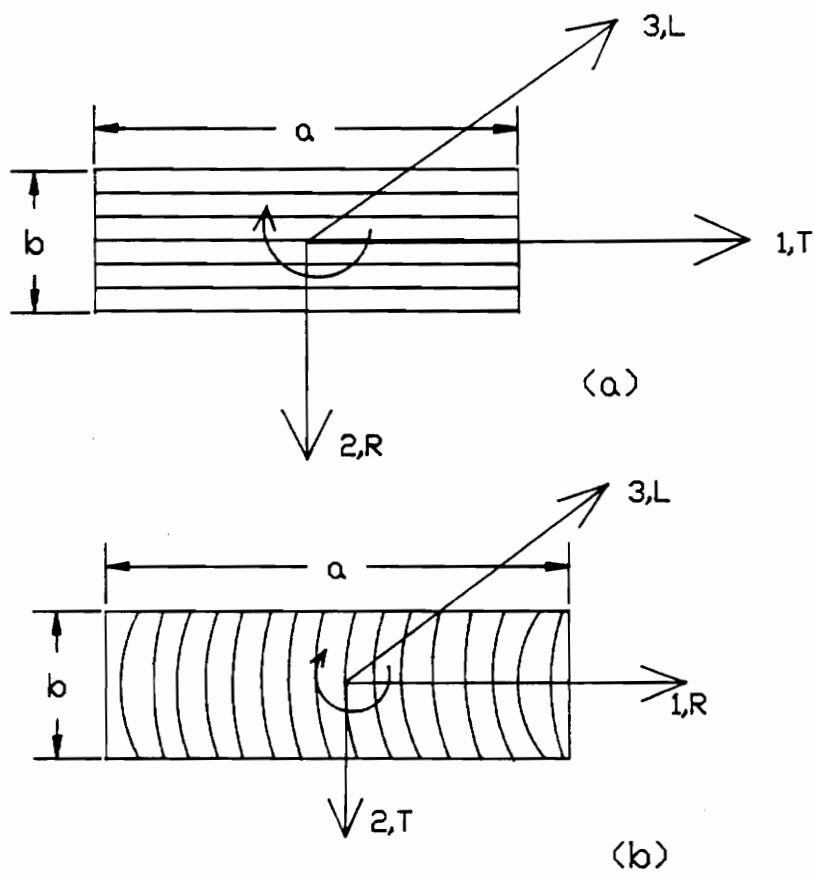


Figure 4.4 Torsion specimen cross section showing the growth ring orientation of a pair of samples to determine shear moduli

In addition to the rectangular cross-sectional bars, six cylindrical torsion specimens with a diameter of one inch and a length of 12 inches were also tested. Circular cross-sectional samples were tested to confirm the orthotropic shear moduli of southern pine calculated using Lekhnitski's solution. The average torsional stiffness of the circular specimens was compared to the analytical torsional stiffness from Lekhnitski's solution for the orthotropic round bars.

2. In the second part, southern pine glulam torsion specimens were tested, and their shear modulus were computed from St. Venant's torsion solution for homogeneous, isotropic bars (Chapter 2, equation [2.34]). Glulam torsion values are then compared to the orthotropic southern pine shear moduli to determine if the difference was significant. Rectangular glulam samples were tested in torsion and their shear elastic constants were computed from St. Venant's torsion solution for homogeneous, isotropic bars (Chapter 2). Nine glulam specimens with rectangular cross-sections, divided in three shape-groups were tested in torsion. The depth-to-width ratios of the glulam samples were the same as those used for the orthotropic samples (i.e., 2, 3, and 4). The samples were prepared with three to six laminae (lamina thickness = 0.35 inch). Since warping is present in torsion samples with rectangular samples, six glulam samples with circular cross-sections were prepared to test in torsion to confirm the shear modulus calculated using torsional stiffness values of the rectangular glulam specimens. The diameter of the cylindrical specimens was one inch. All glulam specimens were also 12 inches long. All the test specimens were cut from southern pine boards obtained from a local lumber yard. Hence, the samples were probably not from the same tree.

All the samples were tested in an INSTRON torsion machine with a load-range capacity of 10,000 in-lbs. The load accuracy was ± 1 in-lb, and the angle of twist accuracy was ± 0.005 degree. Special grips were constructed to accommodate the rectangular cross section of the specimens. The machine allowed free longitudinal displacement of the sample during testing (i.e., unrestrained torsion). Thus, the specimen was free to warp and the requirement of the theory of elasticity that the shear stress distribution be the same at any cross-section, including the end boundaries, was not

violated. To minimize the influence of St. Venant's effect and crushing of the sample ends, rotation was measured away from the grips with two thin aluminum arms fixed to the specimen four inches away from the end grips. The ends of the aluminum arms were attached to LVDT transducers that were secured to the testing machine (Figure 4.5). The change in voltage of the LVDT's was recorded continuously by a data acquisition system. The angle of twist was computed from the LVDT's calibration equation and simple geometry. To eliminate the influence of creep in the response, the specimens were tested at a rate of 3 degrees per minute determined using the guidelines of ASTM standards (3). All tests were carried to an angle of twist of 10 degrees.

Appendix B has the FORTRAN code to iteratively solve the two nonlinear equations of Lekhnitskii's torsion theory for an orthotropic elastic body. Once the shear moduli, G_{LR} and G_{LT} , were computed, a two sample t-test was performed to test if there was a significant difference between G_{LR} and G_{LT} values. Also, the effect of width-to-depth ratio (h/b ratio) was statistically evaluated (using ANOVA procedure) to see if it was significant. Then, St. Venant's isotropic torsion solution (equation [2.34]) was applied to the orthotropic rectangular specimens to determine a shear modulus that would serve as an effective average of G_{LR} and G_{LT} for a southern pine cross-section. A two sample t-test was conducted to test if there was a significant difference between the shear moduli calculated using St. Venant's isotropic torsion theory and G_{LR} , G_{LT} , and the mean of G_{LR} and G_{LT} . For the second phase of the study, the average shear modulus of glulam specimens was statistically compared to G_{LR} , G_{LT} , and the grand mean of G_{LR} and G_{LT} . A T-test was performed to check for any significant differences. Moisture content and specific gravity samples from all the samples were cut about four inches from one end.

4.2.3 Moisture Content and Specific Gravity Measurements

Moisture content and specific gravity were measured according to the ASTM D 2016-74 specifications (3). The oven-drying method was used to calculate the moisture content:



Figure 4.5 Torsion set-up to determine shear modulus

$$\%MC = \frac{\text{weight with water} - \text{OD weight}}{\text{OD weight}} \times 100 \quad [4.1]$$

The oven dry (OD) volume and the weight of the dry wood are necessary for determination of specific gravity. The volume was obtained by an immersion or displacement method, and the OD weight was obtained by weighing the OD specimen. Then, dividing the OD weight by OD volume gives the specific gravity of the specimen.

4.3 Results and Discussion

The longitudinal modulus of elasticity of four straight and three curved glulam beams tested in this study was determined from the properties of individual laminae. Shear modulus of the beams was determined by testing small glulam samples.

4.3.1 Longitudinal Modulus of Elasticity

The longitudinal modulus of elasticity, E_L , of the beams were estimated from the measured Young's modulus along the length of each lamina used in fabricating the beam. E_L measured at three locations along the length of each lamina was used in calculating the beam's Young's modulus. The average of all measured Young's moduli from the laminae was used to estimate the beam longitudinal modulus of elasticity. The coefficient of variation (COV) of Young's modulus among the beams was 23%. The COV of lengthwise modulus of elasticity among the laminae ranged from 3% to 43% with an average coefficient of variation of 19%. Figures 4.6 to 4.12 show the arrangement of laminae in each beam and their longitudinal modulus of elasticity at three sections along the length.

A	B	C	LAMINA #
2.488	1.481	1.231	11
1.224	1.376	2.597	4
2.231	1.250	1.426	12
1.829	1.080	1.794	7
1.917	2.098	2.200	5
1.604	2.112	2.422	10

All E-values are 10E6 psi

Figure 4.6 Placement of laminae and their E-values at three sections along the length of beam B1S

A	B	C	Lamina #
1.914	1.416	1.618	13
1.884	1.456	1.772	14
1.285	1.707	2.379	8
2.051	1.627	2.596	6

Lamina E values are in 10E6 psi

Figure 4.7 Placement of laminae and their E-values at three sections along the length of beam B2S

A	B	C	Lamina #
2.669	2.370	2.030	13
1.254	1.800	1.877	7
1.563	1.916	1.621	3
1.445	1.935	2.835	2
1.809	2.099	2.426	1

All E-values are 10E6 psi

Figure 4.8 Arrangement of laminae and their E-values at three sections along the length of beam B3S

A	B	C	Lamina #
2.512	2.377	2.069	4
2.123	1.796	1.602	15
1.603	2.012	1.966	14
1.232	1.310	1.315	8
1.823	1.541	1.311	9
1.259	1.528	1.059	6
2.356	1.424	2.125	10
2.058	2.011	1.753	12
1.523	2.711	1.738	11
2.355	2.498	2.499	5

All E-values in 10E6 psi

Figure 4.9 Arrangement of laminae and their E-modulus at three sections along the length of beam B4S

A	B	C	Lamina #
2.382	1.736	2.656	12
1.922	1.726	2.570	2
1.613	2.013	2.462	4
1.358	1.779	1.948	8
1.923	1.491	1.502	11
1.726	1.434	1.051	9
1.726	1.486	1.850	6
1.413	2.505	2.091	5
2.291	1.982	1.856	7

All E-values are in 10E6 psi

Figure 4.10 Arrangement of laminae and their E-values at three sections along the length of beam B1C

A	B	C	Lamina #
2.404	1.648	2.576	1
1.556	2.648	2.276	2
2.830	1.872	2.609	9
1.665	2.168	2.431	3

All E-values are in 10E6 psi

Figure 4.11 Arrangement of laminae and their E-modulus at three sections along the length of beam B2C

A	B	C	Lamina #
1.898	1.768	2.332	2
1.906	2.316	2.736	4
1.089	1.615	1.618	6
1.609	1.707	1.935	8
2.303	2.921	2.158	10
2.410	2.152	2.197	11
2.069	2.786	2.526	9
2.373	2.112	1.703	7
1.378	1.244	1.756	5
2.976	1.775	2.656	1
2.709	2.824	1.974	3

All E-values are in 10E6 psi

Figure 4.12 Arrangement of laminae and their E-modulus at three sections along the length of beam B3C

Table 4.2 shows the estimated longitudinal modulus of elasticity and the coefficient of variation for each beam. The Young's modulus was estimated by taking the arithmetic average of E 's of all the laminae used in fabricating the beam. The table includes the number of laminae used to manufacture each beam and the minimum and maximum values of the lamina modulus of elasticity in each beam.

4.3.2 Shear Modulus

Two of the components of the reduced constitutive matrix for glulam beams (Chapter 2) are G_{LR} and G_{LT} . If, however, the beam is assumed to be isotropic in the cross-sectional plane due to the random laminae orientation, then the principal shear moduli G_{LR} and G_{LT} can be replaced by a single shear modulus G . The evident question is "what value of G should be used for southern pine glulam beam?" In this section, the results of the experiments conducted to investigate the assumption of transverse isotropy are presented. In addition, the shear modulus of rectangular glulam samples are computed using Saint-Venant's torsion theory for homogeneous, isotropic material.

Tables 4.3 - 4.5 present the results of the first phase of experiments carried out to compute the shear modulus of glulam beams. The torsional stiffness for each sample was computed from the slope of the torque vs. angle of twist curve obtained experimentally. Lekhnitskii's orthotropic solution (47) was used to compute G_{LR} and G_{LT} . Table 4.3 contains the experimentally obtained torsional stiffness values for all rectangular southern pine samples machined with the material symmetry axes and the geometric axes coincident. The three aspect ratios (a/b) shown in the table were tested to investigate the effect of cross-sectional shape on the shear modulus. To compute G_{LR} and G_{LT} , Lekhnitskii's solution for orthotropic bars was solved using simultaneous equations for two bars of the same aspect ratio but with different growth ring orientations (Figure 4.4). For example, in one sample, the growth rings were parallel to the wider side (commonly called flat-sawn), and the other sample had growth rings oriented perpendicular to the longer side (called

Table 4.2 Torsion test samples with three planes of material symmetry.

SHAPE CATEGORY	NUMBER OF SAMPLES	SIZE (a x b x l) (inches)	GROWTH RING ORIENTATION
SP1	3	1.0 x 0.5 x 12	P
SN1	3	1.0 x 0.5 x 12	N
SP2	3	1.5 x 0.5 x 12	P
SN2	3	1.5 x 0.5 x 12	N
SP3	3	2.0 x 0.5 x 12	P
SN3	3	2.0 x 0.5 x 12	N

NOTE : P = Parallel to longer cross-section dimension.
(Figure 4.4 (a))
N = Normal to longer cross-section dimension.
(Figure 4.4 (b))

quarter-sawn). The computed G_{LR} and G_{LT} values for all the sample combinations are given in Table 4.4. All samples were tested at an average moisture content of 11.12% (COV = 8.2%). The average specific gravity was 0.63 with a COV of 12%.

Table 4.5 presents the mean values of G_{LR} and G_{LT} for each aspect ratio. There was approximately 8% difference between G_{LR} and G_{LT} under each size category. In all cases, the coefficient of variation was less than 3%. The grand means of G_{LR} and G_{LT} , which ignore the shape effect, were 160,870 psi and 150,156 psi.

One-way analysis of variance was performed to determine if there was a significant difference between G_{LR} and G_{LT} for the three aspect ratios tested in the study. At α -level of 0.05, there was no significant difference between the means of three aspect ratio categories. However, a two sample t test indicated that there is a significant difference between G_{LR} and mean G_{LT} , even though the mean values of G_{LR} and G_{LT} of southern pine are quite similar considering the natural variability in wood properties. To determine if the orthotropic shear moduli calculated from Lekhnitski's solution are truly valid and representative of southern pine, samples with circular cross-sections were tested in torsion (Table 4.6). The average torsional stiffness of the circular samples was then compared to the analytical torsional stiffness from Lekhnitski's solution for the orthotropic round bars. Average G_{LR} and G_{LT} values obtained from the rectangular samples were used in Lekhnitski's solution to compute the analytical torsional stiffness value. At the 0.05 α -level, there was no significant difference between the analytical torsional stiffness from Lekhnitski's solution and the measured torsional stiffness of the cylindrical bars. Thus, the values obtained for G_{LR} and G_{LT} from Lekhnitski's solution for orthotropic bars with rectangular cross-section seem valid.

Tables 4.7 and 4.8 present the torsional stiffness values and shear modulus of glulam torsion samples constructed with rectangular and circular cross-sections computed from Saint-Venant's solution for homogeneous, isotropic material. Glulam samples were tested to obtain a representative value for southern pine glulam beam cross-section shear modulus. Since warping defor-

Table 4.3 Aspect ratio and measured torsional stiffness of orthotropic southern pine torsion specimens

Sample ID	Cross-section size (a X b)	Aspect Ratio (a/b)	Torsional Stiffness K (in-lbs/rad)
RN11	0.5' X 1.0'	2	330
RN12	'	'	340
RN13	'	'	350
RP11	'	'	370
RP12	'	'	335
RP13	'	'	375
RN21	0.5' X 1.5'	3	598
RN22	'	'	615
RN23	'	'	608
RP21	'	'	625
RP22	'	'	639
RP23	'	'	617
RN31	0.5' X 2.0'	4	828
RN32	'	'	832
RN33	'	'	838
RP31	'	'	826
RP32	'	'	884
RP33	'	'	931

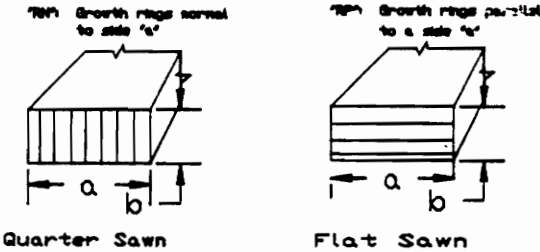


Table 4.4 Combinations of orthotropic samples
within each aspect ratio group.

COMBINATION I.D -----	Aspect Ratio		G_{LR} ---	G_{LT} ---
	a/b ---			
RN11-RP11	2	159,049	153,258	
RN11-RP12	2	160,066	152,993	
RN11-RP13	2	159,598	153,116	
RN12-RP11	2	160,400	149,090	
RN12-RP12	2	161,361	148,855	
RN12-RP13	2	160,955	148,955	
RN13-RP11	2	162,179	144,003	
RN13-RP12	2	163,061	143,880	
RN13-RP13	2	162,742	143,875	
RN21-RP21	3	159,544	156,313	
RN21-RP22	3	162,324	155,907	
RN21-RP23	3	159,684	156,294	
RN22-RP21	3	162,401	147,365	
RN22-RP22	3	163,817	147,182	
RN22-RP23	3	161,153	147,528	
RN23-RP21	3	162,323	147,803	
RN23-RP22	3	163,738	147,621	
RN23-RP23	3	161,051	147,986	
RN31-RP31	4	160,720	149,252	
RN31-RP32	4	158,450	149,457	
RN31-RP33	4	160,856	149,300	
RN32-RP31	4	160,400	152,277	
RN32-RP32	4	158,109	152,496	
RN32-RP33	4	160,509	152,267	
RN33-RP31	4	160,396	152,310	
RN33-RP32	4	158,105	152,531	
RN33-RP33	4	160,505	152,301	

Table 4.5 Mean Values of orthotropic shear moduli for the three cross-section sizes

Cross Section Size	a/b	No. of Combinations	Avg. G_{LR} (psi)	COV %	Avg. G_{LT} (psi)	COV %
0.5" x 1.0"	2	9	161,046	0.87	148,669	2.70
0.5" x 1.5"	3	9	161,782	0.96	150,444	2.86
0.5" x 2.0"	4	9	159,783	0.74	151,355	1.00
Grand Means	-	27	160,870	0.98	150,156	2.36

Table 4.6 Measured and computed torsional stiffness of the orthotropic circular samples (diameter = 1").

SAMPLE	MEASURED K (in.-lbs./rad.)	COMPUTED K (in.-lbs./rad.)	SPECIFIC GRAVITY	MOISTURE CONTENT %
C1	1,302	1,296	0.56	9.4
C2	1,335	1,288	0.62	8.4
C3	1,254	1,288	0.54	9.3
C4	1,293	1,276	0.56	9.4
C5	1,322	1,278	0.55	9.5
C6	1,328	1,251	0.63	9.4
MEAN VALUES	1,306 (COV=2.3%)	1,280 (COV=1.2%)	0.58 (COV=6.4%)	9.2 (COV=4.5%)

mations are present in bars with rectangular cross-sections, torsion samples with circular cross-sections were tested to confirm the shear modulus values obtained using the bars with rectangular cross sections. Cylindrical bars do not undergo warping deformations under torsional loads.

Table 4.9 presents the average shear modulus within each shape category, the overall mean for glulam bars with rectangular cross-sections, and the mean shear modulus of the cylindrical glulam bars. Analysis of variance showed that at α -level of 0.05, the means of the four size groups were not significantly different. The grand average of shear modulus for all glulam bars with rectangular cross sections was 162,051 psi. The average G of the cylindrical samples was 162,017 psi. No significant difference between the glulam samples with rectangular and circular cross-sections were detected at 0.05 α -level.

The G_{LR} and G_{LT} values from the orthotropic samples were statistically compared using two sample t test to the shear modulus of the glulam samples. The results showed that G_{LR} and G were not different statistically at 0.05 α -level. However, G_{LT} and G of glulam samples were different statistically at 0.05 α -level. However, the difference between G_{LT} of orthotropic bars and G of glulam samples was not more than 8 percent. From these results it seems that an average of G_{LR} and G_{LT} yields a value very close to the average shear modulus of glulam samples obtained using Saint-Venant's solution for isotropic, homogeneous materials. Therefore, it appears that Saint-Venant's solution gives a reasonable and a representative value for the shear modulus of a glulam cross-section. Therefore, in this study, the average shear modulus (162,051 psi) of glulam samples with rectangular cross-sections obtained using Saint-Venant's solution of torsion bars was rounded down to 160,000 psi for conservatism, and was used as material property for input to the finite element analysis of southern pine glulam beams.

Table 4.7 Cross Section size, measured torsional stiffness, and computed shear modulus of Glulam torsion bars

Sample I.D	Cross Section size	a/b	K	G
G11	1.0" x 1.0"	1	1,826	162,471
G12			1,700	162,047
G13			1,840	160,061
G21	0.5" x 1.0"	2	370	161,964
G22			380	161,551
G23			368	160,926
G31	0.5" x 1.5"	3	645	161,532
G32			658	163,476
G33			651	162,282
G41	0.5" x 2.0"	4	976	162,875
G42			982	163,464
G43			920	161,960

Table 4.8 Torsional stiffness and shear modulus of glulam bars with circular cross-section.

SAMPLE	DIAMETER	K	G
GC1	1"	1,314	162,218
GC2	1"	1,318	161,906
GC3	1"	1,310	162,373
GC4	1"	1,310	161,569

Table 4.9 Mean Values of G for the rectangular and circular
glulam samples.

===== RECTANGULAR SAMPLES =====						
Cross Section a/b Size	No of Samples	Avg. G (psi)	COV %	Avg Specific Gravity	Avg Moisture Content %	
1.0" x 1.0"	1	3	161,526	0.80	0.61	10.69
1.0" x 0.5"	2	3	161,480	0.32	0.63	10.41
1.5" x 0.5"	3	3	162,430	0.69	0.61	10.73
2.0" x 0.5"	4	3	162,766	0.46	0.56	10.60
=====						
Grand Mean	12	162,051	0.61	0.61	10.60	
=====						
===== CIRCULAR SAMPLES =====						
Diameter = 1"	4	162,017	0.22	0.67	9.74	

4.4 Summary and Conclusions

1. The coefficient of variation (COV) of Young's modulus among the beams was about 23%. The COV of lengthwise modulus of elasticity among the laminae ranged from 3% to 43% with an average COV of 19%. Calculated modulus of elasticity of beams ranged from 1,800,000 psi to 2,220,000 psi.

2. G_{LR} and G_{LT} of orthotropic southern pine specimens were 160,870 psi and 150,160 psi. The two averages differed by less than 8%. There was no significant effect of the aspect ratio on the values of the shear moduli.

3. Based on the torsion results, a southern pine glulam beam can be considered to be isotropic in the cross-section.

4. Shear modulus of glulam specimens was 160,000 psi. The average shear moduli of the glulam rectangular and the circular glulam samples using Saint-Venant's torsion solution for homogeneous, isotropic materials were 162,051 psi and 162,017 psi. Glulam shear modulus differed from orthotropic shear moduli by less than 8%. It differed from the average of G_{LR} and G_{LT} by less than 4%.

CHAPTER 5

5. *GLULAM BEAM ANALYSIS*

5.1 Introduction

For this study, three curved and four straight glued-laminated beams were manufactured in the laboratory. Since the objective of this study was to verify the FE model, given the material properties of the beams, a large sample size was not used. The selected beam sizes covered a wide range of span-to-depth ratios (i.e., 6 to 21) so that shear deflection effects would be considered in verifying the finite element model. The straight beams were subjected to loads in bending about both the principal cross-sectional axes (2- and 3- axes), and in combined bending and axial compression. The curved beams were subjected to bending about only the 2-axis and combined bending and compression. Strains and deflections were measured at various locations. Prior to beam fabrication, each lamina was nondestructively tested to measure the longitudinal elastic modulus. This data was used to estimate the material properties of the beams.

This chapter contains details of fabrication of beams, beam instrumentation for data collection, and experimental apparatus for testing glulam beams in bending and combined bending and compression. Next, the experimental results from the tests conducted on the beams are compared to the results from the finite element analysis. A discussion of the observations and the significance of the results is presented. Some remarks on possible sources of errors and other important considerations are also included. Figure 5.1 shows the flow chart of the testing procedure.

5.2 Fabrication of Glulam Beams

Three curved and four straight glulam beams were manufactured for this study. Clear select structural southern pine boards were used to manufacture the beams. The laminae were classified as No.1 Dense (N1D) or higher grade (Select Structural or SS) according to AITC 117-84 Design Standard Specifications (2). Over 50% of the laminae were categorized as 1/6-2.0E or higher and the remaining were 1/6-1.8E. The average moisture content and specific gravity of the laminae used to fabricate the beams was 8.5% and 0.58. All straight beams and one curved beam were built using 2 inch thick (nominal) and either 4 or 6 inches wide (nominal) laminae. Two curved beams were built using nominal one inch thick laminae. The finished dimensions of all glulam beams are given in Table 5.1.

The beams were manufactured according to the specifications in AITC 117-84-MANUFACTURING (2). Under AITC regulations, structural glulam members should not be fabricated using laminae exceeding a 2-in. net thickness; and, the laminate must include at least four laminae if the bending load is applied to the wide face of the beam. AITC also specifies that the moisture content of the laminae should not exceed 16 percent.

All the beams were manufactured with laminae glued with aliphatic resin adhesive which is easy to apply, safe to handle, and cures at normal room temperature and humidity conditions;

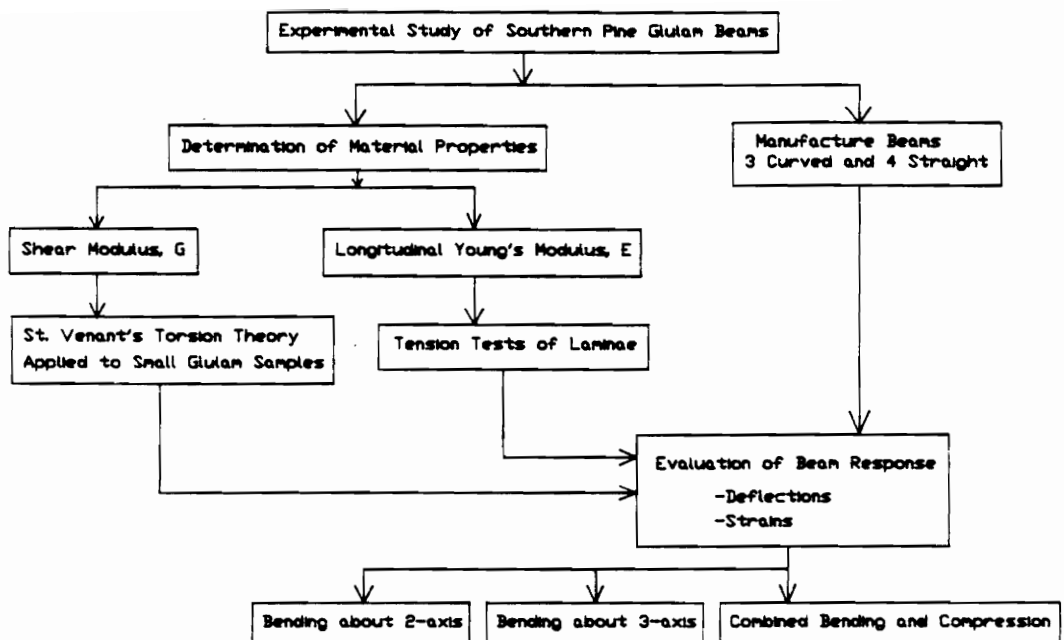


Figure 5.1 Flow chart of the experimental testing procedure

Table 5.1 Geometry of Glulam Beams and their allowable stresses.

BEAM	WIDTH,b (inches)	DEPTH,h (inches)	RADIUS OF CURVATURE,R (feet)
B1S	3.0	8.3125	-
B2S	3.013	5.602	-
B2S	4.865	6.492	-
B4S	4.896	13.823	-
B1C	2.994	5.984	50
B2C	3.014	5.568	50
B3C	4.914	7.546	50

NOTE : S = Straight and C = Curved

ALLOWABLE STRESSES*

F_{bx} (psi)	F_{by} (psi)	F_c (psi)	F_{cs} (psi)	F_{cs} (psi)	F_{vx} (psi)	F_{vy} (psi)
2100	2400	1800	650	2400	200	175

* For combination symbol 57 from Table 2 AITC 117 - 84 Design Standard Specifications for Structural Glued Laminated Timber of Softwood Species.

however, all beams were kept clamped for at least 24 hours to allow the adhesive to fully cure. A similar type of glue (room temperature setting PVA-type) was used by Bodig and Goodman (9) for plate shear tests of wood. They found for short term tests this adhesive performed adequately. However, for long term tests, significant creep deformations may occur when using aliphatic resin. Since the present study involved tests of short duration it was assumed that glue-line creep would not significantly influence the test results.

The laminae were arranged randomly within each beam. Since the curing time for the resin is about 30 minutes, the process of spreading the glue, assembling the laminae, and the initial clamping of the laminae was carried out within 30 minutes. Wooden caul boards were used to distribute clamping pressure to the laminae to avoid damaging the surface laminae. Clamping pressure was applied along the length of the beam using two parallel rows of bar clamps, spaced six inches apart. Clamping was carried from the center of the beam to both the ends. Initially, moderate pressure was applied; once all the clamps were installed, they were tightened to apply maximum pressure.

The curved beams were manufactured to a radius of curvature of 50 ft. The curvature was obtained by using a specially constructed curved wooden form to which the laminae of the curved beam were pressed and clamped.

The beams were cured over night at a temperature of 20 degrees centigrade and 55 to 65 percent relative humidity. Once the clamps were removed, the beams were left untouched and protected for at least two days. Before machining to finished sizes and lengths, the excess glue on the faces of the beams was scrapped using a metal scraper to avoid nicking the planer knives. The moisture content and the specific gravity samples were cut from each laminae before they were glued into beams.

Since the beams were tested at service loads, it was important to determine the allowable stresses specified by the code. Based on the laminae E-Rated grades, the design values for combi-

nation number 57 from AITC 117-84 Design Standard Specifications were used to determine the allowable stresses for the beams (Table 5.1).

5.3 Testing of Glulam Beams

The three curved beams were subjected to bending loads about their 2-axis and combined bending (about 2-axis) and longitudinal compression. Three of the four straight beams were loaded in bending (about 2 and 3 axes) and in combined bending (about 2 or 3 axes) and compression. The deepest straight beam (SB 4) was not tested under combined bending and compression loads because of the size limitations of the testing set-up. It was only tested in bending about its 2-axis. All beam testings were carried out in the Mechanical Testing Laboratory at Brooks Forest Products Center at Virginia Polytechnic Institute and State University. The temperature was maintained around 20° centigrade and the relative humidity was between 55% and 65%.

A 20,000 lbs. Baldwin-Lima-Hamilton (BLH) load cell (Model U3G2) was used to measure the bending loads; and, a 10,000 lbs. BLH load cell (Model U3G2B) was used to measure the axial loads. Loads were read continuously during each test. The load cell calibration equations, incorporated into the computer code, automatically converted the measured voltage into load (Appendix A). Three Celesco PT101 position (displacement) transducers were used to measure the glulam beam deflections under bending and combined loads (Figure 5.2). The displacement transducers had a measurement range of 10 inches and an accuracy of 0.1%. They were calibrated using an Instron extensometer (Model A18-38). The range of the extensometer was 0 to 1 inch with an accuracy of 0.00002 inch. Voltage readings were recorded at known displacements, and a calibration equation was derived statistically. These equations were incorporated into the data acquisition program (Appendix A). These transducers had 0.15% accuracy at full scale range (10 inches) and a resolution of 0.002 inch (range dependent). They were arranged in a Wheatstone bridge cir-

cuit to the data acquisition system. Laboratory developed Clip-on Electrical Transducers (CET) were used to measure strain at the midsection of the beams.

5.3.1 In-Plane Bending

Figures 5.3 and 5.4 show the testing set-up used to test the beams in bending about their principal axes (2 and 3 axes). All beams were loaded in "third point" bending on a 15,000 lbs capacity laboratory built universal testing machine. The tests were carried out according to ASTM D 198-84 specifications except that the rate of loading was manually controlled. The maximum loads that the beams were subjected to was achieved within 90 seconds. Loads were recorded using a 20,000 lb. load-cell that was installed within the bending test frame. Beams were instrumented with CET gages at the mid-section of the beam test span to measure strains along the depth. Also, three displacement transducers were installed under the beam along its length to record the deflections. Loads, strains, and deflections were recorded continuously using the 9000 series HP-data acquisition system. The HP-basic code to measure and store the data is given in Appendix A.

Beams that were 8 ft long were tested with a span of 83 inches. Beams that were 10 ft long were tested with spans of 83 inches and 114 inches. And 12 ft long beams were tested at 83, 114, and 132 inches test spans. Table 5.2 gives details about the tests performed on each beam and the effective spans for each test. The longer beams were tested at different spans to study the stress distribution in beams with a variety of length-to-depth ratios and to compare the experimental and the analytical results.

5.3.2 Combined Bending and Compression

Figures 5.5-5.7 show the set-up used to test the beams in combined bending and compression. Small initial bending and compression loads (500 lbs and 500 lbs) were applied to remove any slack

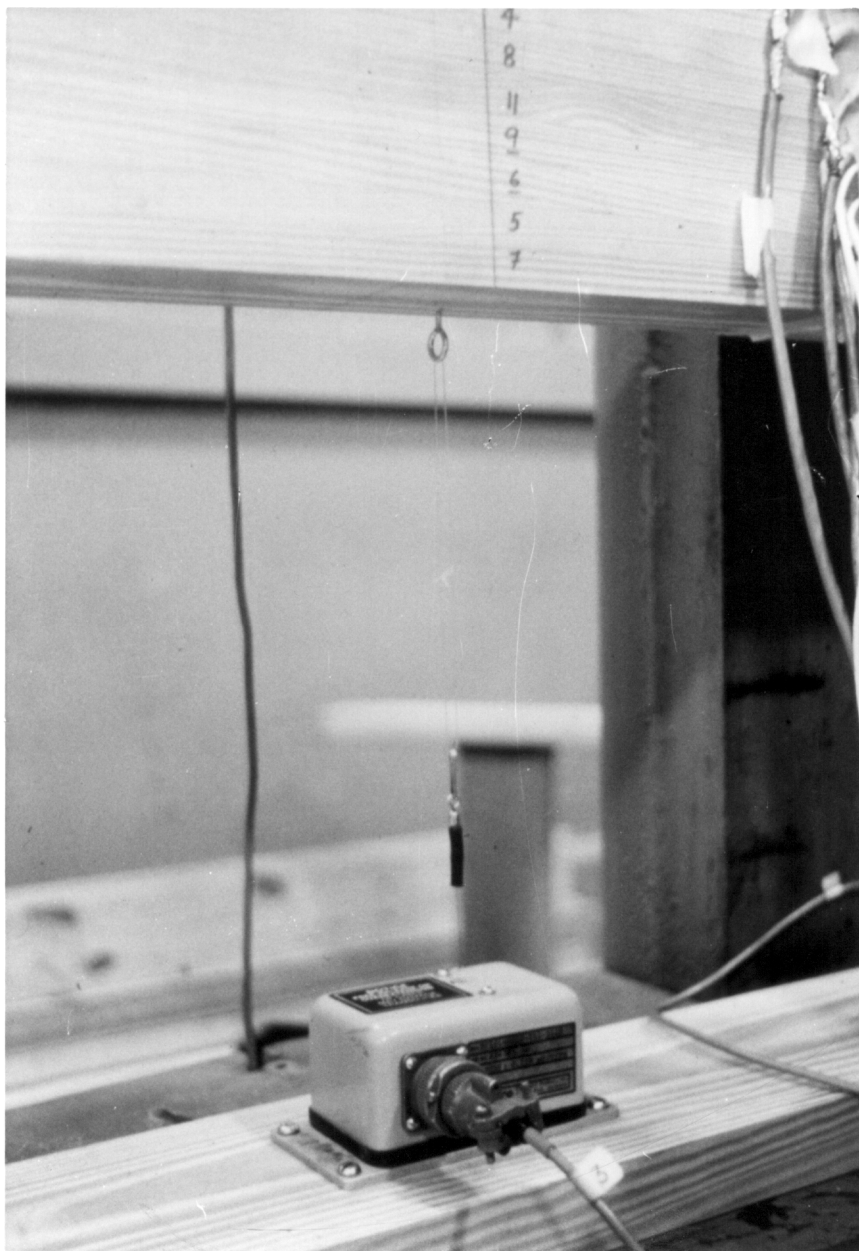


Figure 5.2 Displacement transducer used to measure beam deflections

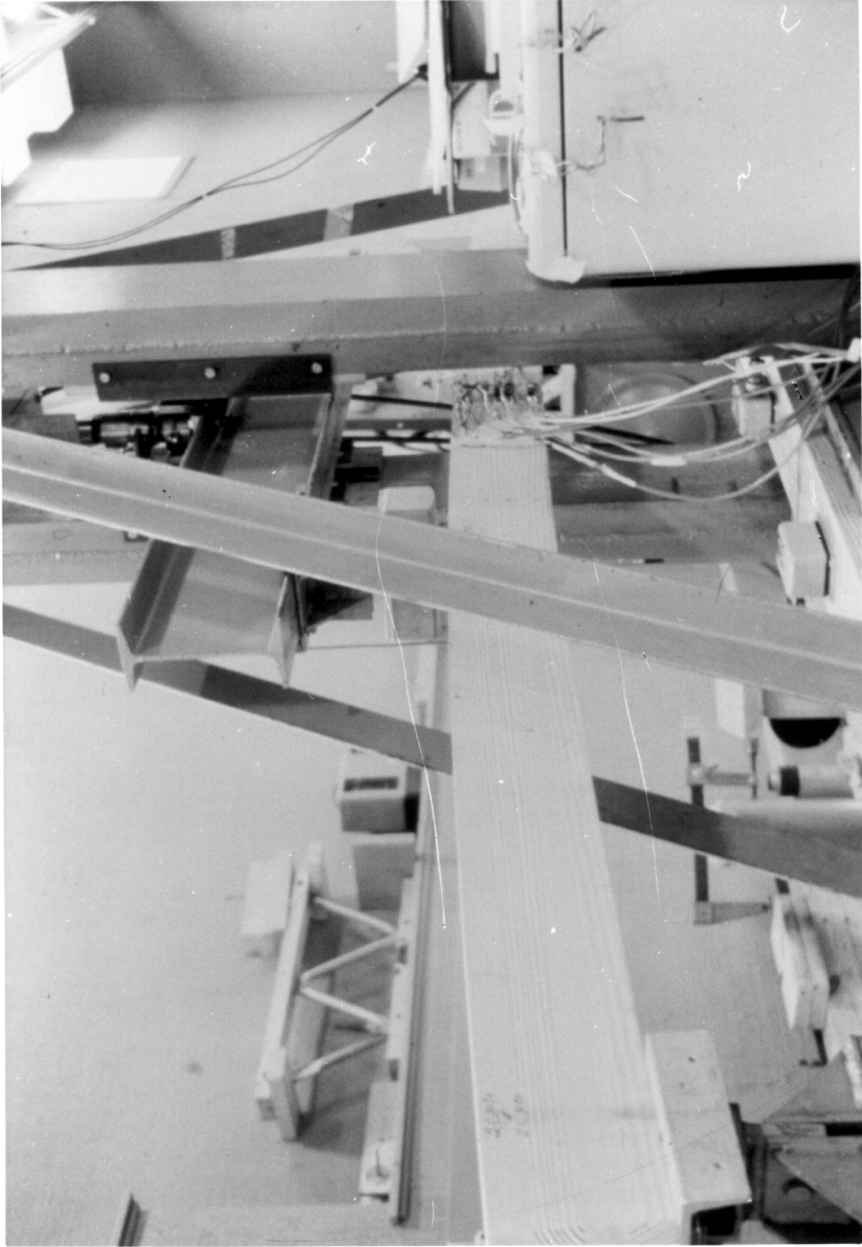


Figure 5.3 Bending set-up to test glulam beams in simple bending about 2-or 3- axis

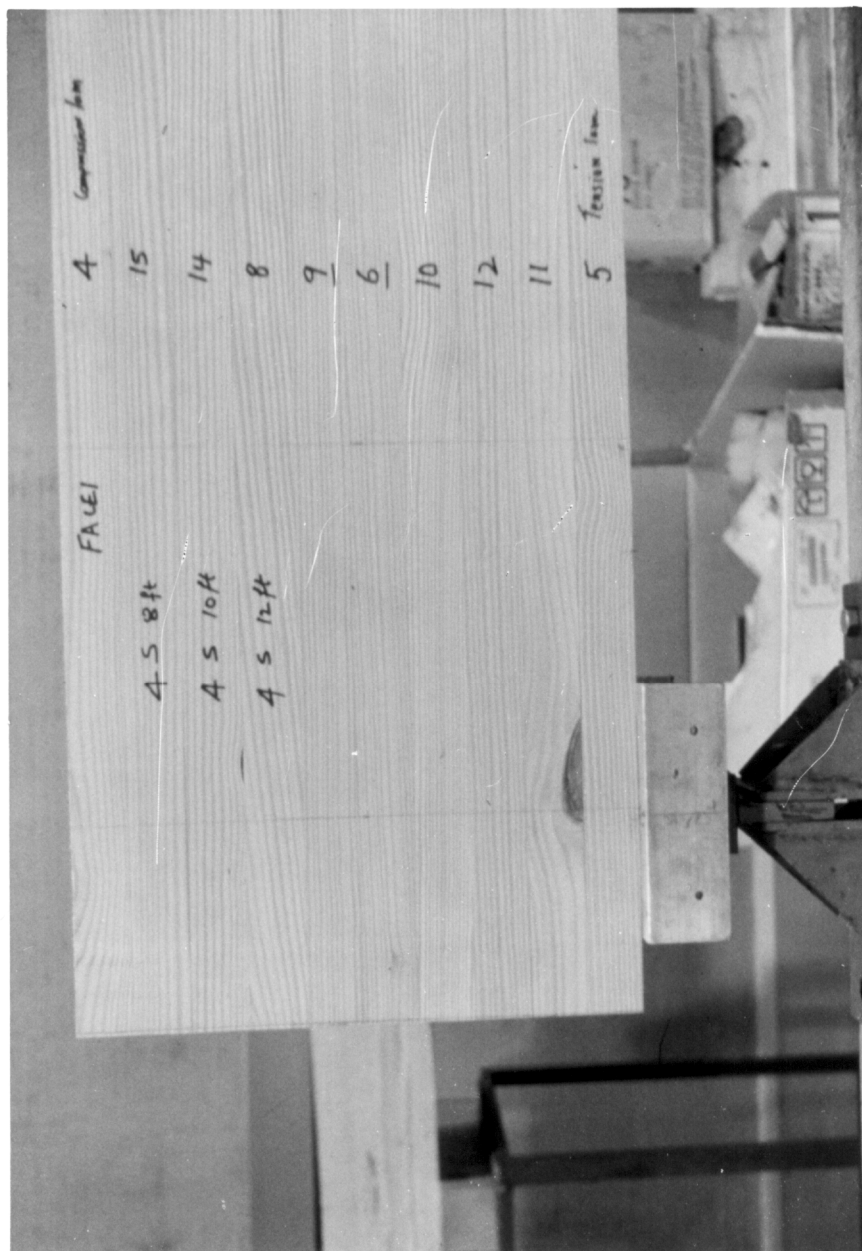


Figure 5.4 End support in the beam bending set-up

Table 5.2 Details of tests performed on each beam and the effective spans for each test.

BEAM ID	EFFECTIVE SPAN (inches)	TYPE OF LOADING
B1S83	83	BENDING ABOUT 3-3 AXIS
B1S83	83	BENDING ABOUT 2-2 AXIS
B1S114	114	BENDING ABOUT 3-3 AXIS
B1S114	114	BENDING ABOUT 2-2 AXIS
B2S83	83	BENDING ABOUT 3-3 AXIS
B2S83	83	BENDING ABOUT 2-2 AXIS
B2S114	114	BENDING ABOUT 3-3 AXIS
B2S114	114	BENDING ABOUT 2-2 AXIS
B3S83	83	BENDING ABOUT 3-3 AXIS
B3S83	83	BENDING ABOUT 2-2 AXIS
B3S114	114	BENDING ABOUT 3-3 AXIS
B3S114	114	BENDING ABOUT 2-2 AXIS
B3S132	132	BENDING ABOUT 3-3 AXIS
B3S132	132	BENDING ABOUT 2-2 AXIS
B4S83	83	BENDING ABOUT 3-3 AXIS
B4S114	114	BENDING ABOUT 3-3 AXIS
B4S132	132	BENDING ABOUT 3-3 AXIS
B1S108	108	BENDING & COMPRESSION ABOUT 3-3 AXIS
R1S108	108	BENDING & COMPRESSION ABOUT 2-2 AXIS
B2S108	108	BENDING & COMPRESSION ABOUT 3-3 AXIS
B2S108	108	BENDING & COMPRESSION ABOUT 2-2 AXIS
B3S130	130	BENDING & COMPRESSION ABOUT 3-3 AXIS
B3S130	130	BENDING & COMPRESSION ABOUT 2-2 AXIS
B1C83	83	BENDING ABOUT 3-3 AXIS
B2C83	83	BENDING ABOUT 3-3 AXIS
B2C114	114	BENDING ABOUT 3-3 AXIS
B3C83	83	BENDING ABOUT 3-3 AXIS
B3C114	114	BENDING ABOUT 3-3 AXIS
B3C132	132	BENDING ABOUT 3-3 AXIS
B1C83	81	BENDING & COMPRESSION ABOUT 3-3 AXIS
B2C109	109	BENDING & COMPRESSION ABOUT 3-3 AXIS
B3C130	130	BENDING & COMPRESSION ABOUT 3-3 AXIS

in the equipment. Deflection and strain readings taken at this point were subtracted from the subsequent strain readings to get the induced strains. Once the initial strain reading was taken, only bending loads were applied to a maximum of 1,500 lbs. Once the strains were read at maximum bending loads, compression loads were applied in increments of about 1000 lbs until a maximum compression load of around 6000 lbs was achieved. At every increment of load, strain and deflection values were recorded. Bending loads were recorded using a 20,000 lbs load cell, and compression loads were read by a 10,000 lbs load cell.

Moisture content and specific gravity were measured according to the ASTM D 2016-74 specifications (3). The oven-drying method was used to calculate the moisture content as mentioned in chapter 4.

5.4 Results and Discussion

The experimental results obtained from testing full size glulam beams were compared to the analytical results obtained from the finite element analysis with ABAQUS (34). All beams were tested only within their elastic range. Normal strain at the midspan and deflections at three locations along the length of the beams were recorded. Loads were applied symmetrically for all simple bending tests. For one curved beam, asymmetrical bending loads were applied when the beams were tested in combined bending and compression. Strain and deflection measured at several locations on each beam were compared to the analytical results for four load conditions: 1) bending about the major axis, 2) bending about the minor axis, 3) combined compression and bending about the major axis, and 4) combined compression and bending about the minor axis. Curved beams were subjected to only the first three load conditions. Since an experimental apparatus was not available to perform a true biaxial bending test, beams were subjected to bending about both the major and the minor axes. The superposition principle should be valid since the beams were

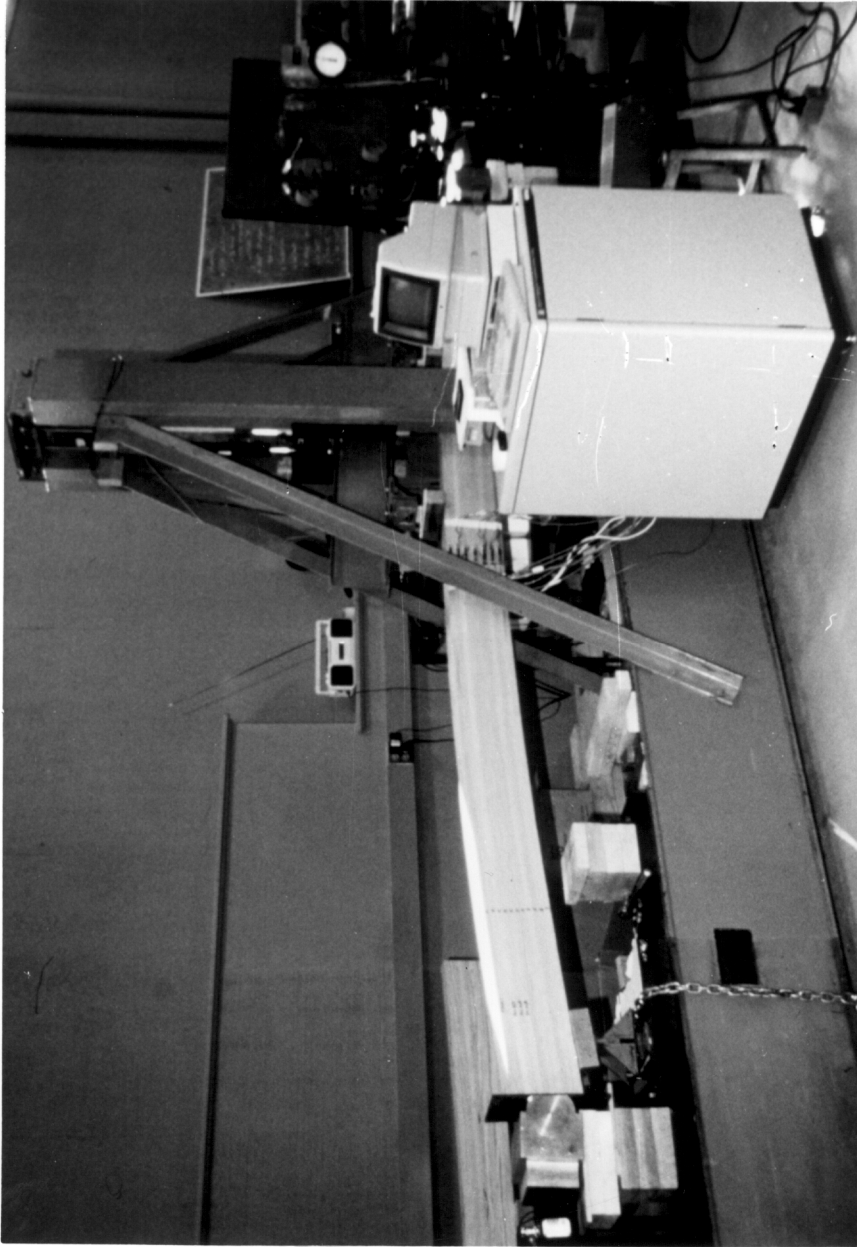


Figure 5.5 Experimental set-up to test glulam beams under combined bending and compression loads

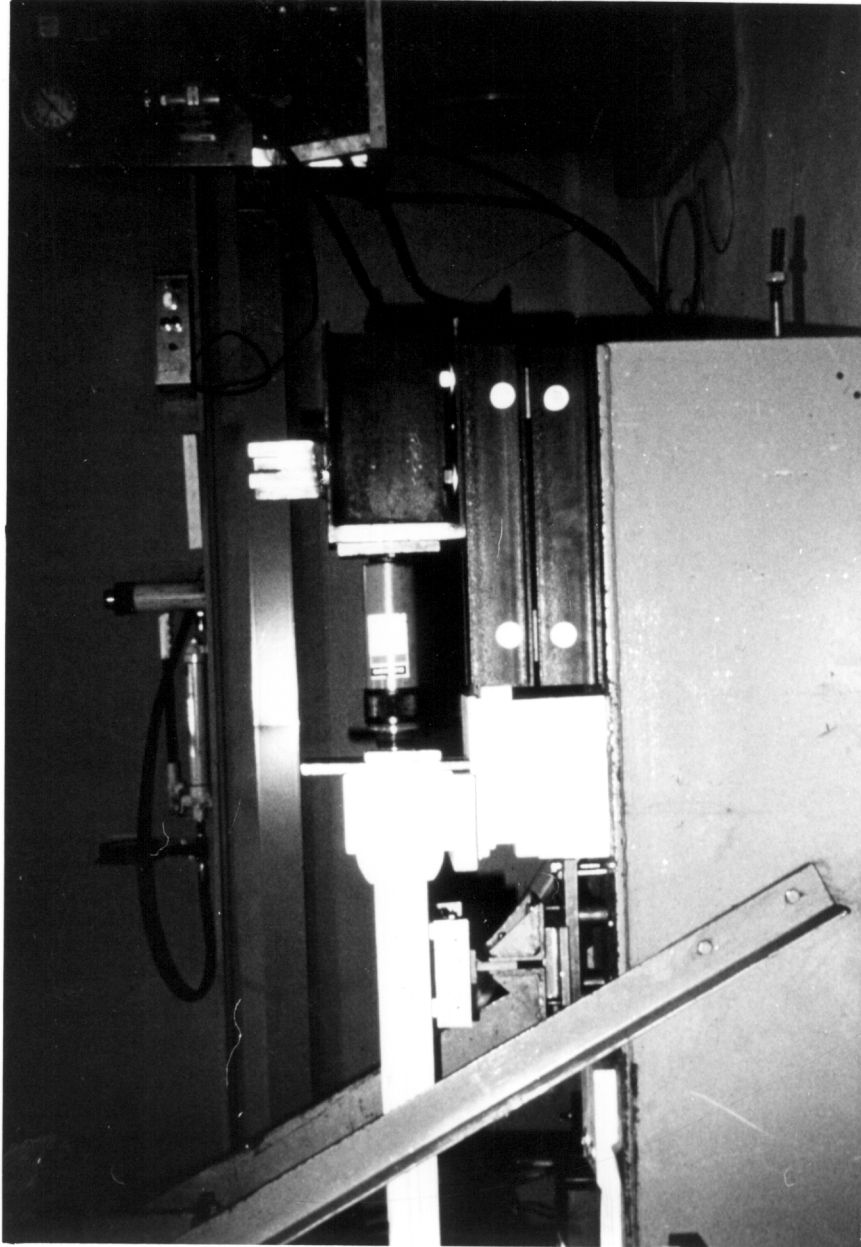


Figure 5.6 Combined bending and compression set-up for beams
--boundary condition on the side from where axial
loads were applied

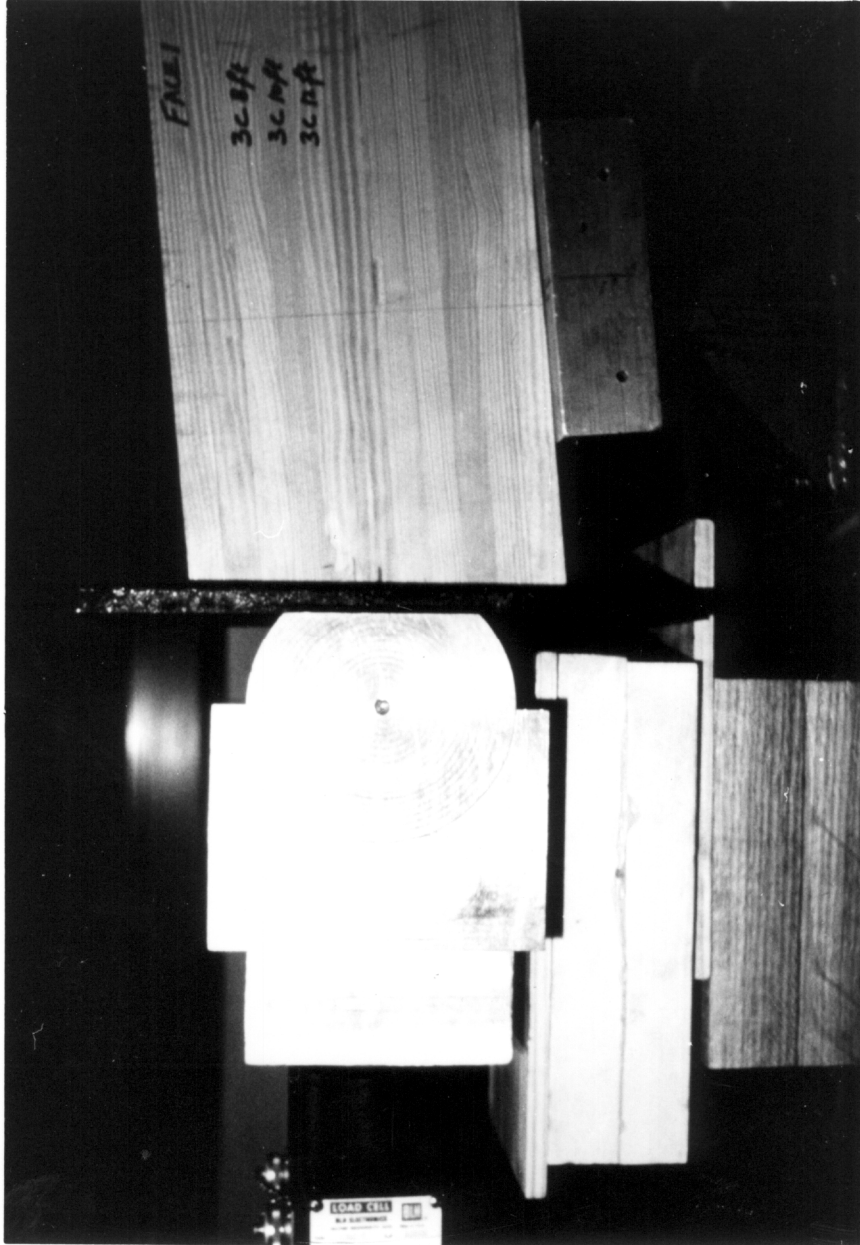


Figure 5.7 Combined bending and compression set-up --
boundary condition on the side where load cell
was placed

stressed within their linear range. Therefore, all comparisons in this study were done for bending about both the axes, and for simultaneous bending and axial compression.

Each beam was tested five times with each load condition and data was collected using load cells, clip gages, and displacement transducers. At each measurement location strain and deflection were plotted against load. For each load condition, regression lines were computed from the five test replications to relate strain to load and deflection to load at each measured location. Then the experimental and the analytical results were compared at a small and a large load at each location.

5.4.1 Simple Bending About the Major Axis

All beams were tested in simple bending about their major axis (3-axis) under two equal concentrated symmetric loads applied at third-points. Experimental and analytical results were compared at the third-point locations at loads of 250 and 500 or 750 lbs. The finite element mesh for all the beams is shown in Figure 5.8. The mesh consisted of seven elements and 15 nodes. Pinned and roller supports were used to model the experimental boundary conditions.

Tables 5.3 to 5.17 present the comparison between the measured and predicted strain for all the beams. Experimental and analytical strain values were compared at five or seven different points from the centroidal axis at each measurement location. The tables include the percent error between the experimental and the analytical values.

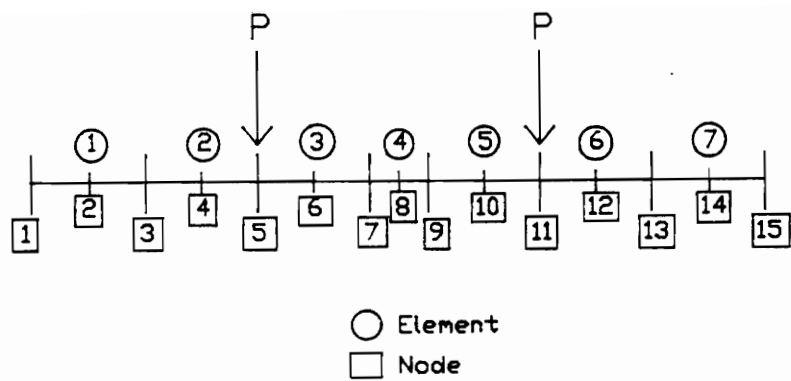


Figure 5.8 Finite element mesh used to analyze all beams in bending about the major and the minor axes

Table 5.3 Beam B1S83: Comparison of the experimental and the analytical strain in bending about the 3-axis.

LOAD (lbs.)	DISTANCE FROM CENTROIDAL AXIS (inches)	EXPERIMENTAL STRAIN (microstrain)	ANALYTICAL STRAIN (microstrain)	% ERROR

P=250	3.438	-79	-92	16.5
	2.031	-54	-54	0.0
	0.594	-21	-16	23.8
	-0.031	-7	1	85.7
	-0.781	20	21	5.0
	-2.156	59	58	1.7
	-3.578	104	96	7.7
P=500	3.438	-232	-276	19.0
	2.031	-166	-163	1.8
	0.594	-63	-48	23.8
	-0.031	-17	2	88.2
	-0.781	48	63	31.2
	-2.156	161	173	7.4
	-3.578	283	287	1.4

Table 5.4 Beam B1S114: Comparison of the experimental and the analytical strain in bending about 3-axis.

LOAD (lbs.)	DISTANCE FROM CENTROIDAL AXIS (inches)	EXPERIMENTAL STRAIN (microstrain)	ANALYTICAL STRAIN (microstrain)	% ERROR
P=250	3.438	-116	-126	8.6
	2.031	-79	-75	5.1
	0.594	-28	-22	21.4
	-0.031	-5	1	80.0
	-0.781	24	29	20.8
	-2.156	68	79	16.2
	-3.578	134	132	1.5
P=750	3.438	-348	-379	8.9
	2.031	-223	-224	0.5
	0.594	-78	-65	16.7
	-0.031	-18	3	117.0
	-0.781	64	86	34.3
	-2.156	196	238	21.4
	-3.578	365	394	7.9

Table 5.5 Beam B2S83: Comparison of the experimental and the analytical strain in bending about 3-axis.

LOAD (lbs.)	DISTANCE FROM CENTROIDAL AXIS (inches)	EXPERIMENTAL STRAIN (microstrain)	ANALYTICAL STRAIN (microstrain)	% ERROR
P=250	2.109	-168	-183	8.9
	0.688	-49	-60	22.4
	-0.063	10	6	40.0
	-0.750	69	65	5.8
	-2.141	181	185	2.2
P=750	2.109	-456	-548	20.2
	0.688	-133	-179	34.6
	-0.063	30	16	46.7
	-0.750	204	195	4.4
	-2.141	513	556	8.4

Table 5.6 Beam B2S114: Comparison of the experimental and the analytical strain in bending about 3-axis.

LOAD (lbs.)	DISTANCE FROM CENTROIDAL AXIS (inches)	EXPERIMENTAL STRAIN (microstrain)	ANALYTICAL STRAIN (microstrain)	% ERROR

P=250	2.109	-243	-251	3.3
	0.688	-70	-82	17.1
	-0.063	14	8	42.8
	-0.750	101	89	11.9
	-2.141	264	254	3.8
P=750	2.109	-626	-752	20.1
	0.688	-181	-245	35.4
	-0.063	40	22	45.0
	-0.750	278	267	4.0
	-2.141	704	763	8.4

Table 5.7 B3S83: Comparison of the experimental and the analytical strain in bending about 3-axis.

LOAD (lbs.)	DISTANCE FROM CENTROIDAL AXIS (inches)	EXPERIMENTAL STRAIN (microstrain)	ANALYTICAL STRAIN (microstrain)	% ERROR
P=250	2.766	-68	-87	27.9
	1.875	-52	-59	13.5
	0.766	-13	-24	84.6
	0.078	5	-2	140.0
	-0.719	29	23	20.7
	-1.750	56	55	1.8
	-2.688	90	85	5.6
P=750	2.766	-192	-261	35.9
	1.875	-147	-177	20.4
	0.766	-36	-72	100.0
	0.078	10	-7	170.0
	-0.719	78	68	12.8
	-1.750	149	165	10.7
	-2.688	242	254	5.0

Table 5.8 Beam B3S132: Comparison of the experimental and the analytical strain in bending about 3-axis.

LOAD (lbs.)	DISTANCE FROM CENTROIDAL AXIS (inches)	EXPERIMENTAL STRAIN (microstrain)	ANALYTICAL STRAIN (microstrain)	% ERROR

P=250	2.703	-117	-135	15.4
	1.719	-80	-86	7.5
	0.750	-38	-38	0.0
	-0.078	-9	4	144.4
	-0.797	23	40	73.9
	-1.859	63	93	47.6
	-2.828	130	142	9.2
P=750	2.703	-343	-406	18.4
	1.719	-229	-258	12.7
	0.750	-105	-113	7.6
	-0.078	-20	12	160.0
	-0.797	75	120	60.0
	-1.859	176	279	58.5
	-2.828	358	425	18.7

Table 5.9 Beam B4S83: Comparison of the experimental and the analytical strain in bending about 3-axis.

LOAD (lbs.)	DISTANCE FROM CENTROIDAL AXIS (inches)	EXPERIMENTAL STRAIN (microstrain)	ANALYTICAL STRAIN (microstrain)	% ERROR

P=250	5.844	-23	-20	13.0
	3.938	-12	-14	16.7
	1.969	-5	-7	40.0
	0.141	-2	-1	50.0
	-1.906	8	7	12.5
	-3.906	12	14	16.7
	-5.875	21	20	5.0
P=750	5.844	-61	-61	0.0
	3.938	-45	-41	8.9
	1.969	-19	-20	5.3
	0.141	-1	-1	0.0
	-1.906	17	20	17.6
	-3.906	40	41	2.5
	-5.875	66	61	7.6

Table 5.10 Beam B4S114: Comparison of the experimental and the analytical strain in bending about 3-axis.

LOAD (lbs.)	DISTANCE FROM CENTROIDAL AXIS (inches)	EXPERIMENTAL STRAIN (microstrain)	ANALYTICAL STRAIN (microstrain)	% ERROR
P=250	5.844	-26	-28	7.7
	3.938	-19	-19	0.0
	1.906	-10	-9	10.0
	0.047	2	0	100.0
	-1.906	9	9	0.0
	-3.938	18	19	5.6
	-5.922	30	28	6.7
P=750	5.844	-55	-56	1.8
	3.938	-35	-37	5.7
	1.906	-13	-18	38.5
	0.047	3	0	100.0
	-1.906	28	18	35.7
	-3.938	43	37	14.0
	-5.922	65	56	13.8

Table 5.11 Beam B4S132: Comparison of the experimental and the analytical strain in bending about 3-axis.

LOAD (lbs.)	DISTANCE FROM CENTROIDAL AXIS (inches)	EXPERIMENTAL STRAIN (microstrain)	ANALYTICAL STRAIN (microstrain)	% ERROR
P=250	5.844	-33	-32	3.0
	3.938	-23	-22	4.3
	1.906	-13	-10	23.1
	0.047	0	0	0.0
	-1.906	11	10	9.1
	-3.938	20	22	10.0
	-5.922	36	33	8.3
P=750	5.844	-85	-97	14.1
	3.938	-65	-65	0.0
	1.906	-31	-32	3.2
	0.047	0	-1	100.0
	-1.906	38	32	15.8
	-3.938	64	65	1.6
	-5.922	109	98	10.1

Table 5.12 Beam B1C83: Comparison of the experimental and the analytical strain in bending about 3-axis.

LOAD (lbs.)	DISTANCE FROM CENTROIDAL AXIS (inches)	EXPERIMENTAL STRAIN (microstrain)	ANALYTICAL STRAIN (microstrain)	% ERROR

P=250	2.562	-174	-177	1.7
	1.688	-120	-117	2.5
	0.828	-62	-57	8.1
	0.047	-3	-3	0.0
	-0.859	64	59	7.8
	-1.750	124	121	2.4
	-2.594	201	180	10.4
P=750	2.562	-435	-532	22.3
	1.688	-292	-350	19.9
	0.828	-156	-172	10.2
	0.047	-11	-10	9.1
	-0.859	158	178	12.7
	-1.750	304	363	19.4
	-2.594	483	538	11.4

Table 5.13 Beam B2C83: Comparison of the experimental and the analytical strain in bending about 3-axis.

LOAD (lbs.)	DISTANCE FROM CENTROIDAL AXIS (inches)	EXPERIMENTAL STRAIN (microstrain)	ANALYTICAL STRAIN (microstrain)	% ERROR
P=250	2.156	-202	-155	23.3
	0.813	-76	-58	23.7
	0.000	-7	0	100.0
	-0.672	48	48	0.0
	-2.063	192	148	22.9
P=750	2.156	-580	-465	19.8
	0.813	-215	-175	18.6
	0.000	-20	0	100.0
	-0.672	133	145	9.0
	-2.063	527	445	15.6

Table 5.14 Beam B2C114: Comparison of the experimental and the analytical strain in bending about 3-axis.

LOAD (lbs.)	DISTANCE FROM CENTROIDAL AXIS (inches)	EXPERIMENTAL STRAIN (microstrain)	ANALYTICAL STRAIN (microstrain)	% ERROR
P=250	2.156	-274	-213	22.3
	0.813	-102	-80	21.6
	0.000	-10	0	100.0
	-0.672	63	66	4.8
	-2.063	232	204	12.1
P=750	2.156	-797	-638	19.9
	0.813	-291	-241	17.2
	0.000	-26	0	100.0
	-0.672	186	199	7.0
	-2.063	668	611	8.5

Table 5.15 Beam B3C83: Comparison of the experimental and the analytical strain in bending about 3-axis.

LOAD (lbs.)	DISTANCE FROM CENTROIDAL AXIS (inches)	EXPERIMENTAL STRAIN (microstrain)	ANALYTICAL STRAIN (microstrain)	% ERROR
P=250	3.266	-55	-61	10.9
	2.266	-48	-42	12.5
	1.250	-18	-23	27.8
	0.063	-3	-1	68.7
	-1.188	20	22	10.0
	-2.234	36	42	16.7
	-3.203	69	60	13.0
P=750	3.266	-162	-182	12.3
	2.266	-128	-127	1.0
	1.250	-50	-70	4.0
	0.063	-4	-4	0.0
	-1.188	61	66	8.2
	-2.234	104	125	20.2
	-3.203	195	179	8.2

Table 5.16 Beam B3C114: Comparison of the experimental and the analytical strain in bending about 3-axis.

LOAD (lbs.)	DISTANCE FROM CENTROIDAL AXIS (inches)	EXPERIMENTAL STRAIN (microstrain)	ANALYTICAL STRAIN (microstrain)	% ERROR

P=250	3.297	-72	-84	16.7
	2.312	-66	-59	10.6
	1.312	-32	-34	6.2
	0.078	-13	-2	84.6
	-1.250	25	32	28.0
	-2.250	48	58	20.8
	-3.250	84	83	1.2
P=750	3.297	-220	-253	15.0
	2.312	-193	-178	7.8
	1.312	-94	-101	7.4
	0.078	-33	-6	81.8
	-1.250	75	96	28.0
	-2.250	142	173	21.8
	-3.250	242	250	3.3

Table 5.17 Beam B3C132: Comparison of the experimental and the analytical strain in bending about 3-axis.

LOAD (lbs.)	DISTANCE FROM CENTROIDAL AXIS (inches)	EXPERIMENTAL STRAIN (microstrain)	ANALYTICAL STRAIN (microstrain)	% ERROR
P=250	3.297	-77	-98	27.3
	2.312	-75	-68	9.3
	1.312	-38	-39	2.6
	0.078	-18	-2	88.9
	-1.250	29	37	27.6
	-2.250	62	67	8.1
	-3.250	102	96	5.9
P=750	3.297	-253	-293	15.8
	2.312	-221	-206	6.8
	1.312	-111	-117	5.4
	0.078	-46	-7	84.8
	-1.250	79	111	40.5
	-2.250	173	200	15.6
	-3.250	282	289	2.5

For all beams, the largest difference between the experimental and the analytical results occurred near the centroidal axis. The reason for this discrepancy was probably due to the small magnitude of strain in the vicinity of the neutral axis. Accurately measuring such small strains is beyond the capability of the clip-on transducers used in this study. However, the experimental and the analytical results agree very well at most locations away from the neutral axis. Generally, as the strain increased the error decreased (i.e. at points located further from the neutral axis). There were a few locations where the error was between 15% and 35%. The strain distribution through the depth of a beam is influenced by the properties of each lamina and the material inhomogeneity within the lamina. In most cases, the absolute value of the analytical predictions were greater than the experimentally measured strain. This was true especially in the lower half of the beams where tensile stresses are present. When a glulam beam is loaded in bending below the proportional limit, strain is assumed to vary linearly through the depth. Within the linear elastic region, stress is proportional to strain throughout the cross sections of the beams. The modulus of elasticity is a material property that relates these two quantities. Therefore, if the moduli of elasticity of two adjacent laminae are not equal, there will be a stress discontinuity. Although the strains in two adjacent laminae are equal at the interface, a greater stress develops in the stiffer lamina.

Figures 5.9, 5.10, 5.11, 5.12, 5.13, 5.14 show the experimental and the analytical strain through the depth in straight (Figures 5.9-5.11) and curved beams (Figures 5.12-5.14) at two magnitudes of loads. Figures 5.15, 5.16, 5.17, 5.18, 5.19, and 5.20 show the comparison between measured and predicted deflections along the length of the beams.

Deflections were measured at three locations along the length of the beams. Deflection was always measured at the mid-point of the beam span. Tables 5.18 to 5.32 present the deflection measurements for all the beams tested in simple bending about the major axis. There was very good agreement between the experimental and the analytical deflections. The majority of the analytical results differed from measured deflections by less than 10%. Generally, the analytical predictions were greater than the experimental measurements indicating that the model was conservative.

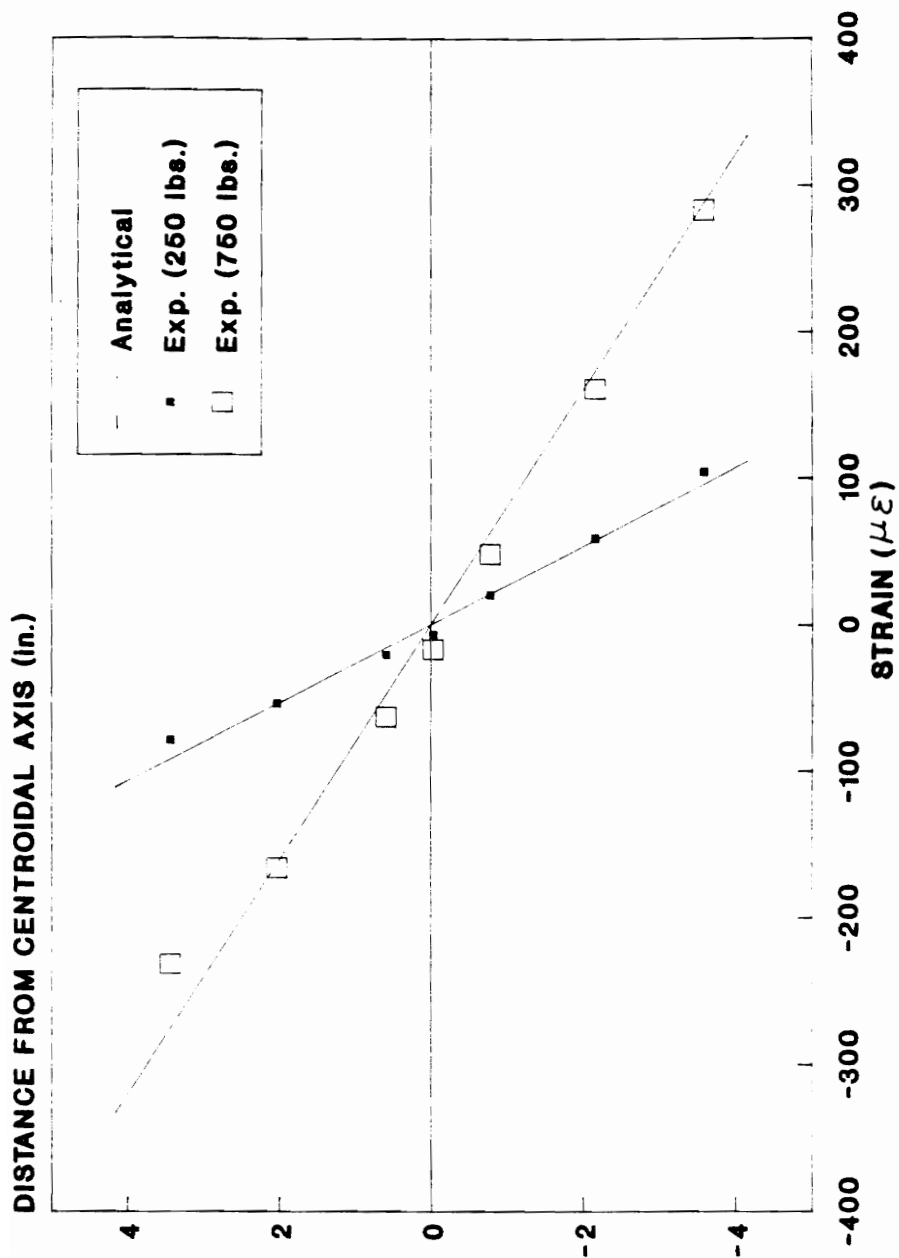


Figure 5.9 Comparison of the experimental and the analytical normal strain in beam B1S83 under bending in the direction of 2-axis

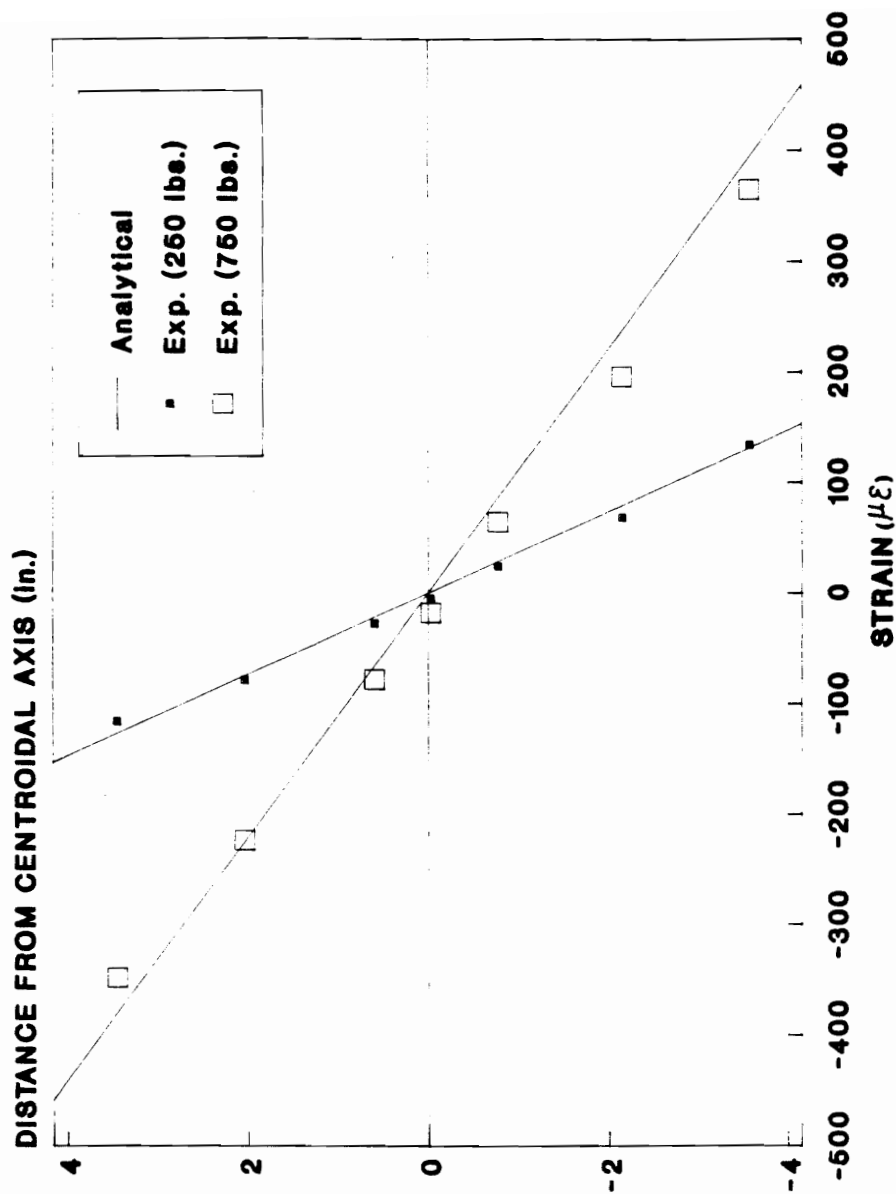


Figure 5.10 Comparison of the experimental and the analytical normal strain in beam B1S114 under bending in the direction of 2-axis

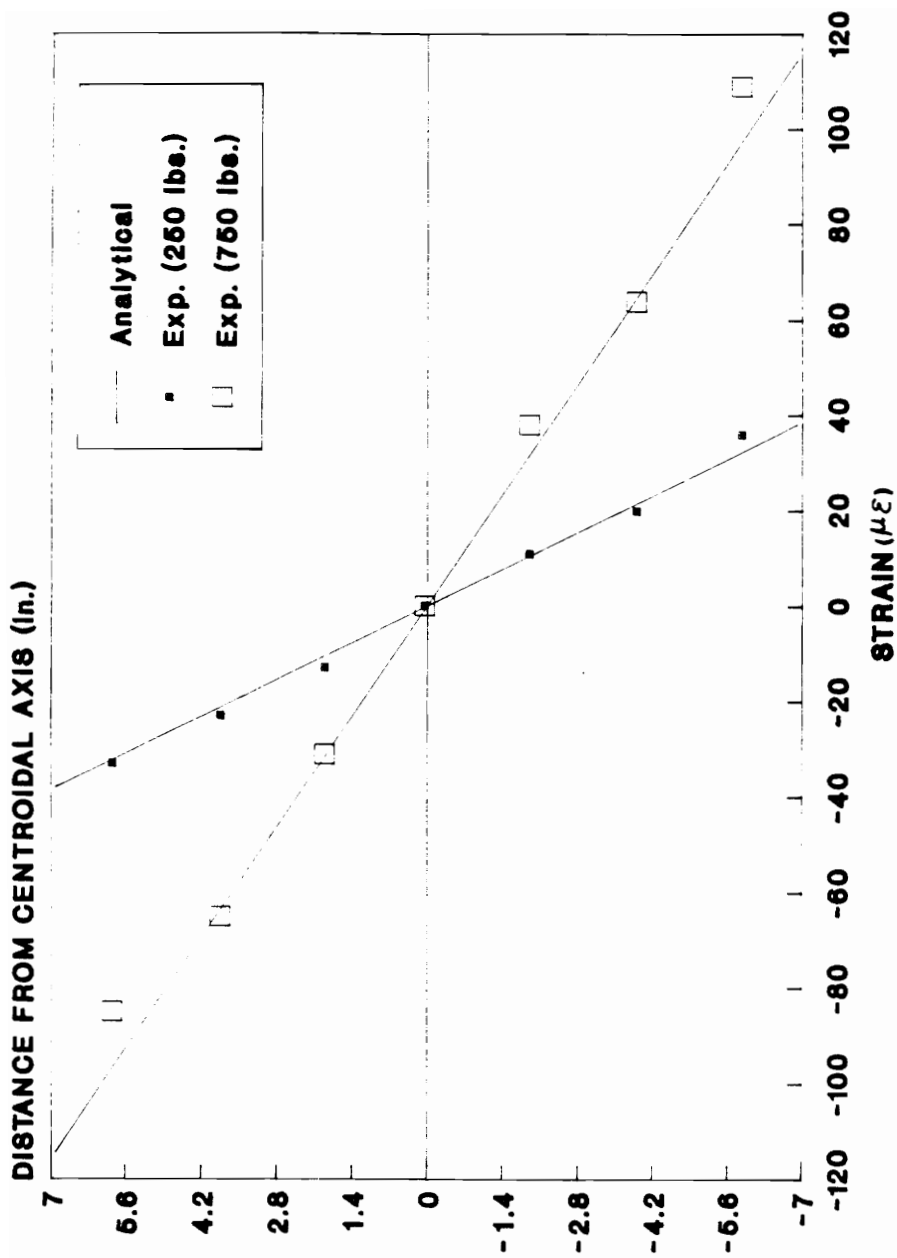


Figure 5.11 Comparison of the experimental and the analytical normal strain in beam B4S132 under bending in the direction of 2-axis

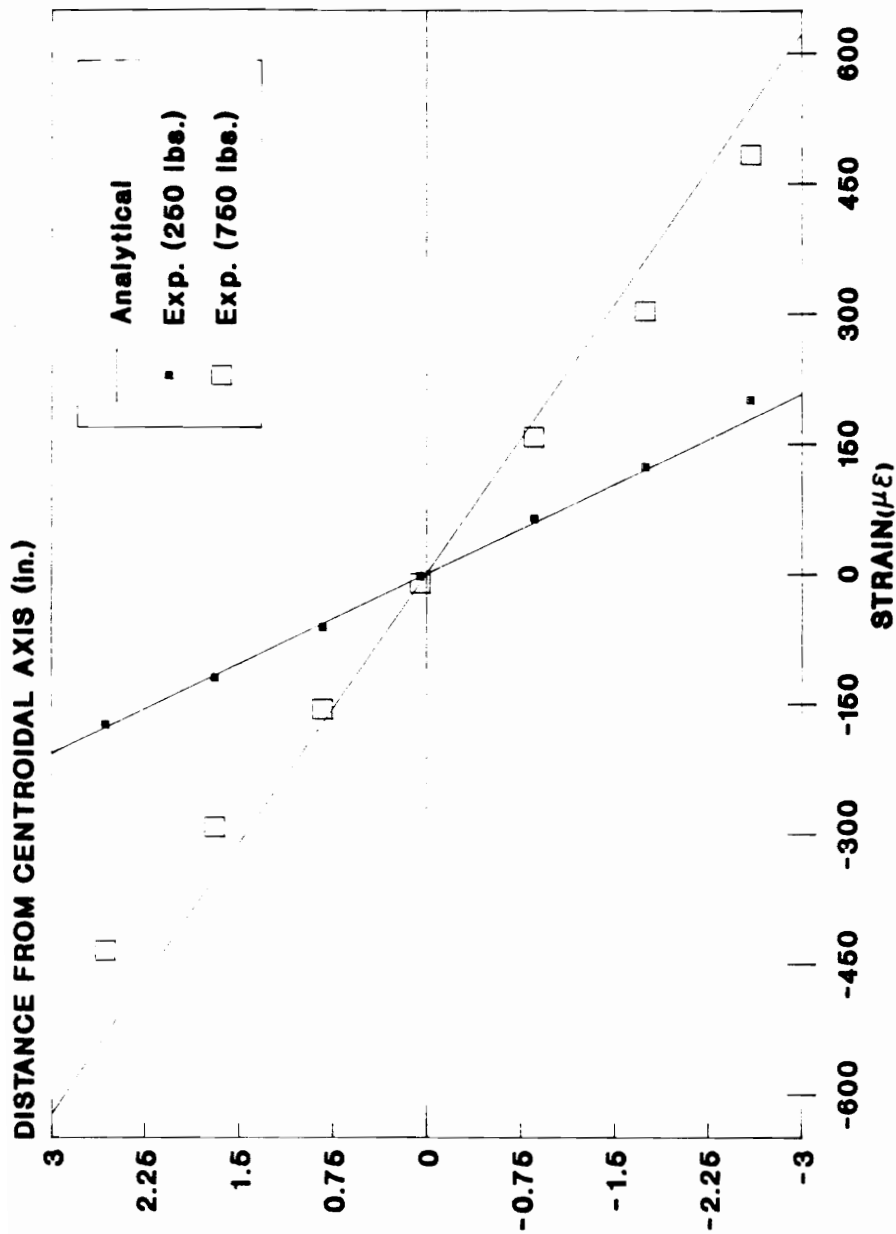


Figure 5.12 Comparison of the experimental and the analytical normal strain in beam B1C83 under bending in the direction of 2-axis

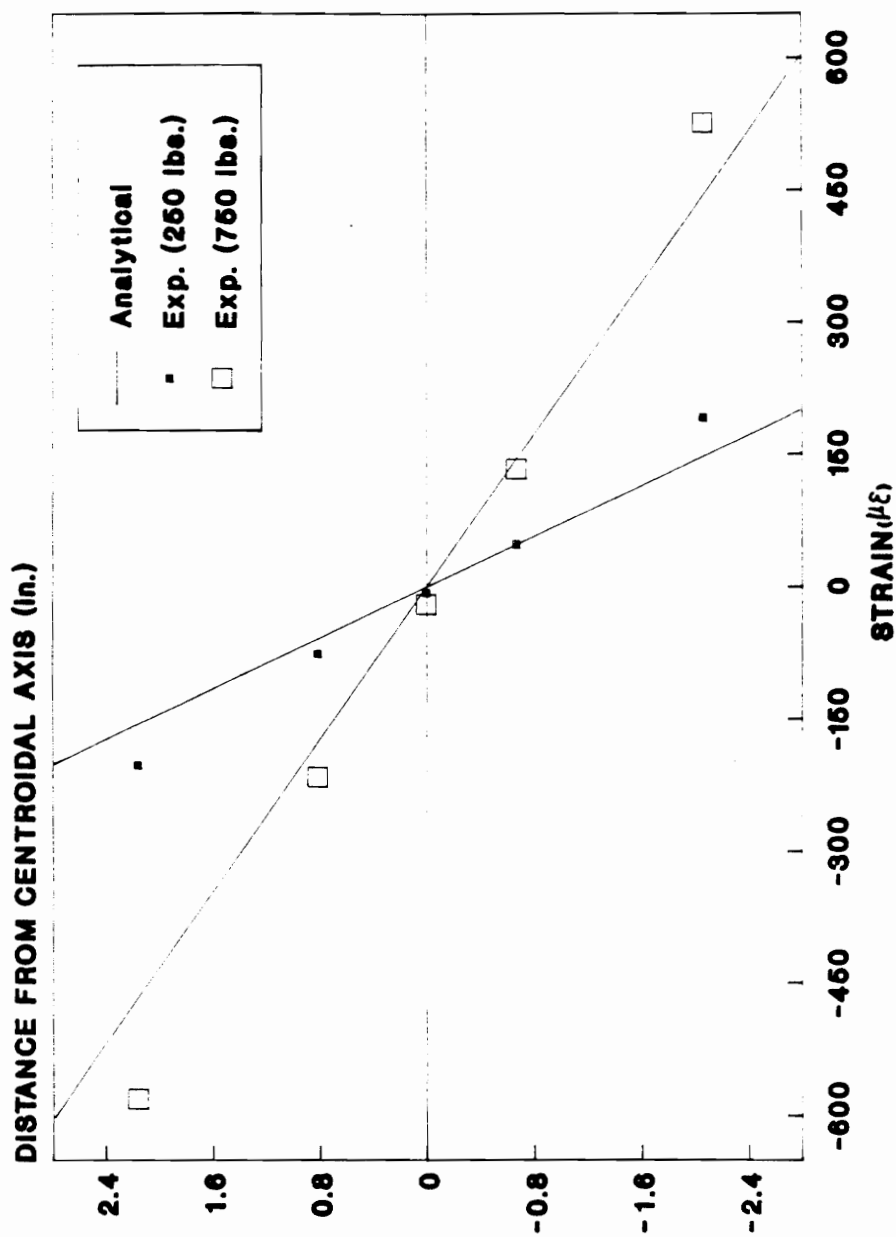


Figure 5.13 Comparison of the experimental and the analytical normal strain in beam B2C83 under bending in the direction of 2-axis

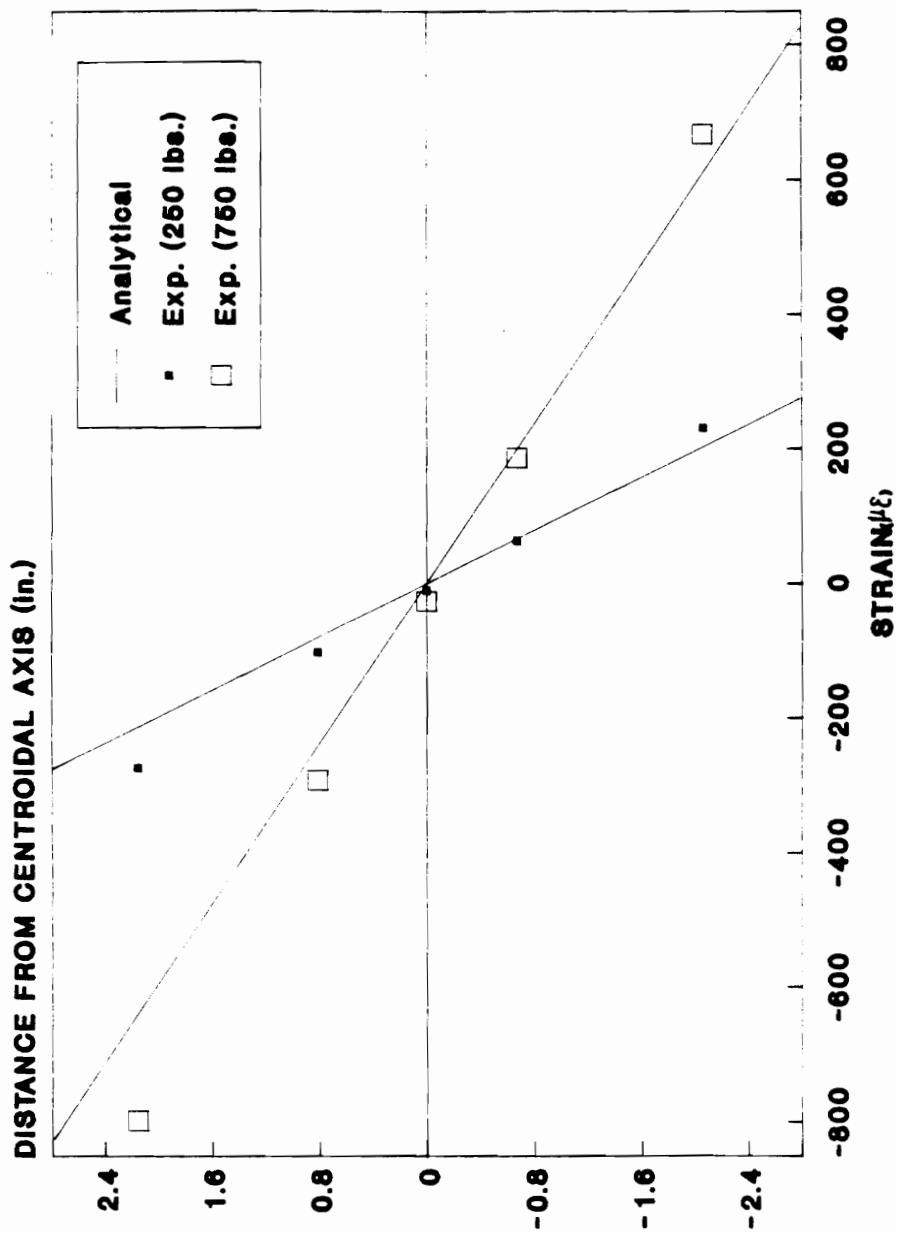


Figure 5.14 Comparison of the experimental and the analytical normal strain in beam B2C114 under bending in the direction of 2-axis

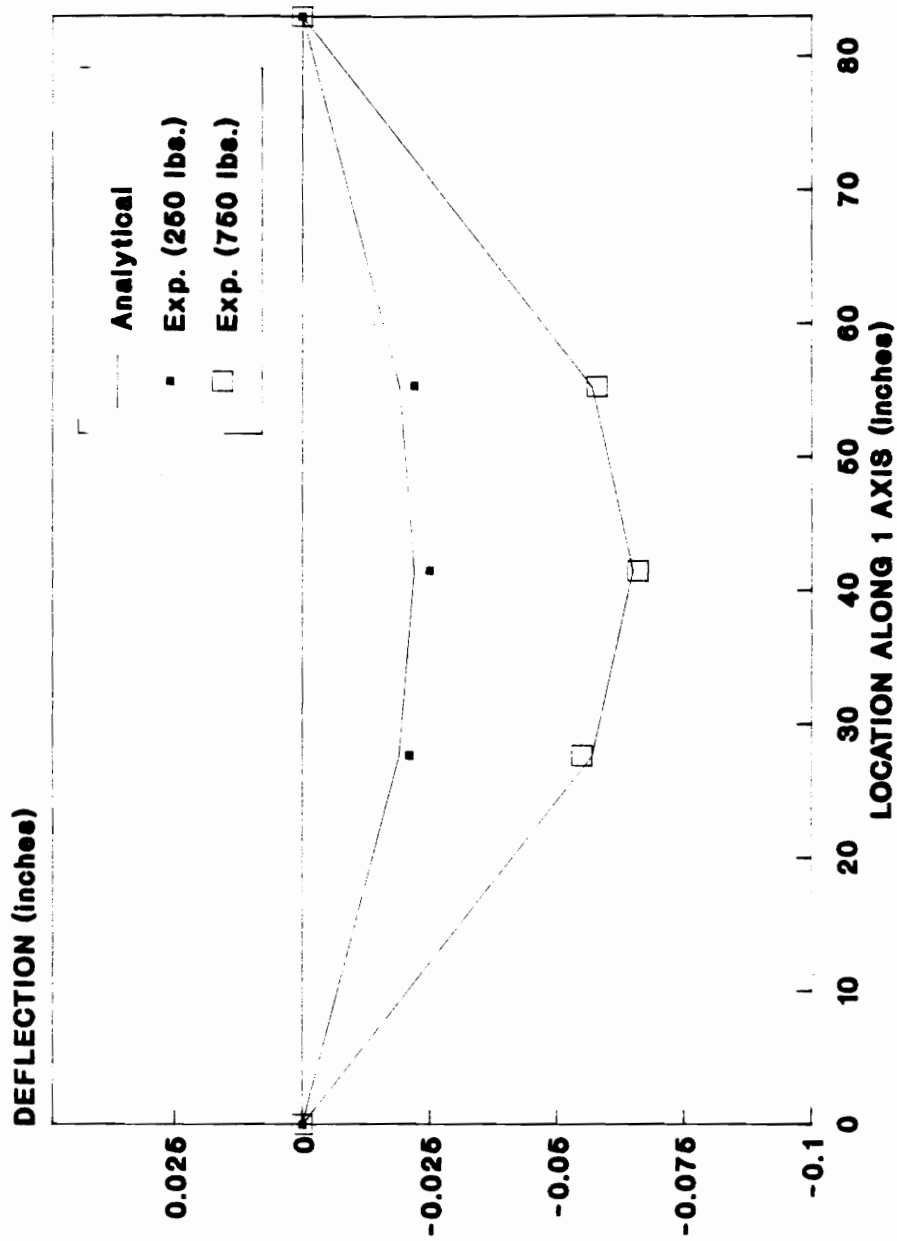


Figure 5.15 Comparison of the experimental and the analytical deflections for beam B1S83 under bending in the direction of 2-axis

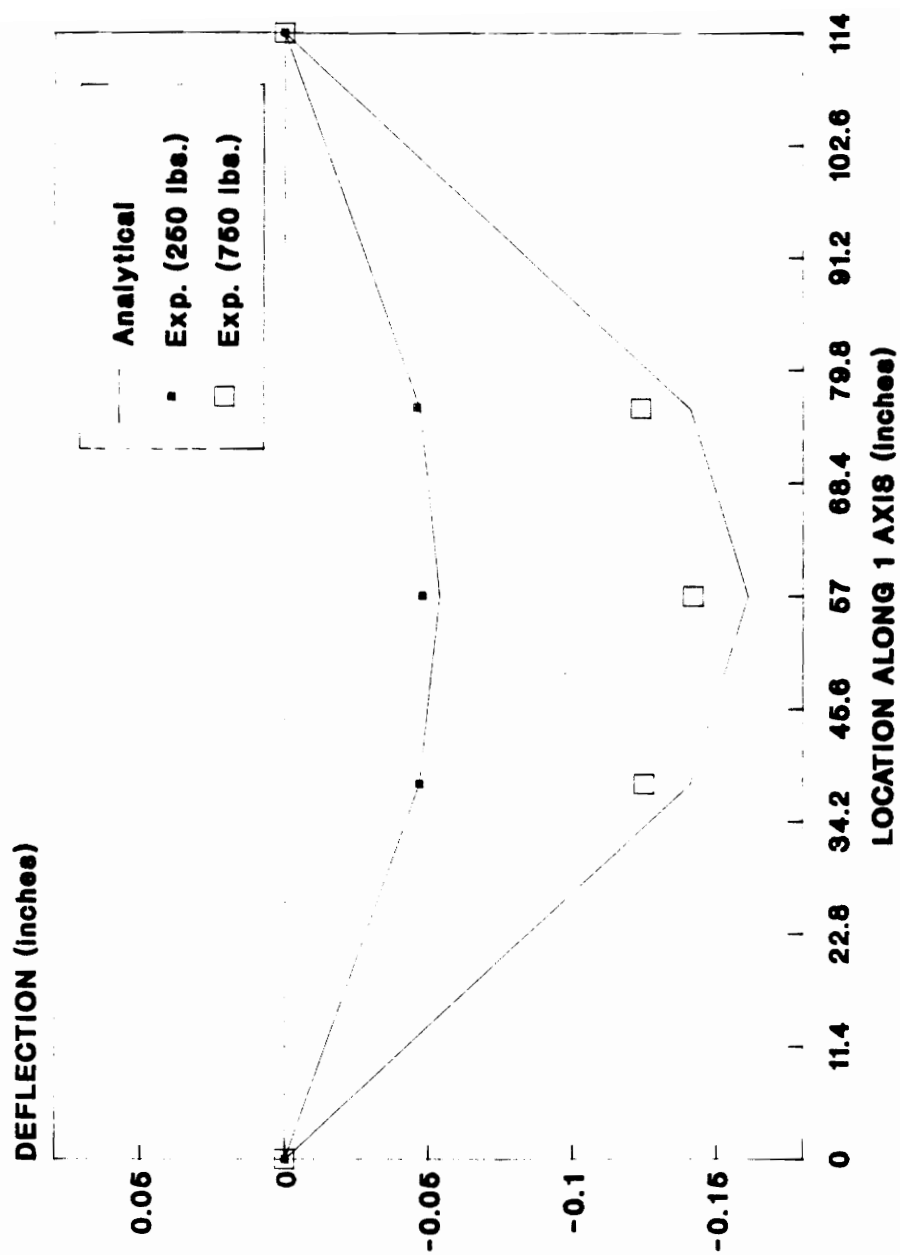


Figure 5.16 Comparison of the experimental and the analytical deflections for beam B1S114 under bending in the direction of 2-axis

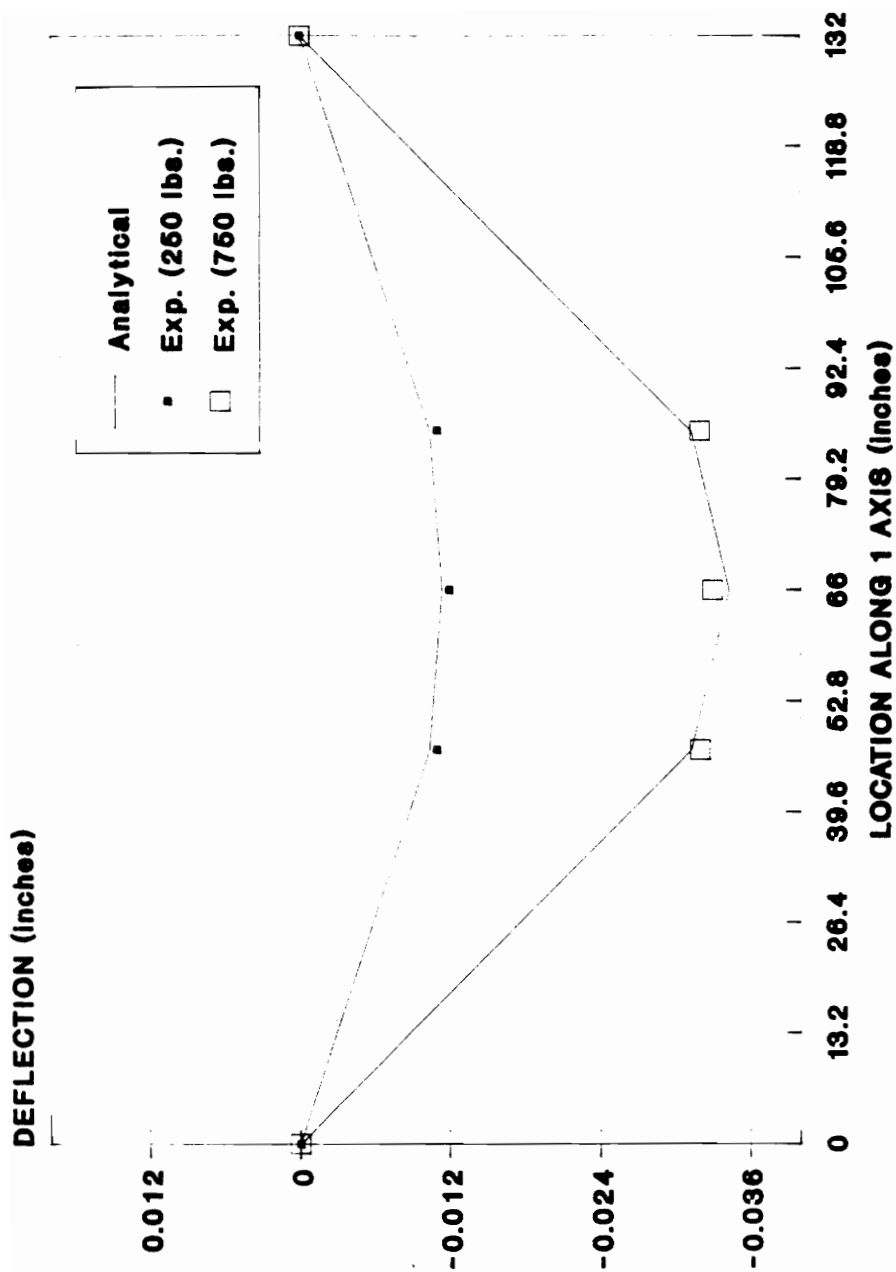


Figure 5.17 Comparison of the experimental and the analytical deflections for beam B4S132 under bending in the direction of 2-axis

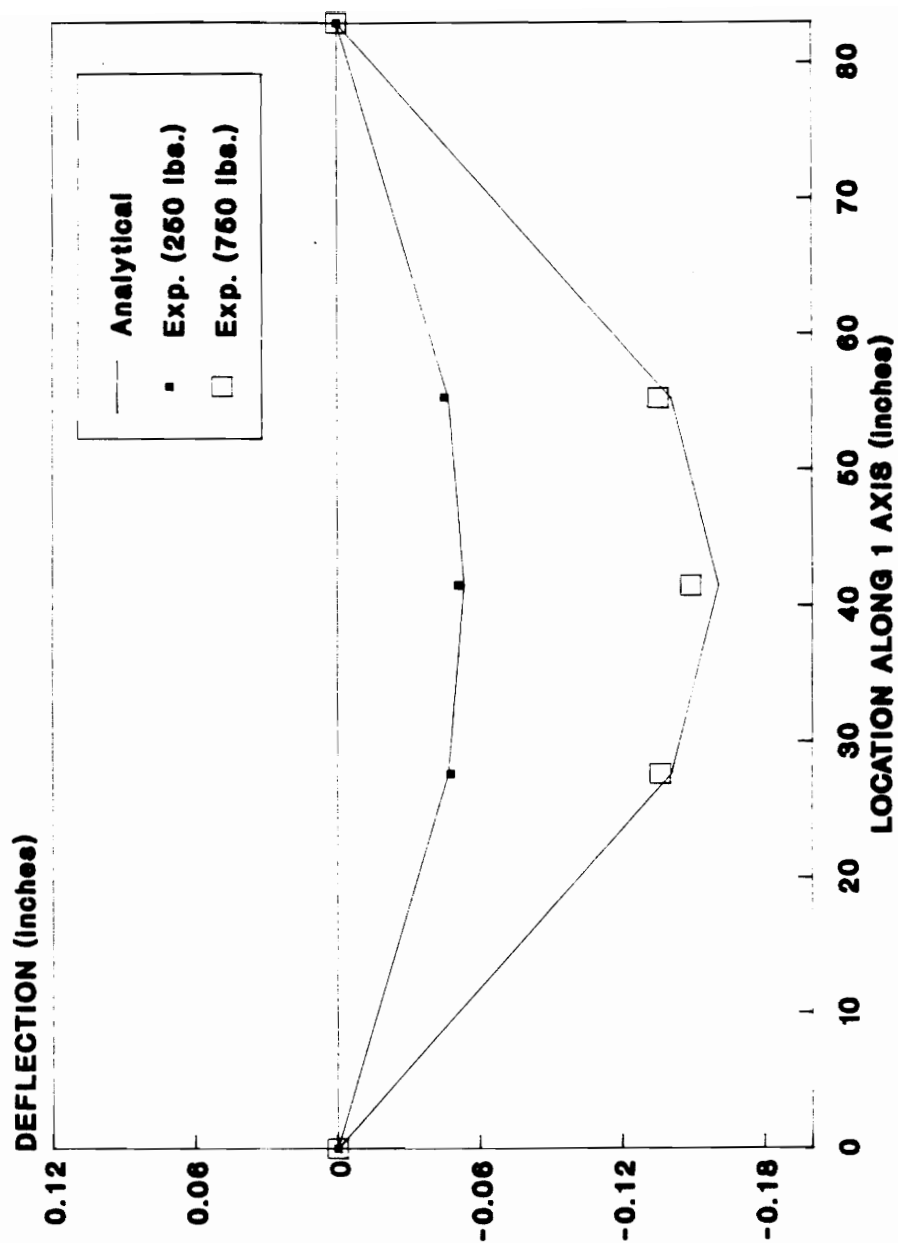


Figure 5.18 Comparison of the experimental and the analytical deflections for beam B1C83 under bending in the direction of 2-axis

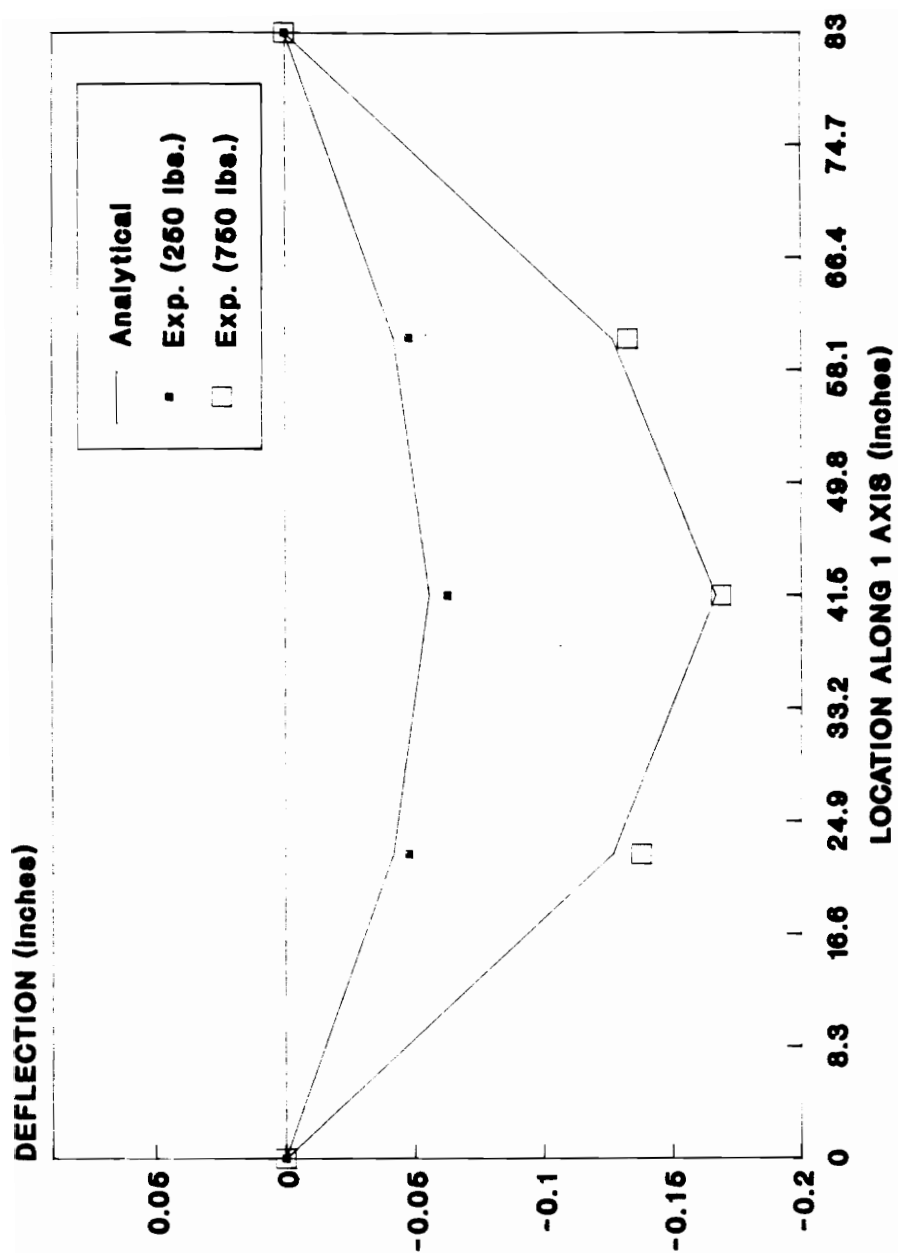


Figure 5.19 Comparison of the experimental and the analytical deflections for beam B2C83 under bending in the direction of 2-axis

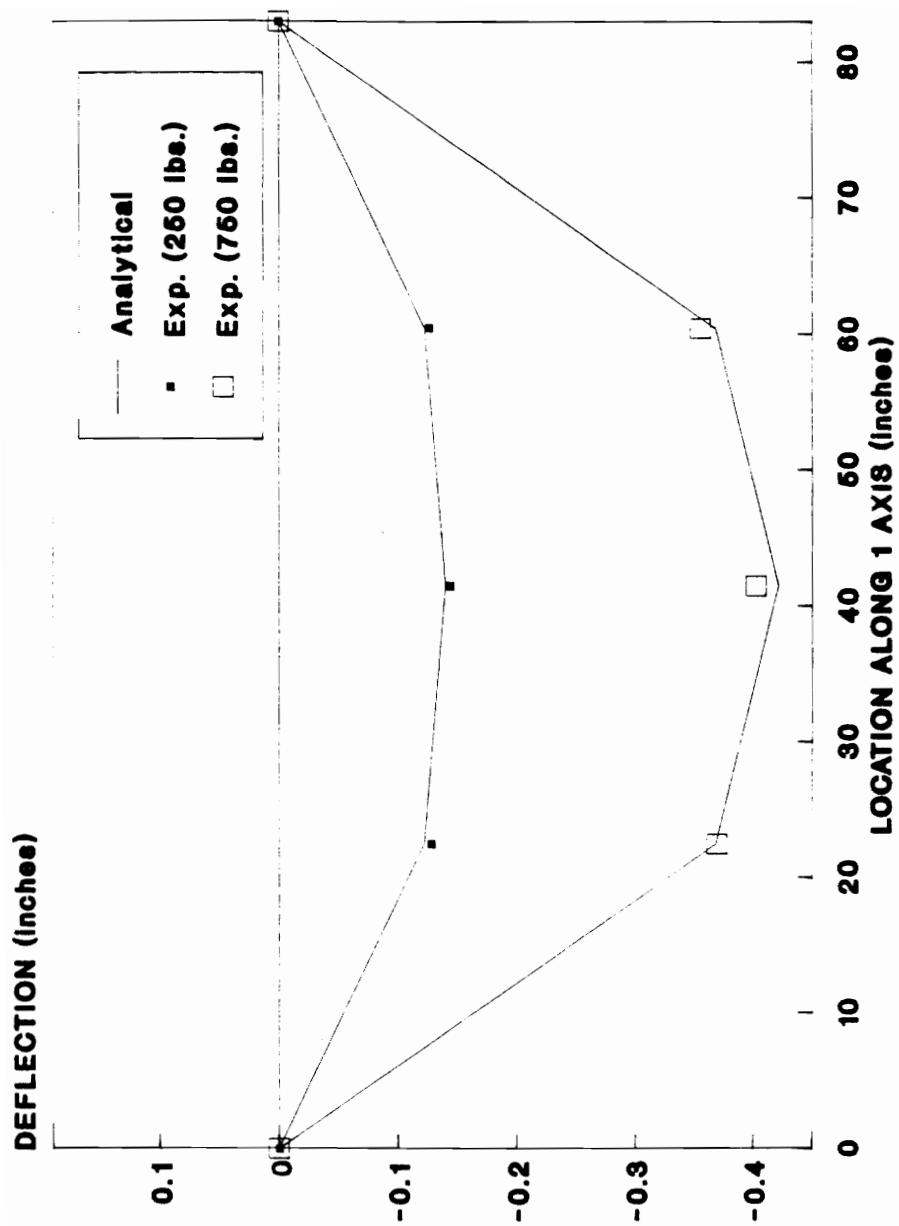


Figure 5.20 Comparison of the experimental and the analytical deflections for beam B2C114 under bending in the direction of 2-axis

Table 5.18 Beam B1S83: Comparison of the experimental and the analytical deflections in bending about 3-axis.

LOAD (lbs.)	LOCATION LENGTHWISE (inches)	EXPERIMENTAL DEFLECTION (inches)	ANALYTICAL DEFLECTION (inches)	ERROR %
P=250	27.67	-0.021	-0.019	9.5
	41.50	-0.025	-0.022	12.0
	55.33	-0.022	-0.019	13.6
P=750	27.67	-0.055	-0.057	3.6
	41.50	-0.066	-0.065	1.5
	55.33	-0.058	-0.057	1.7

All the experimental strain results presented above were measured only on one side of the beams. Strain measured on both the sides are presented for straight beam S2 and curved beam C3 tested over a span of 83 inches (Figures 5.21 and 5.22). Due to the varying modulus of elasticity across the width of a beam, the strain values of the two faces differed slightly. However, the strain distribution of both the faces show similar trends.

5.4.2 Simple Bending About the Minor Axis

Biaxial bending stresses can be simulated by testing a beam separately under simple bending about both its major and minor axes provided that the stresses are kept below the proportional limit. In this study, in comparing the experimental and the analytical strain and deflection values, the method of superposition was assumed to be valid. Therefore, simple bending about the two principal axes of the cross-section was conducted and the results were compared instead of directly performing biaxial bending tests. In this section, the experimental and the analytical values for flatwise bending (bending about the minor axis) are presented. Only three straight beams were subjected to flatwise bending. A finite element mesh similar to Figure 5.8 was used to analyze a beam subjected to edgewise bending. Pin and roller supports were used to model the experimental boundary conditions.

Table 5.19 Beam B1S114: Comparison of the experimental and the analytical deflections in bending about 3-axis.

LOAD (lbs.)	LOCATION LENGTHWISE (inches)	EXPERIMENTAL DEFLECTION (inches)	ANALYTICAL DEFLECTION (inches)	ERROR %

P=250	38.00	-0.047	-0.047	0.0
	57.00	-0.048	-0.054	12.5
	76.00	-0.046	-0.047	2.2
P=750	38.00	-0.125	-0.141	12.8
	57.00	-0.142	-0.161	13.4
	76.00	-0.124	-0.141	13.7

Table 5.20 Beam B2S83: Comparison of the experimental and the analytical deflections in bending about 3-axis.

LOAD (lbs.)	LOCATION LENGTHWISE (inches)	EXPERIMENTAL DEFLECTION (inches)	ANALYTICAL DEFLECTION (inches)	ERROR %
P=250	22.50	-0.050	-0.050	0.0
	41.50	-0.061	-0.067	9.8
	60.50	-0.049	-0.050	2.0
P=750	22.50	-0.138	-0.151	9.4
	41.50	-0.177	-0.200	13.0
	60.50	-0.139	-0.151	8.6

Table 5.21 Beam B2S114: Comparison of the experimental and the analytical deflections in bending about 3-axis.

LOAD (lbs.)	LOCATION LENGTHWISE (inches)	EXPERIMENTAL DEFLECTION (inches)	ANALYTICAL DEFLECTION (inches)	ERROR %
P=250	38.00	-0.146	-0.147	0.7
	57.00	-0.165	-0.169	2.4
	76.00	-0.145	-0.147	1.4
P=750	38.00	-0.391	-0.442	13.0
	57.00	-0.432	-0.506	17.1
	76.00	-0.386	-0.442	14.5

Table 5.22 Beam B3S83: Comparison of the experimental and the analytical deflections in bending about 3-axis.

LOAD (lbs.)	LOCATION LENGTHWISE (inches)	EXPERIMENTAL DEFLECTION (inches)	ANALYTICAL DEFLECTION (inches)	ERROR %
P=250	22.50	-0.017	-0.019	11.8
	41.50	-0.023	-0.025	8.7
	60.50	-0.020	-0.019	5.0
P=750	22.50	-0.049	-0.056	14.3
	41.50	-0.064	-0.074	15.6
	60.50	-0.052	-0.056	7.7

Table 5.23 Beam B3S132: Comparison of the experimental and the analytical deflections in bending about 3-axis.

LOAD (lbs.)	LOCATION LENGTHWISE (inches)	EXPERIMENTAL DEFLECTION (inches)	ANALYTICAL DEFLECTION (inches)	ERROR %

P=250	47.00	-0.090	-0.086	4.4
	66.00	-0.097	-0.095	2.1
	85.00	-0.087	-0.086	1.1
P=750	47.00	-0.235	-0.259	10.2
	66.00	-0.260	-0.286	10.0
	85.00	-0.227	-0.259	14.1

Table 5.24 Beam B4S83: Comparison of the experimental and the analytical deflections in bending about 3-axis.

LOAD (lbs.)	LOCATION LENGTHWISE (inches)	EXPERIMENTAL DEFLECTION (inches)	ANALYTICAL DEFLECTION (inches)	ERROR %
P=250	22.50	-0.002	-0.002	0.0
	41.50	-0.004	-0.003	25.0
	60.50	-0.002	-0.002	0.0
P=750	22.50	-0.009	-0.008	11.1
	41.50	-0.011	-0.010	9.1
	60.50	-0.010	-0.008	20.0

Table 5.25 Beam B4S114: Comparison of the experimental and the analytical deflections in bending about 3-axis.

LOAD (lbs.)	LOCATION LENGTHWISE (inches)	EXPERIMENTAL DEFLECTION (inches)	ANALYTICAL DEFLECTION (inches)	ERROR %

P=250	38.00	-0.008	-0.007	12.5
	57.00	-0.009	-0.008	11.1
	76.00	-0.007	-0.007	0.0
P=750	38.00	-0.022	-0.020	9.1
	57.00	-0.023	-0.023	0.0
	76.00	-0.021	-0.020	4.8

Table 5.26 Beam B4S132: Comparison of the experimental and the analytical deflections in bending about 3-axis.

LOAD (lbs.)	LOCATION LENGTHWISE (inches)	EXPERIMENTAL DEFLECTION (inches)	ANALYTICAL DEFLECTION (inches)	ERROR %
P=250	47.00	-0.011	-0.010	9.1
	66.00	-0.012	-0.011	8.3
	85.00	-0.011	-0.010	9.1
P=750	47.00	-0.032	-0.031	3.1
	66.00	-0.033	-0.034	3.0
	85.00	-0.032	-0.031	3.1

Table 5.27 Beam B1C83: Comparison of the experimental and the analytical deflections in bending about 3-axis.

LOAD (lbs.)	LOCATION LENGTHWISE (inches)	EXPERIMENTAL DEFLECTION (inches)	ANALYTICAL DEFLECTION (inches)	ERROR %
P=250	27.67	-0.048	-0.047	2.1
	41.50	-0.051	-0.054	5.9
	55.33	-0.045	-0.047	4.4
P=750	27.67	-0.136	-0.141	3.7
	41.50	-0.149	-0.161	8.1
	55.33	-0.136	-0.141	3.7

Table 5.28 Beam B2C83: Comparison of the experimental and the analytical deflections in bending about 3-axis.

LOAD (lbs.)	LOCATION LENGTHWISE (inches)	EXPERIMENTAL DEFLECTION (inches)	ANALYTICAL DEFLECTION (inches)	ERROR %
P=250	22.50	-0.048	-0.042	12.5
	42.50	-0.063	-0.056	11.1
	60.50	-0.048	-0.042	12.5
P=750	22.50	-0.138	-0.127	8.0
	42.50	-0.169	-0.167	1.2
	60.50	-0.133	-0.127	4.5

Table 5.29 Beam B2C114: Comparison of the experimental and the analytical deflections in bending about 3-axis.

LOAD (lbs.)	LOCATION LENGTHWISE (inches)	EXPERIMENTAL DEFLECTION (inches)	ANALYTICAL DEFLECTION (inches)	ERROR %

P=250	22.50	-0.129	-0.123	4.6
	41.50	-0.145	-0.141	2.8
	60.50	-0.127	-0.123	3.1
P=750	22.50	-0.370	-0.369	0.3
	41.50	-0.403	-0.422	4.7
	60.50	-0.356	-0.369	3.7

Table 5.30 Beam B3C83: Comparison of the experimental and the analytical deflections in bending about 3-axis.

LOAD (lbs.)	LOCATION LENGTHWISE (inches)	EXPERIMENTAL DEFLECTION (inches)	ANALYTICAL DEFLECTION (inches)	ERROR %
P=250	22.50	-0.013	-0.011	15.4
	41.50	-0.017	-0.015	11.8
	60.50	-0.010	-0.011	10.0
P=750	22.50	-0.037	-0.034	8.1
	41.50	-0.048	-0.045	6.2
	60.50	-0.037	-0.034	8.1

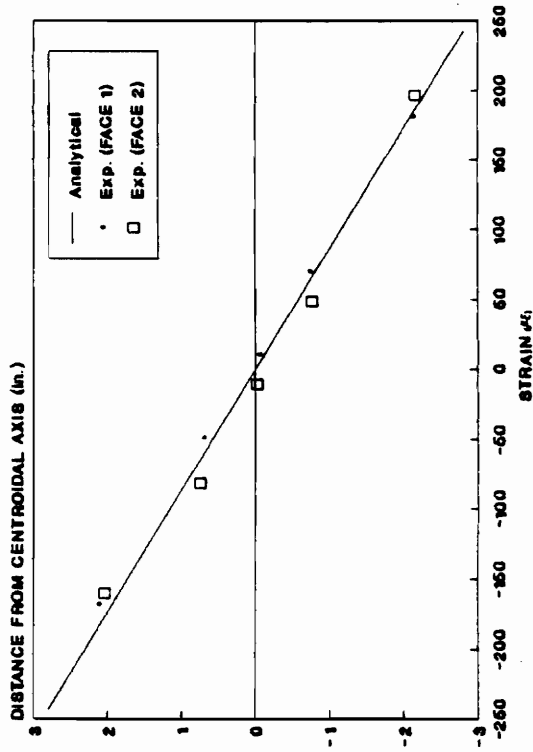
Table 5.31 Beam B3C114: Comparison of the experimental and the analytical deflections in bending about 3-axis.

LOAD (lbs.)	LOCATION LENGTHWISE (inches)	EXPERIMENTAL DEFLECTION (inches)	ANALYTICAL DEFLECTION (inches)	ERROR %
P=250	38.00	-0.031	-0.033	6.4
	57.00	-0.035	-0.037	5.7
	76.00	-0.033	-0.033	0.0
P=750	38.00	-0.095	-0.098	3.2
	57.00	-0.102	-0.112	9.8
	76.00	-0.090	-0.098	8.9

Table 5.32 Beam B3C132: Comparison of the experimental and the analytical deflections in bending about 3-axis.

LOAD (lbs.)	LOCATION LENGTHWISE (inches)	EXPERIMENTAL DEFLECTION (inches)	ANALYTICAL DEFLECTION (inches)	ERROR %
P=250	47.00	-0.051	-0.052	2.0
	66.00	-0.055	-0.057	3.6
	85.00	-0.052	-0.052	0.0
P=750	47.00	-0.142	-0.156	9.8
	66.00	-0.163	-0.172	5.5
	85.00	-0.146	-0.156	6.8

P = 250 lbs.



P = 750 lbs.

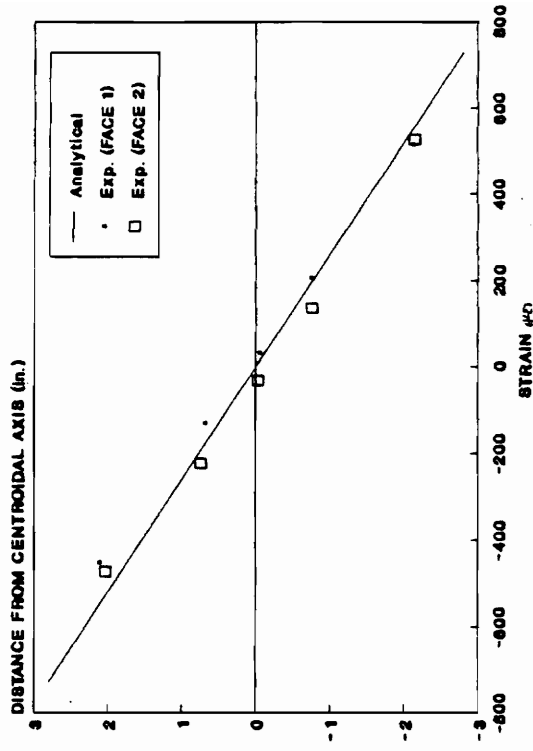
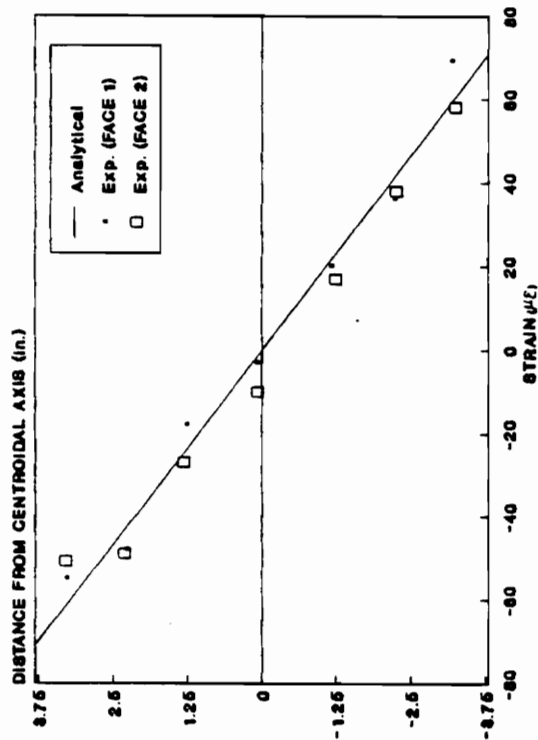


Figure 5.21 Beam B2S83 -- comparison of strain distribution between faces 1 and 2 under bending in the direction of 2-axis

P = 250 lbs.



P = 750 lbs.

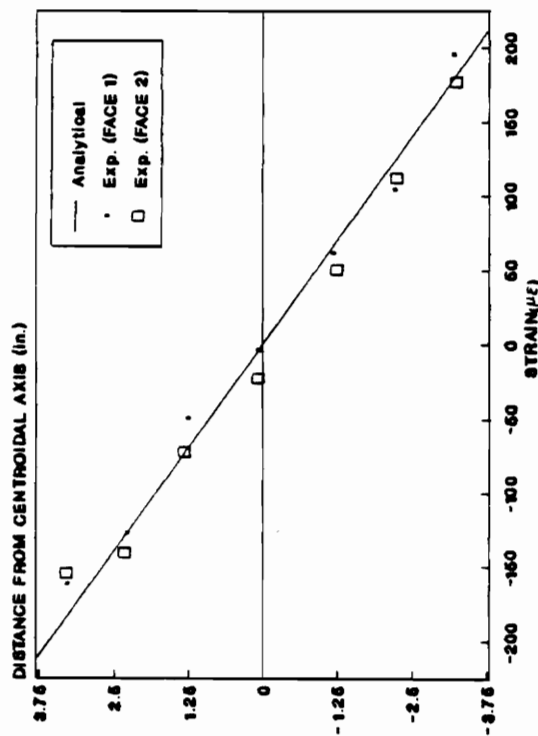


Figure 5.22 Beam B3C83 -- comparison of strain distribution between faces 1 and 2 under bending in the direction of 2-axis

Tables 5.33 to 5.38 present the comparison of the experimental and the analytical strain results at two magnitudes of third-point loads. Beams were subjected to two equal concentrated symmetric loads at third-points. Except for the locations adjacent to or directly on the centroidal axis, the experimental and the analytical strain values showed good agreement. The percent error (difference between experimental and analytical strain) at most locations was less than 10%. Figure 5.23 shows a typical strain distribution in a straight beam subjected to flatwise bending.

Tables 5.39 to 5.44 compare the experimental and the analytical deflection readings of the straight beams in flatwise bending. Except for beam B1S (span of 114 inches), there was good agreement between the deflections at 250 lbs. However, at 750 lbs the experimental and the analytical deflections of beams B1S (span = 114 inches), B2S (span = 114 inches), and B3S (span = 83 inches) differed by 12% to 25%. Figure 5.24 shows a typical comparison between the experimental and the analytical deflections at three locations along the length of a straight beam. The principal of superposition was not used to combine the edgewise and the flatwise bending strain to obtain biaxial bending strain because of the way the strains were measured experimentally. It was not possible to measure strain at the same location in both edgewise and flatwise bending.

5.4.3 Combined Bending and Compression

Beams B1S, B2S, B3S, B1C, B2C, and B3C were subjected to combined stresses. Straight beams were tested in bending about the major axis and compression, as well as, in bending about the minor axis and compression. Whereas, curved beams were only tested in bending about the

Table 5.33 Beam B1S83: Comparison of the experimental and the analytical strain in bending about 2-axis.

LOAD (lbs.)	DISTANCE FROM CENTROIDAL AXIS (inches)	EXPERIMENTAL STRAIN (microstrain)	ANALYTICAL STRAIN (microstrain)	% ERROR
P=250	1.031	-250	-212	15.2
	0.031	-24	-6	75.0
	-1.000	193	205	6.2
P=500	1.031	-464	-424	8.6
	0.031	-51	-13	74.5
	-1.000	363	411	13.2

Table 5.34 Beam B1S114: Comparison of the experimental and the analytical strain in bending about 2-axis.

LOAD (lbs.)	DISTANCE FROM CENTROIDAL AXIS (inches)	EXPERIMENTAL STRAIN (microstrain)	ANALYTICAL STRAIN (microstrain)	% ERROR

P=250	0.969	-268	-273	1.9
	-0.062	24	18	25.0
	-1.078	271	304	12.2
P=500	0.969	-516	-547	6.0
	-0.062	48	35	27.1
	-1.078	534	608	13.8

Table 5.35 Beam B2S83: Comparison of the experimental and the analytical strain in bending about 2-axis.

LOAD (lbs.)	DISTANCE FROM CENTROIDAL AXIS (inches)	EXPERIMENTAL STRAIN (microstrain)	ANALYTICAL STRAIN (microstrain)	% ERROR
P=250	1.063	-334	-318	4.8
	0.031	-28	-9	67.9
	-1.000	299	299	0.0
P=500	1.063	-620	-636	2.6
	0.031	-50	-19	62.0
	-1.000	555	599	7.9

Table 5.36 Beam B2S114: Comparison of the experimental and the analytical strain in bending about 2-axis.

LOAD (lbs.)	DISTANCE FROM CENTROIDAL AXIS (inches)	EXPERIMENTAL STRAIN (microstrain)	ANALYTICAL STRAIN (microstrain)	% ERROR
P=250	1.063	-428	-437	2.1
	0.031	-14	-13	7.1
	-1.000	382	-411	7.6
P=750	1.063	-831	-874	5.2
	0.031	-31	-26	16.1
	-1.000	739	-822	11.2

Table 5.37 Beam B3S83: Comparison of the experimental and the analytical strain in bending about 2-axis.

LOAD (lbs.)	DISTANCE FROM CENTROIDAL AXIS (inches)	EXPERIMENTAL STRAIN (microstrain)	ANALYTICAL STRAIN (microstrain)	% ERROR
P=250	1.906	-107	-107	0.0
	0.922	-53	-52	1.9
	0.031	-1	-2	100.0
	-0.859	55	48	12.7
	-1.906	132	107	18.9
P=750	1.906	-306	-321	4.9
	0.922	-146	-155	6.2
	0.031	-1	-5	400.0
	-0.859	155	144	7.1
	-1.906	364	321	11.8

Table 5.38 Beam B3S132: Comparison of the experimental and the analytical strain in bending about 2-axis.

LOAD (lbs.)	DISTANCE FROM CENTROIDAL AXIS (inches)	EXPERIMENTAL STRAIN (microstrain)	ANALYTICAL STRAIN (microstrain)	% ERROR

P=250	1.906	-166	-170	2.4
	0.922	-84	-82	2.4
	0.031	2	-3	250.0
	-0.859	86	77	10.5
	-1.906	208	170	18.3
P=750	1.906	-482	-510	5.8
	0.922	-237	-247	4.2
	0.031	4	-8	300.0
	-0.859	243	230	5.3
	-1.906	576	510	11.5

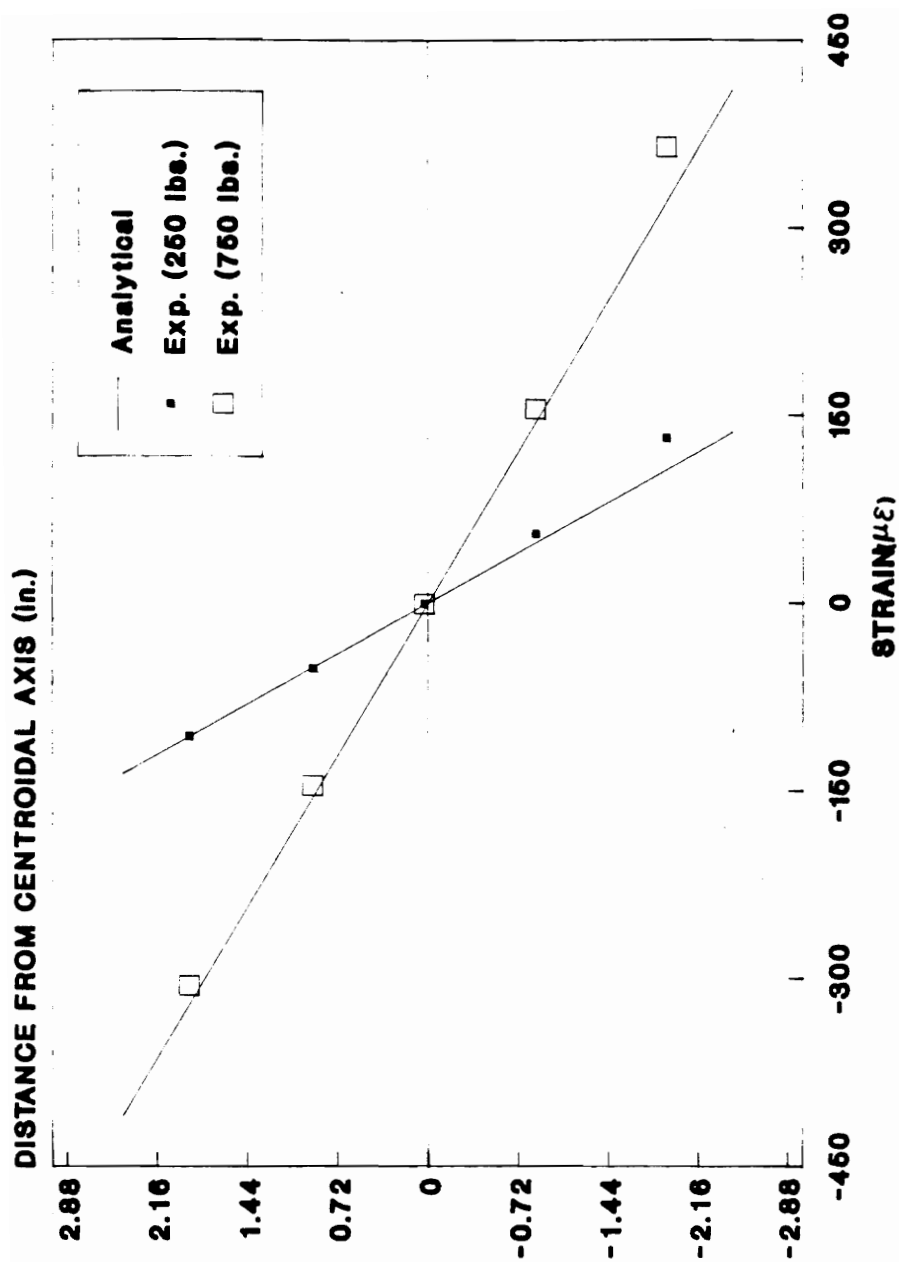


Figure 5.23 Comparison of the experimental and the analytical normal strain in beam B3S83 under bending in the direction of 3-axis

Table 5.39 Beam B1S83: Comparison of the experimental and the analytical deflections in bending about 2-axis.

LOAD (lbs.)	LOCATION LENGTHWISE (inches)	EXPERIMENTAL DEFLECTION (inches)	ANALYTICAL DEFLECTION (inches)	ERROR %
P=250	22.50	-0.120	-0.116	3.3
	41.50	-0.151	-0.153	1.3
	60.50	-0.122	-0.116	4.9
P=500	22.50	-0.214	-0.231	7.9
	41.50	-0.276	-0.306	10.9
	60.50	-0.217	-0.231	6.4

Table 5.40 Beam B1S114: Comparison of the experimental and the analytical deflections in bending about 2-axis.

LOAD (lbs.)	LOCATION LENGTHWISE (inches)	EXPERIMENTAL DEFLECTION (inches)	ANALYTICAL DEFLECTION (inches)	ERROR %

P=250	38.00	-0.293	-0.342	16.7
	57.00	-0.328	-0.393	19.8
	76.00	-0.284	-0.342	20.4
P=500	38.00	-0.563	-0.685	21.7
	57.00	-0.628	-0.787	25.3
	76.00	-0.549	-0.685	24.8

Table 5.41 Beam B2S83: Comparison of the experimental and the analytical deflections in bending about 2-axis.

LOAD (lbs.)	LOCATION LENGTHWISE (inches)	EXPERIMENTAL DEFLECTION (inches)	ANALYTICAL DEFLECTION (inches)	ERROR %

P=250	22.50	-0.163	-0.168	3.1
	41.50	-0.207	-0.223	7.7
	60.50	-0.159	-0.168	5.7
P=500	22.50	-0.349	-0.336	3.7
	41.50	-0.439	-0.445	1.4
	60.50	-0.338	-0.336	0.6

Table 5.42 Beam B2S114: Comparison of the experimental and the analytical deflections in bending about 2-axis.

LOAD (lbs.)	LOCATION LENGTHWISE (inches)	EXPERIMENTAL DEFLECTION (inches)	ANALYTICAL DEFLECTION (inches)	ERROR %

P=250	38.00	-0.476	-0.499	4.8
	57.00	-0.522	-0.573	9.8
	76.00	-0.449	-0.499	11.1
P=750	38.00	-0.888	-0.998	12.4
	57.00	-0.973	-1.146	17.8
	76.00	-0.839	-0.998	19.0

Table 5.43 Beam B3S83: Comparison of the experimental and the analytical deflections in bending about 2-axis.

LOAD (lbs.)	LOCATION LENGTHWISE (inches)	EXPERIMENTAL DEFLECTION (inches)	ANALYTICAL DEFLECTION (inches)	ERROR %
P=250	22.50	-0.030	-0.032	6.7
	41.50	-0.037	-0.043	16.2
	60.50	-0.030	-0.032	6.7
P=750	22.50	-0.084	-0.097	15.5
	41.50	-0.110	-0.128	16.4
	60.50	-0.084	-0.097	15.5

Table 5.44 Beam B3S132: Comparison of the experimental and the analytical deflections in bending about 2-axis.

LOAD (lbs.)	LOCATION LENGTHWISE (inches)	EXPERIMENTAL DEFLECTION (inches)	ANALYTICAL DEFLECTION (inches)	ERROR %
P=250	47.00	-0.150	-0.152	1.3
	66.00	-0.174	-0.168	3.4
	85.00	-0.151	-0.152	6.6
P=750	47.00	-0.384	-0.456	18.8
	66.00	-0.448	-0.504	12.5
	85.00	-0.388	-0.456	17.5

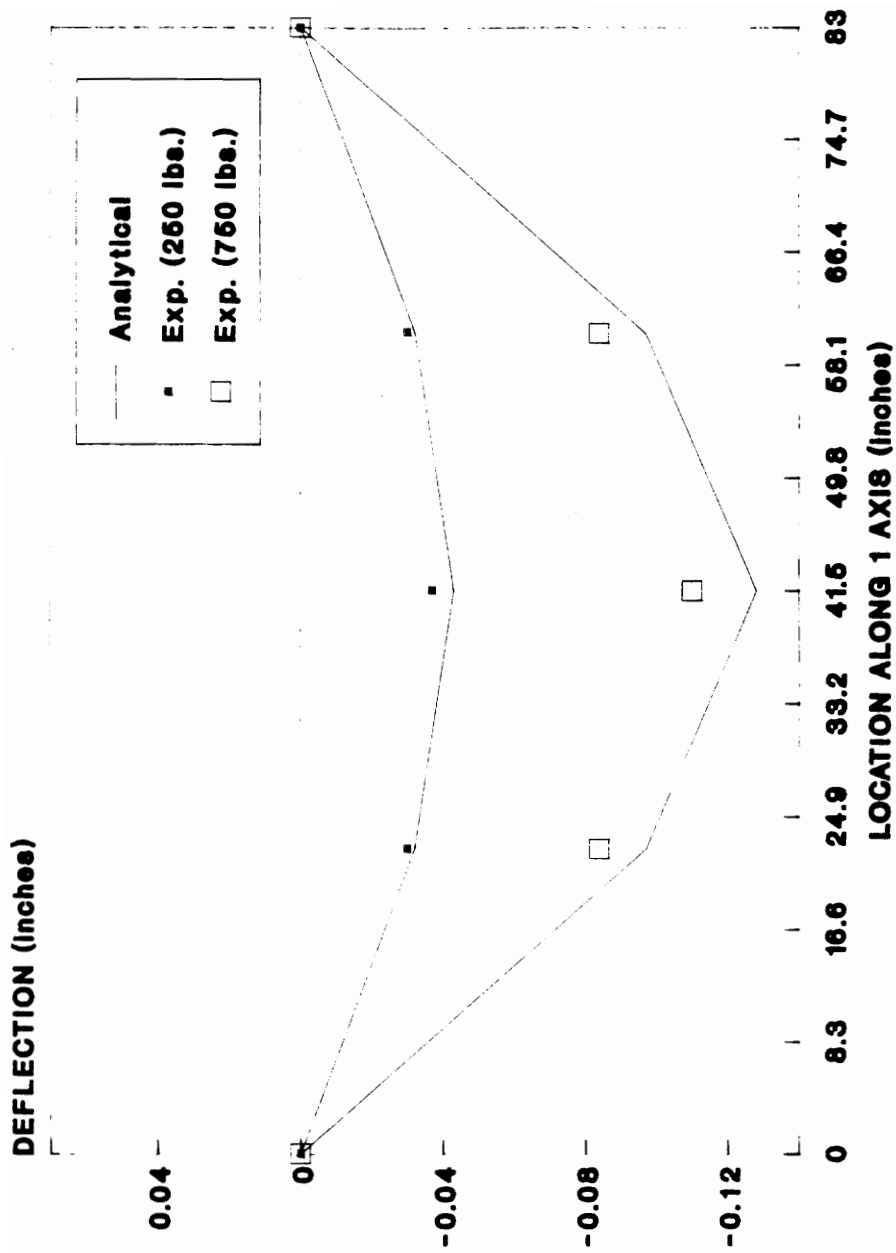
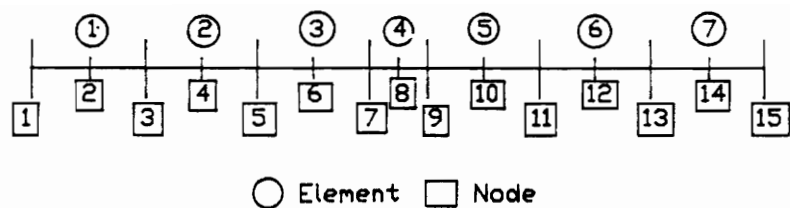


Figure 5.24 Comparison of the experimental and the analytical deflections for beam B3S83 under bending in the direction of 3-axis

major axis and compression loads. All tests were conducted within the elastic range of the beams. Two equal and concentrated bending loads were applied in all cases. However, except for beam B1S, loads were not applied symmetrically for all the beams. Figure 5.25 shows the finite element mesh of each beam that was tested in combined bending and compression. The figure also presents, in a table form, the locations where loads were applied.

To test the beams, bending loads were applied first; then, axial loads were applied to a desired level while maintaining the applied bending load. To model the experimental set-up, straight and curved beams were modelled in the finite element analysis with pin-pin and pin-roller boundary conditions throughout the analysis. But, for the curved beams, to accurately model the experimental procedures after the bending load was applied, the nodes receiving the bending load were restrained in the 2-direction to restrict vertical movement during the subsequent application of the compression loads. If the nodes were not restrained, the beam would regain its original curvature due to the compression load. In the experimental set-up, the load heads restricted the curved beams from regaining their original curvature.

Tables 5.45 to 5.53 compare the experimental strain measurements to the analytical strain predictions for all the straight and curved beams tested in combined bending and compression. The results for straight beams show a better agreement between the experimental and the analytical strain in the compression zone. The experimental and the analytical results, however, show a similar trend in strain readings along the depth of the beams from top to bottom. There was a greater error at the three loads on the compression side than on the tension side. In addition, there was less error between the experimental and the analytical values along the depth of the beam when the beams were subjected to flatwise bending (bending about the minor axis or 2-axis).



Beam ID	Nodes where load (P) was applied
B1S108	5 & 13
B2S108	5 & 13
B3S130	11 & 13
B1C81	3 & 9
B2C109	5 & 13
B3C130	11 & 13

Figure 5.25 Finite element mesh used to analyze beams in combined bending and compression (table shows where load, P, was applied)

Table 5.45 Beam B1S108: Comparison of the experimental and the analytical strain in combined bending about 3-axis and compression.

LOAD (lbs.)	DISTANCE FROM CENTROIDAL AXIS (inches)	EXPERIMENTAL STRAIN (microstrain)	ANALYTICAL STRAIN (microstrain)	% ERROR
P=750	3.469	-235	-309	31.5
Q=0	2.031	-188	-181	3.7
	0.609	-59	-54	8.5
	-0.125	-9	11	22.2
	-0.812	46	72	56.5
	-2.188	154	195	26.6
	-3.562	296	317	7.1
P=750	3.469	-341	-356	4.4
Q=2000	2.031	-268	-227	15.3
	0.609	-113	-99	12.4
	-0.125	-71	-33	53.5
	-0.812	27	28	3.7
	-2.188	151	152	0.7
	-3.562	306	276	9.8
P=750	3.469	-494	-452	8.5
Q=6000	2.031	-384	-320	16.7
	0.609	-171	-190	11.1
	-0.125	-148	-122	17.6
	-0.812	-47	-59	25.5
	-2.188	115	67	41.7
	-3.562	314	193	38.5

Table 5.46 Beam B1S108: Comparison of the experimental and the analytical strain in combined bending about 2-axis and compression.

LOAD (lbs.)	DISTANCE FROM CENTROIDAL AXIS (inches)	EXPERIMENTAL STRAIN (microstrain)	ANALYTICAL STRAIN (microstrain)	% ERROR
P=500	1.062	-410	-484	18.0
Q=0	0.969	-345	-441	27.8
	0.062	-39	-28	28.2
	-0.969	377	441	17.0
	-1.047	442	477	7.9
P=500	1.062	-532	-566	6.4
Q=2000	0.969	-479	-520	8.6
	0.062	-98	-75	23.5
	-0.969	399	431	8.0
	-1.047	478	469	1.9
P=500	1.062	-630	-656	4.1
Q=6000	0.969	-595	-607	2.0
	0.062	-147	-122	17.1
	-0.969	429	428	0.2
	-1.047	510	470	7.8

Table 5.47 Beam B2S108: Comparison of the experimental and the analytical strain in combined bending about 3-axis and compression.

LOAD (lbs.)	DISTANCE FROM CENTROIDAL AXIS (inches)	EXPERIMENTAL STRAIN (microstrain)	ANALYTICAL STRAIN (microstrain)	% ERROR
P=750	2.109	-429	-607	41.5
Q=0	0.672	-175	-193	10.3
	-0.094	-4	27	-
	-0.766	159	220	38.4
	-2.141	505	616	22.0
P=750	2.109	-540	-692	28.1
Q=2000	0.672	-287	-265	7.7
	-0.094	-89	-38	57.3
	-0.766	146	162	11.0
	-2.141	528	570	8.0
P=750	2.109	-827	-868	5.0
Q=6000	0.672	-499	-411	17.6
	-0.094	-227	-167	26.4
	-0.766	-7	47	-
	-2.141	458	484	5.7

Table 5.48 Beam B2S108: Comparison of the experimental and the analytical strain in combined bending about 2-axis and compression.

LOAD (lbs.)	DISTANCE FROM CENTROIDAL AXIS (inches)	EXPERIMENTAL STRAIN (microstrain)	ANALYTICAL STRAIN (microstrain)	% ERROR

P=500	1.078	-716	-716	0.0
Q=0	0.047	-36	-31	13.9
	-0.938	599	623	4.0
P=500	1.078	-866	-865	0.1
Q=2000	0.047	-118	-101	14.4
	-0.938	624	629	0.8

Table 5.49 Beam B3S130: Comparison of the experimental and the analytical strain in combined bending about 3-axis and compression.

LOAD (lbs.)	DISTANCE FROM CENTROIDAL AXIS (inches)	EXPERIMENTAL STRAIN (microstrain)	ANALYTICAL STRAIN (microstrain)	% ERROR
P=750	2.734	-280	-393	40.4
Q=0	1.719	-234	-247	5.5
	0.703	-75	-101	34.7
	-0.047	-26	7	-
	-0.812	63	117	85.7
	-1.828	198	263	32.8
	-2.860	372	411	10.5
P=750	2.734	-349	-431	23.5
Q=2000	1.719	-293	-283	3.4
	0.703	-121	-135	11.6
	-0.047	-51	-25	51.0
	-0.812	41	87	-
	-1.828	203	235	15.8
	-2.860	405	386	4.7
P=750	2.734	-440	-509	15.7
Q=6000	1.719	-386	-356	7.8
	0.703	-198	-202	2.0
	-0.047	-112	-89	20.5
	-0.812	-12	27	-
	-1.828	168	180	7.1
	-2.860	386	336	13.0

Table 5.50 Beam B3S130: Comparison of the experimental and the analytical strain in combined bending about 2-axis and compression.

LOAD (lbs.)	DISTANCE FROM CENTROIDAL AXIS (inches)	EXPERIMENTAL STRAIN (microstrain)	ANALYTICAL STRAIN (microstrain)	% ERROR
P=750	2.000	-522	-512	1.9
Q=0	1.000	-253	-256	1.2
	-0.047	-12	12	-
	-0.875	209	224	7.2
	-1.891	483	484	0.2
P=750	2.000	-623	-560	10.1
Q=2000	1.000	-305	-296	3.0
	-0.047	-42	-20	52.4
	-0.875	199	199	0.0
	-1.891	503	467	7.2
P=750	2.000	-719	-606	15.7
Q=4000	1.000	-359	-335	6.7
	-0.047	-72	-51	29.2
	-0.875	193	173	10.4
	-1.891	533	448	15.9

Table 5.51 Beam B1C81: Comparison of the experimental and the analytical strain in combined bending about 3-axis and compression.

LOAD (lbs.)	DISTANCE FROM CENTROIDAL AXIS (inches)	EXPERIMENTAL STRAIN (microstrain)	ANALYTICAL STRAIN (microstrain)	% ERROR
P=750	2.531	-393	-513	30.5
Q=0	1.719	-316	-348	10.1
	0.812	-117	-164	40.2
	0.000	0	0	0.0
	-0.922	169	187	10.6
	-1.797	248	364	46.8
	-2.688	434	544	10.1
P=750	2.531	-462	-573	24.0
Q=2000	1.719	-391	-409	4.6
	0.812	-182	-224	23.1
	0.000	-69	-60	13.0
	-0.922	88	128	45.4
	-1.797	198	305	54.0
	-2.688	422	486	15.2
P=750	2.531	-592	-698	17.9
Q=6000	1.719	-513	-531	3.5
	0.812	-300	-345	15.0
	0.000	-190	-179	5.8
	-0.922	-64	10	-
	-1.797	101	189	87.1
	-2.688	274	372	35.8

Table 5.52 Beam B2C109: Comparison of the experimental and the analytical strain in combined bending about 3-axis and compression.

LOAD (lbs.)	DISTANCE FROM CENTROIDAL AXIS (inches)	EXPERIMENTAL STRAIN (microstrain)	ANALYTICAL STRAIN (microstrain)	% ERROR
P=750	2.141	-555	-520	6.3
Q=0	0.781	-230	-190	17.4
	0.000	-44	0	100.0
	-0.672	108	163	50.9
	-2.094	450	509	13.1
P=750	2.141	-628	-572	8.9
Q=2000	0.781	-294	-243	17.3
	0.000	-97	-54	44.3
	-0.672	45	109	-
	-2.094	391	453	15.9
P=750	2.141	-754	-677	10.2
Q=6000	0.781	-421	-349	17.1
	0.000	-204	-161	21.1
	-0.672	-91	1	-
	-2.094	242	344	42.1

Table 5.53 Beam B3C130: Comparison of the experimental and the analytical strain in combined bending about 3-axis and compression.

LOAD (lbs.)	DISTANCE FROM CENTROIDAL AXIS (inches)	EXPERIMENTAL STRAIN (microstrain)	ANALYTICAL STRAIN (microstrain)	% ERROR

P=750	3.344	-233	-284	21.9
Q=0	2.359	-196	-201	2.6
	1.344	-115	-114	0.9
	0.109	-7	-9	28.6
	-1.250	90	106	17.8
	-2.219	192	189	1.6
	-3.281	285	279	2.1
P=750	3.344	-255	-314	23.1
Q=2000	2.359	-223	-229	2.7
	1.344	-143	-141	1.4
	0.109	-34	-35	2.9
	-1.250	59	82	38.9
	-2.219	160	166	3.8
	-3.281	246	257	4.5
P=750	3.344	-251	-373	48.6
Q=6000	2.359	-224	-286	27.7
	1.344	-171	-196	14.6
	0.109	-78	-86	10.2
	-1.250	-9	34	-
	-2.219	73	120	64.4
	-3.281	131	214	63.4

Figures 5.26 to 5.29 show typical experimental and analytical strain distributions in two of the straight beams under combined bending and axial loads. Analytical, as well as, experimental strain readings at three loads converged on the side where the beam was under tension. The observations seem to indicate that the outer laminae on the tension side of the beams were being subjected to large tensile strains. Whereas the laminae on the compression side were undergoing further compression. In all cases, the neutral axis shifted downwards. The neutral planes and the centroidal planes of the beams do not coincide. The shift of the neutral plane was, however, very small relative to the depth of the beams. The shift in the neutral axis was due to increasing compressive stresses.

Figure 5.30 shows the distribution of strain under combined bending and compression loads in a curved beam. No convergence of strain distributions at three levels of loads was noticed. In the majority of the beams, the analytical results were conservative and predicted higher strain than the experimental strain values.

Tables 5.54 to 5.62 show the deflection readings for straight and curved beams tested under combined loads. Except for deflection readings of beams B2C, B3C, and B2S in flatwise bending, the experimental and the analytical results of the rest of the beams agree very well. The percent difference between the experimental and the analytical results was less than 10%. For beams B2C, B3C, and B2S the percent error was between 20-40%. In all cases, the analytical deflections were larger than the experimental deflections. The measured deflections were lower than the predicted ones because the displacement transducers were fixed, but the beams were being translated horizontally due to the axial loads. Therefore, the displacement chord in the transducer was moving horizontally, but not vertically down. Thus, the recorded deflections were smaller. Figures 5.31 and 5.32 show examples of deflection results in a straight and a curved beam.

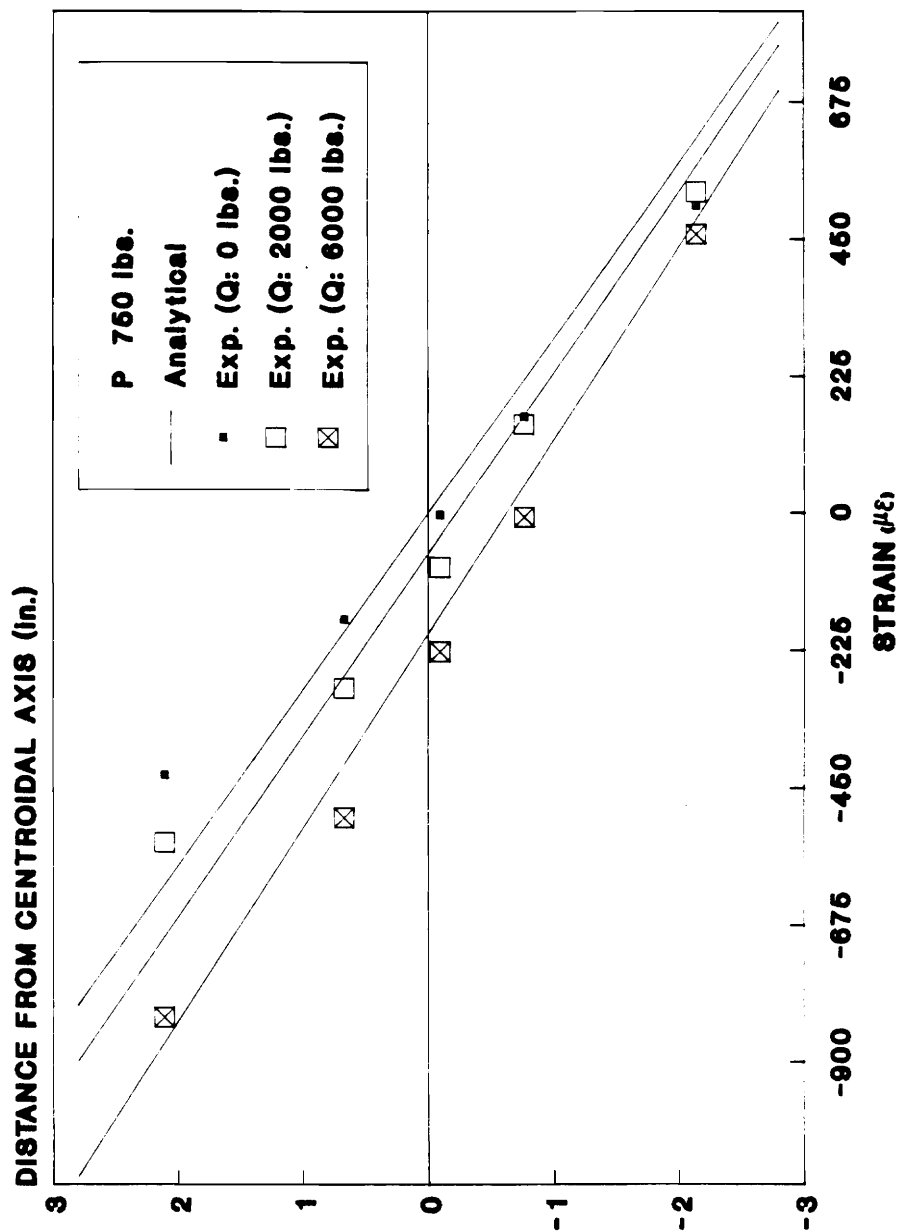


Figure 5.26 Comparison of strain distribution in beam B2S108 under combined bending in 2-direction and axial compression

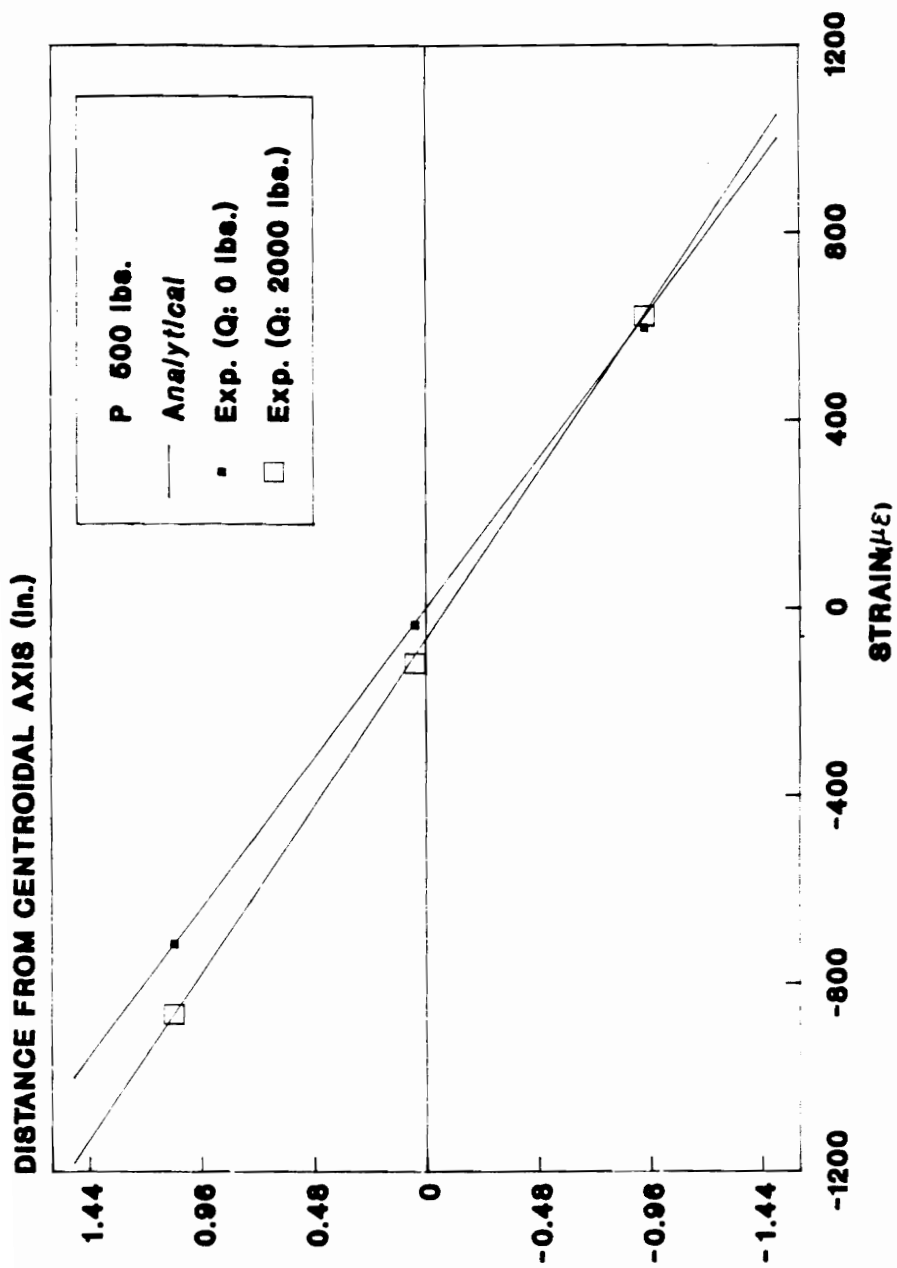


Figure 5.27 Comparison of strain distribution in beam B2S108 under combined bending in 3-direction and axial compression

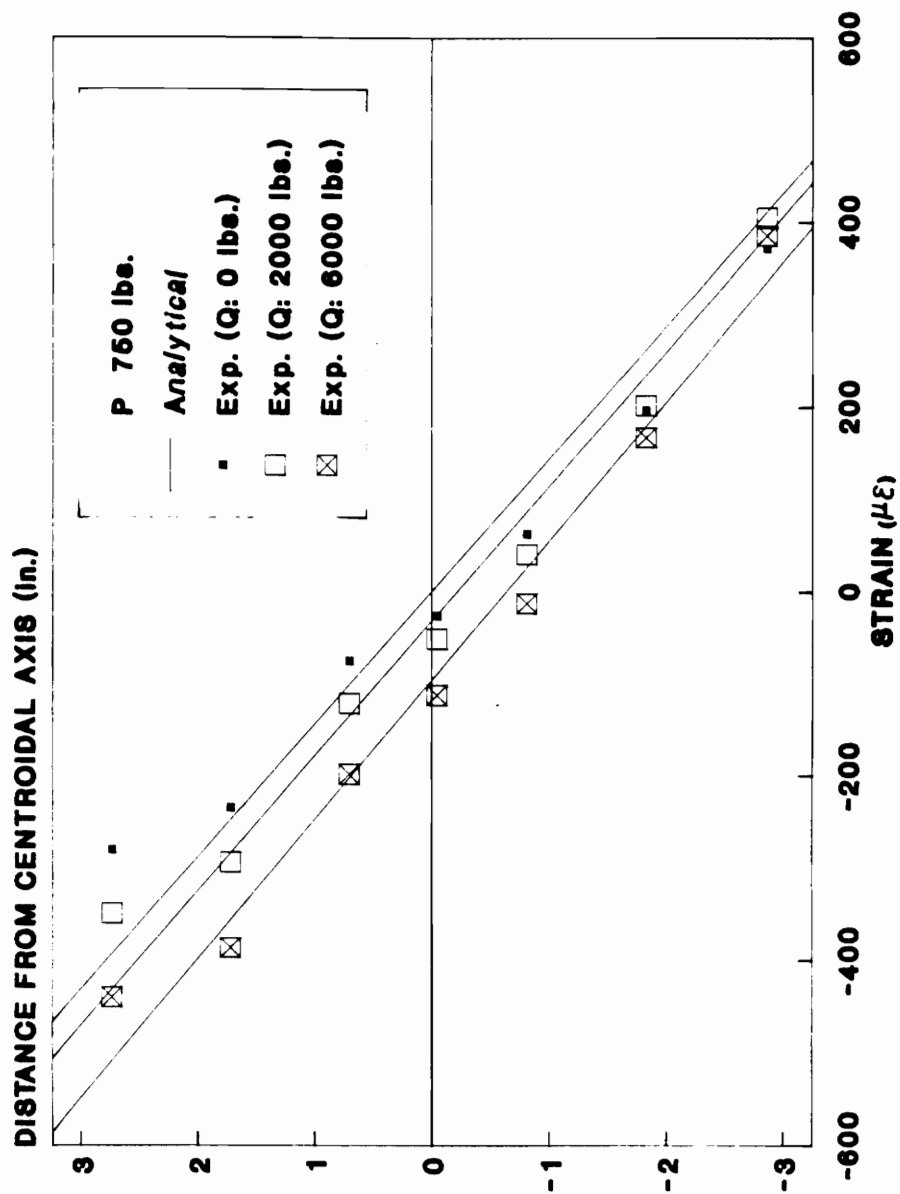


Figure 5.28 Comparison of strain distribution in beam B3S130 under combined bending in 2-direction and axial compression

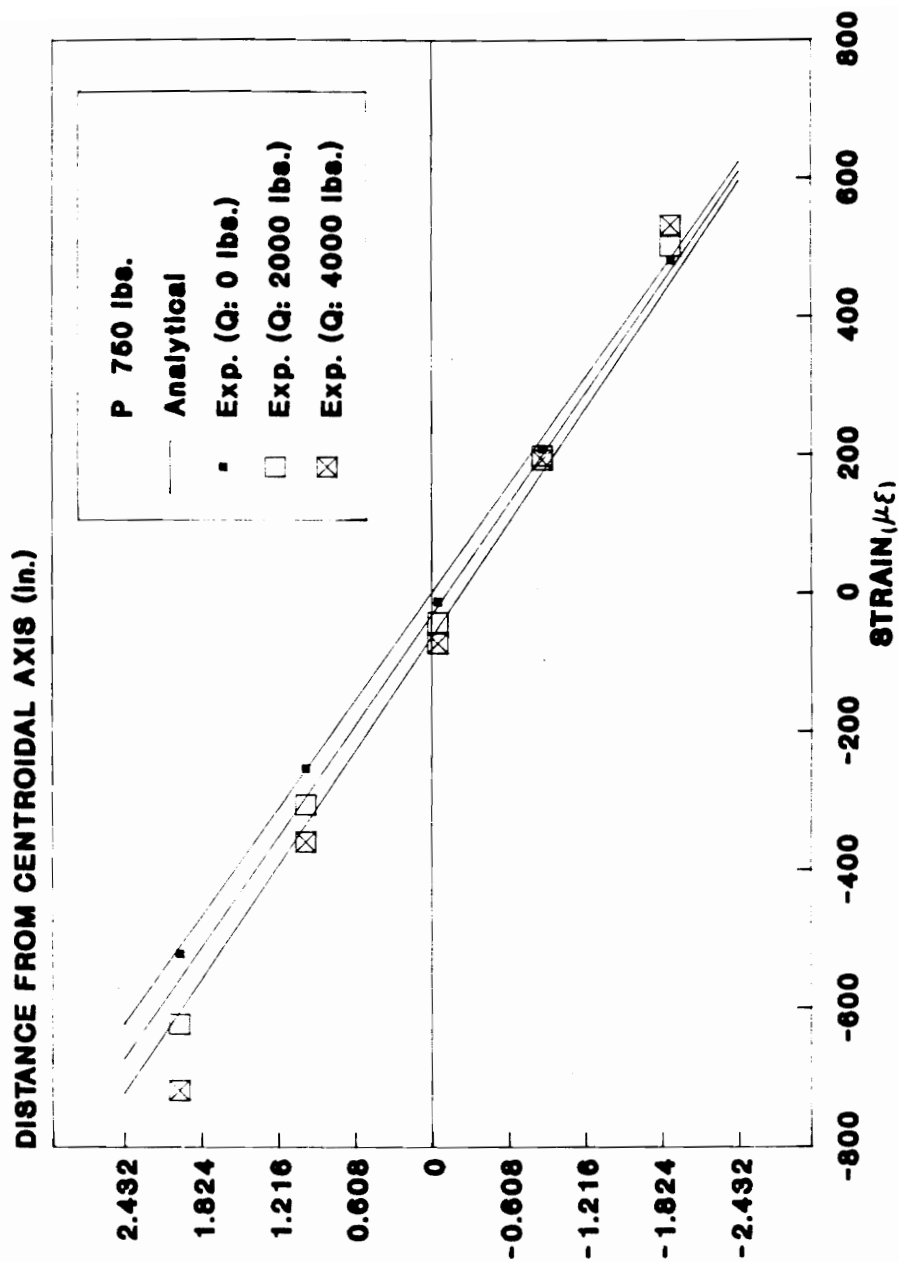


Figure 5.29 Comparison of strain distribution in beam B3S130 under combined bending in 3-direction and axial compression

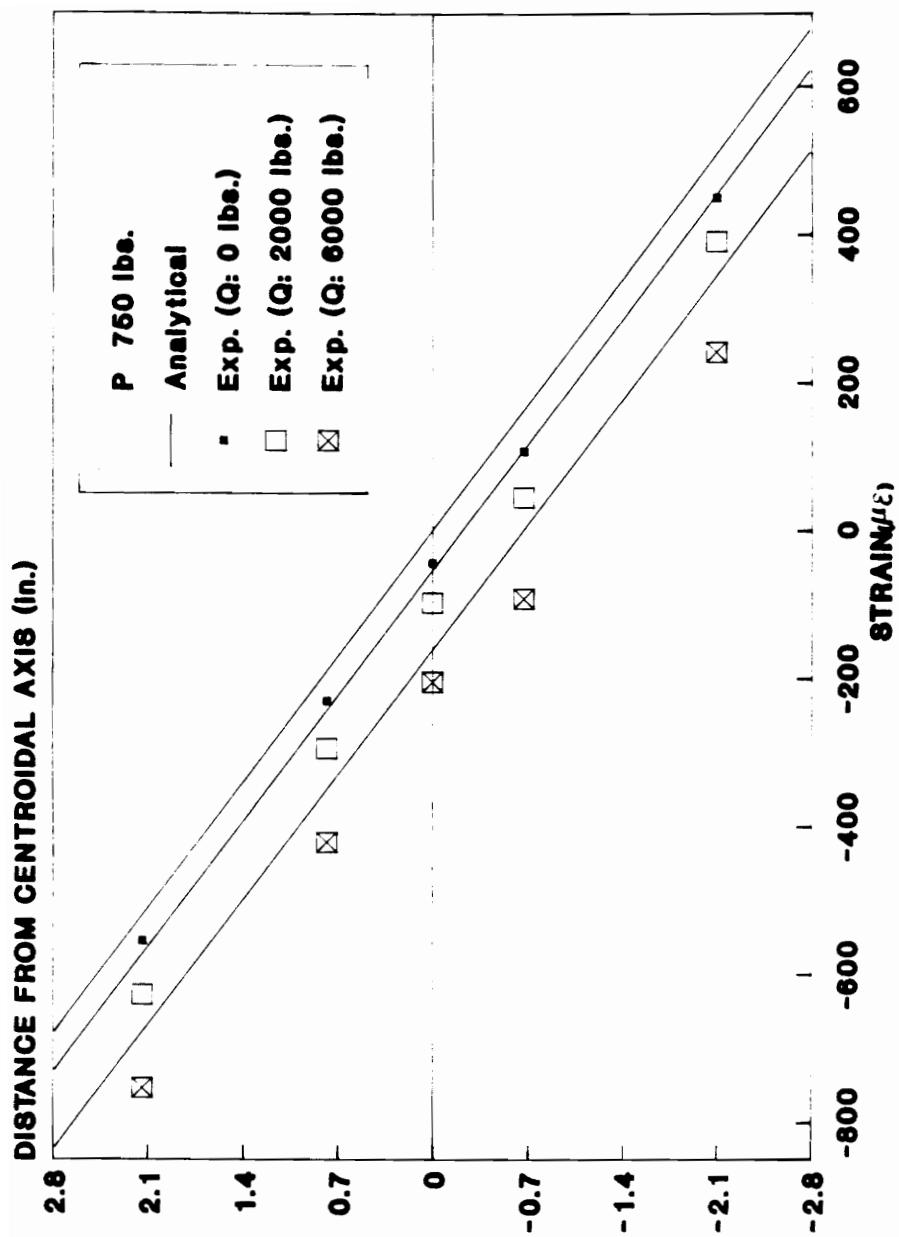


Figure 5.30 Comparison of strain distribution in beam B2C114 under combined bending in 2-direction and axial compression

Table 5.54 Beam B1S108: Comparison of the experimental and the analytical deflections in bending about 3-axis and compression.

LOAD (lbs.)	LOCATION LENGTHWISE (inches)	EXPERIMENTAL DEFLECTION (inches)	ANALYTICAL DEFLECTION (inches)	ERROR %
P=750 Q=0	43.25	-0.092	-0.112	21.7
	54.06	-0.099	-0.116	17.2
	89.75	-0.062	-0.063	1.6
P=0 Q=2000	43.25	-0.105	-0.113	7.6
	54.06	-0.116	-0.118	1.7
	89.75	-0.072	-0.064	11.1
P=0 Q=6000	43.25	-0.116	-0.115	0.9
	54.06	-0.125	-0.120	4.0
	89.75	-0.078	-0.065	16.7

Table 5.55 Beam B1S108: Comparison of the experimental and the analytical deflections in bending about 2-axis and compression.

LOAD (lbs.)	LOCATION LENGTHWISE (inches)	EXPERIMENTAL DEFLECTION (inches)	ANALYTICAL DEFLECTION (inches)	ERROR %

P=250	43.25	-0.499	-0.538	7.8
Q=0	54.06	-0.521	-0.566	8.6
	89.75	-0.293	-0.300	2.4
P=0	43.25	-0.524	-0.578	10.3
Q=2000	54.06	-0.548	-0.608	10.9
	89.75	-0.303	-0.322	6.3
P=0	43.25	-0.602	-0.627	4.2
Q=6000	54.06	-0.624	-0.659	5.6
	89.75	-0.346	-0.348	0.6

Table 5.56 Beam B2S108: Comparison of the experimental and the analytical deflections inbending about 3-axis and compression.

LOAD (lbs.)	LOCATION LENGTHWISE (inches)	EXPERIMENTAL DEFLECTION (inches)	ANALYTICAL DEFLECTION (inches)	ERROR %
P=750 Q=0	43.25	-0.276	-0.348	26.1
	54.06	-0.280	-0.365	30.4
	89.75	-0.161	-0.195	21.1
P=0 Q=2000	43.25	-0.285	-0.359	26.0
	54.06	-0.291	-0.376	29.2
	89.75	-0.166	-0.201	21.1
P=0 Q=6000	43.25	-0.390	-0.382	2.0
	54.06	-0.399	-0.401	0.5
	89.75	-0.213	-0.214	0.5

Table 5.57 Beam B2S108: Comparison of the experimental and the analytical deflections in bending about 2-axis and compression.

LOAD (lbs.)	LOCATION LENGTHWISE (inches)	EXPERIMENTAL DEFLECTION (inches)	ANALYTICAL DEFLECTION (inches)	ERROR %
P=750 Q=0	43.25	-0.754	-0.784	4.0
	54.06	-0.782	-0.824	5.4
	89.75	-0.434	-0.434	0.9
P=750 Q=2000	43.25	-0.861	-0.871	1.2
	54.06	-0.898	-0.916	2.0
	89.75	-0.491	-0.485	1.2

Table 5.58 Beam B3S130: Comparison of the experimental and the analytical deflections inbending about 3-axis and compression.

LOAD (lbs.)	LOCATION LENGTHWISE (inches)	EXPERIMENTAL DEFLECTION (inches)	ANALYTICAL DEFLECTION (inches)	ERROR %
P=750	65.00	-0.214	-0.253	18.2
Q=0	74.25	-0.215	-0.254	18.1
	102.20	-0.149	-0.173	16.1
P=0	65.00	-0.237	-0.257	8.4
Q=2000	74.25	-0.239	-0.258	7.9
	02.20	-0.165	-0.176	6.7
P=0	65.00	-0.242	-0.266	9.9
Q=6000	74.25	-0.246	-0.267	8.5
	02.20	-0.170	-0.181	6.5

Table 5.59 Beam B3S130: Comparison of the experimental and the analytical deflections in bending about 2-axis and compression.

LOAD (lbs.)	LOCATION LENGTHWISE (inches)	EXPERIMENTAL DEFLECTION (inches)	ANALYTICAL DEFLECTION (inches)	ERROR %
P=750	65.00	-0.396	-0.445	12.4
Q=0	74.25	-0.402	-0.446	10.9
	102.20	-0.283	-0.303	7.1
P=0	65.00	-0.438	-0.458	4.6
Q=2000	74.25	-0.439	-0.459	4.6
	102.20	-0.310	-0.311	0.3
P=0	65.00	-0.467	-0.471	-0.9
Q=4000	74.25	-0.467	-0.472	1.1
	102.20	-0.320	-0.319	0.3

Table 5.60 Beam B1C81: Comparison of the experimental and the analytical deflections in bending about 3-axis and compression.

LOAD (lbs.)	LOCATION LENGTHWISE (inches)	EXPERIMENTAL DEFLECTION (inches)	ANALYTICAL DEFLECTION (inches)	ERROR %
P=750 Q=0	27.00	-0.129	-0.131	1.6
	40.50	-0.136	-0.150	10.3
	54.00	-0.129	-0.131	0.2
P=0 Q=2000	27.00	-0.132	-0.131	0.8
	40.50	-0.141	-0.150	6.4
	54.00	-0.133	-0.131	1.5
P=0 Q=6000	27.00	-0.132	-0.132	0.8
	40.50	-0.141	-0.150	6.4
	54.00	-0.133	-0.131	1.5

Table 5.61 Beam B2C109: Comparison of the experimental and the analytical deflections in bending about 3-axis and compression.

LOAD (lbs.)	LOCATION LENGTHWISE (inches)	EXPERIMENTAL DEFLECTION (inches)	ANALYTICAL DEFLECTION (inches)	ERROR %

P=750	43.62	-0.251	-0.302	20.3
Q=0	54.69	-0.263	-0.317	20.5
	90.37	-0.152	-0.173	13.8
P=0	43.62	-0.262	-0.302	15.3
Q=2000	54.69	-0.275	-0.316	14.9
	90.37	-0.159	-0.173	8.8
P=0	43.62	-0.218	-0.302	38.5
Q=6000	54.69	-0.235	-0.315	34.0
	90.37	-0.136	-0.173	27.2

Table 5.62 Beam B3C130: Comparison of the experimental and the analytical deflections inbending about 3-axis and compression.

LOAD (lbs.)	LOCATION LENGTHWISE (inches)	EXPERIMENTAL DEFLECTION (inches)	ANALYTICAL DEFLECTION (inches)	ERROR %

P=750	65.00	-0.124	-0.152	22.6
Q=0	74.25	-0.125	-0.153	22.4
	102.20	-0.096	-0.104	8.3
P=0	65.00	-0.124	-0.151	21.8
Q=2000	74.25	-0.125	-0.153	22.4
	102.20	-0.093	-0.104	11.8
P=0	65.00	-0.062	-0.149	140.0
Q=6000	74.25	-0.059	-0.153	159.0
	102.20	-0.042	-0.104	148.0

5.5 Sources of Error

There were many possible sources of error that gave rise to differences between the experimental and the analytical results. Some of the possible experimental sources of error were:

1. The clip-on transducers were not sensitive to very small strain at the neutral axis of the beams. A possible method of improving the sensitivity would be to bond more sensitive foil gages to clip-on transducers. Thus, smaller strain in the wood could be accurately measured.

2. The correct placement of CET on the specimen is crucial. If the base plates are not set close to the calibration gage length, errors can be introduced in the strain measurement. Also, alignment of the CET with the specimen geometric axes is important.

3. The rotary potentiometer used to measure deflections should be replaced by highly accurate LVDT (Linear Variable Differential Transformer). The resolution of the potentiometers used in this study was not sufficient to accurately read very small displacements.

4. While conducting beam tests, bending loads were applied continuously by the loading ram. Therefore, the data acquisition system has to read all the channels very fast so that all channel readings will correspond to the same load level. This was hard to achieve, and contributes to the errors.

5. Large differences in the experimental and the analytical results for combined bending and compression loads were primarily due to the experimental set-up. Ideally, it is desirable to have two concentrated loads in the form of dead weights on the beam while applying the compression load. Thus, as the locations on the beams where bending loads are applied are being translated horizontally due to compression loads, the bending loads also would translate. In other words, the bending loads should be able to translate horizontally, while the compression load is being applied.

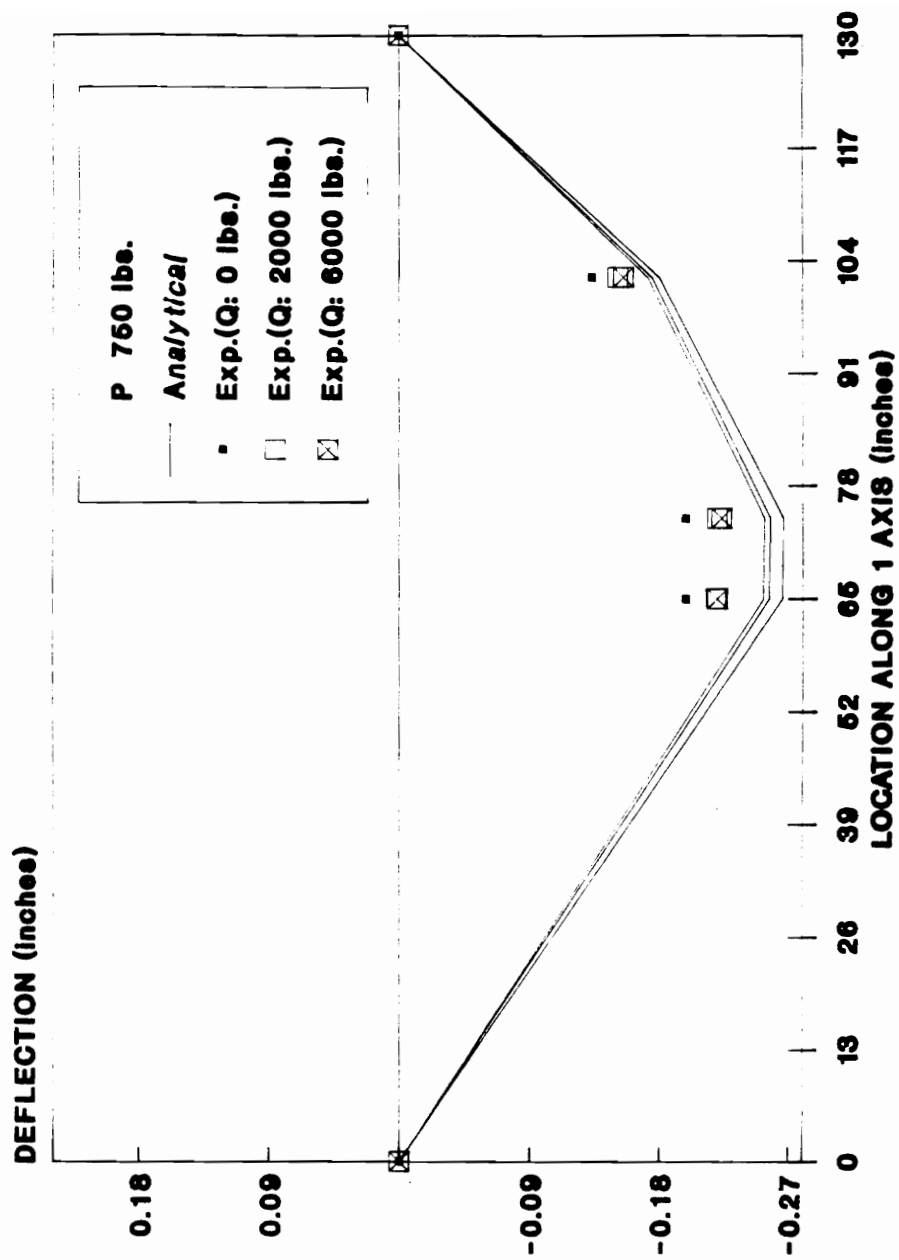


Figure 5.31 Comparison of deflections for beam B3S130 under combined bending in 2-direction and axial compression

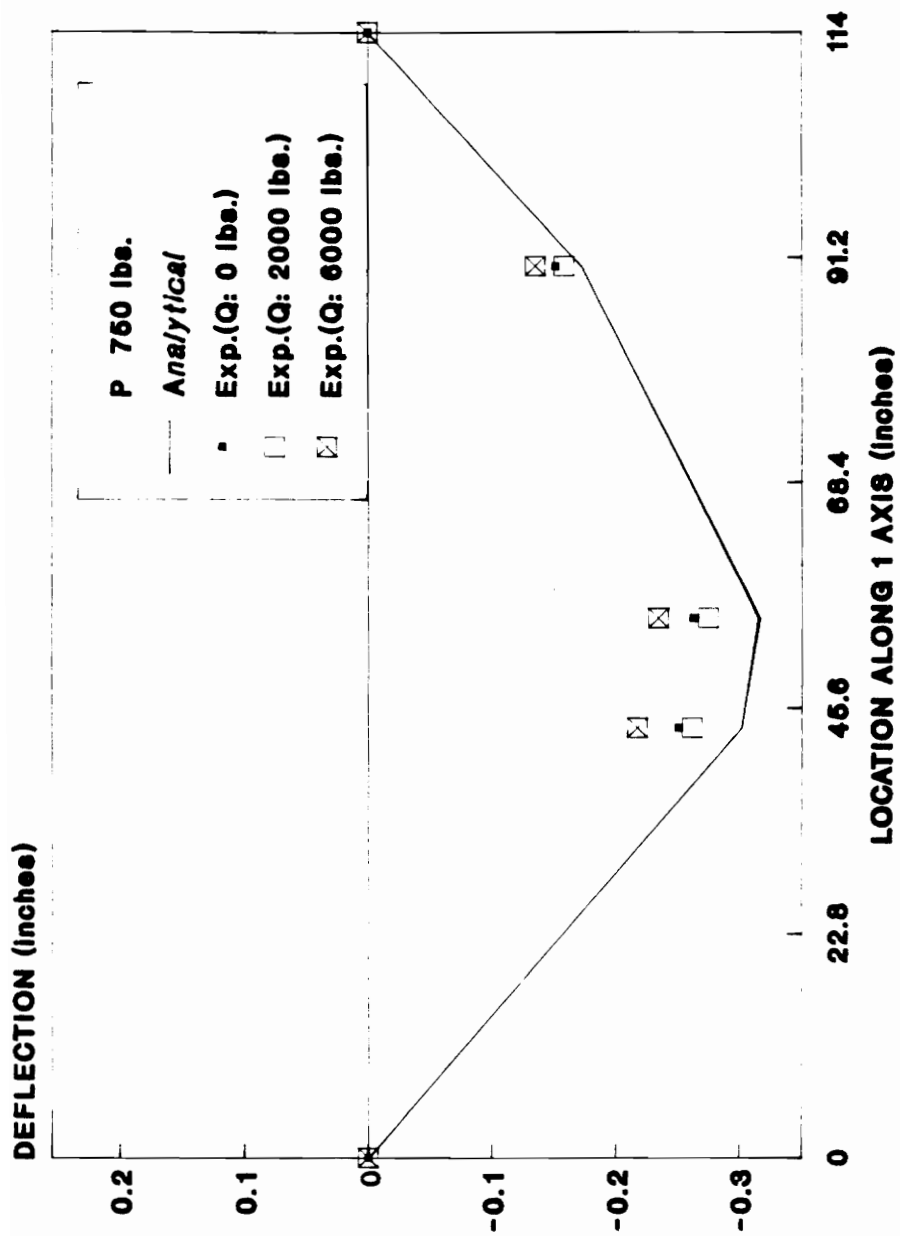


Figure 5.32 Comparison of deflections for beam B2C114 under combined bending in 2-direction and axial compression

6. In addition, the boundary conditions probably were not accurately modelled in the finite element analysis to simulate the combined bending and compression test. It was difficult to exactly depict the boundary conditions of the experiment in the lab to model it accurately.

7. Lastly, errors in the results were inevitable because of the variations in stiffness properties within the beams themselves due to the nature of wood.

5.6 Summary and Conclusions

Considering the possible sources of errors mentioned in the previous section, over 80% of the experimental and the analytical results were in very good agreement with each other (i.e. less than 10% error). The study on the beams indicates that southern pine glulam beams can be modelled accurately using the finite element analysis with a stiffness matrix that contains only the longitudinal modulus of elasticity of the beam and the shear modulus of the cross-section of the beam.

The experimental and the analytical strain and deflection measurements of glulam beams in bending about the major and the minor axes agreed well for most cases. Differences of less than 10% between the experimental measurements and the analytical predictions were found for bending about the major and the minor axes for all locations through the depth of the beams except in the vicinity of the neutral axis. The difference between the measured and the predicted strain and deflection measurements for glulam beams tested in combined bending and compression ranged mostly between 0% and 40%. This difference could be attributed to several causes including the idealized modelling of the boundary conditions, the experimental set-up for combined loading, the sensitivity of the CET to small strains around the neutral axis, and the low resolution of the displacement transducers.

In conclusion, comparison of the experimental and the analytical results show that a three-noded isoparametric beam element accurately predicts the behavior of glulam beams under flatwise

and edgewise bending loads, as well as under combined bending and compression loads. The model is based on simplified assumptions of transverse isotropy and global modulus of

CHAPTER 6

6. SUMMARY, CONCLUSIONS, AND RECOMMENDATIONS FOR FUTURE RESEARCH

6.1 Introduction

The preceeding chapters presented the experimental methods used to verify the analytical model to predict the behavior of glulam space beams. They also contain the experimental and the analytical results of the behavoir of glulam beams under in-plane bending about the major and the minor axes, and combined compression and bending loads. The following chapter summerizes the results and presents the conclusions drawn from this study.

6.2 Summary and Conclusions

1. Southern pine glulam beams can be modelled accurately using the finite element analysis with a stiffness matrix that contains only the longitudinal modulus of elasticity of the beam and the shear modulus of the cross-section of the beam.

2. Torsion tests conducted on orthotropic southern pine specimens with rectangular cross-sections revealed that the values of shear moduli, G_{LR} and G_{LT} , were very close to each other. The two averages differed by less than 8%. The average values of the principal shear moduli G_{LR} and G_{LT} of the orthotropic samples are: $G_{LR} = 160,870$ psi and $G_{LT} = 150,156$ psi. The test results showed that there was no significant effect of the aspect ratio on the values of the shear moduli.

3. Shear modulus of glulam specimens was taken to be 160,000 psi. The average shear moduli of the glulam rectangular and the circular glulam samples were 162,051 psi and 162,017 psi, respectively. These values were obtained using Saint Venant's torsion solution for homogeneous, isotropic materials. Glulam shear modulus was not very much different from G_{LR} and G_{LT} of the orthotropic southern pine specimens. Glulam shear modulus differed from orthotropic shear moduli by less than 8%. It differed from the average of G_{LR} and G_{LT} (155,513 psi) by less than 4%.

4. Based on the torsion results, the shear modulus of a glulam beam cross-section can be calculated using Saint Venant's torsion solution for homogeneous, isotropic materials. This greatly simplifies the formulation of a 3-D beam finite element model.

5. A simple and reusable clip-on electrical transducer (CET) was fabricated and used to measure the strains in the glulam beams. The reproducibility and the accuracy of the results was reasonably good and acceptable. CET was proven to be an economical, an accurate, and a reliable strain measuring device for wood.

6. In addition, a study conducted on the effect of strain gage size on strain measurements showed that 2 inch gage length was suitable to record strain in southern pine beams.

7. The experimental and the analytical strain and deflection measurements of glulam beams in bending about the major and the minor axes agreed well for most cases. Differences of less than

10% between the experimental measurements and analytical predictions were found for bending about the major and the minor axes for all locations through the depth of the beams except in the vicinity of the neutral axis. The differences between the measured and the predicted strain and deflection measurements for glulam beams tested in combined bending and compression ranged mostly between 0% and 40%. This difference between the experimental and the analytical results were attributed to several causes including the idealized modelling of the boundary conditions, the experimental set-up for combined loading, the sensitivity of the CET to small strains around the neutral axis, and the low resolution of the displacement transducers.

In conclusion, the results show that a three-noded isoparametric beam element accurately predicts the response of the glulam beams tested in this study. Due to wood's variability, the reduction of material properties in the constitutive matrix is an attractive feature compared to a complex matrix used in a continuum element analysis. Particularly since we don't really know the material properties on a pointwise basis, which is necessary for a continuum analysis. This is especially true for commercial glulam beams where all we know are published design values.

6.3 Recommendations for Future Work

Work should be done to improve the measuring devices, such as deflection transducers and the clip-on electrical transducers. CET should be improved to make it more sensitive to very small strain such as those occurring closer to the neutral axis of beams subjected to bending loads. Stability of the CET should also be improved for better reproducibility. It is also important to find a method of installing the CET shoes on the wooden specimens.

Research should be conducted to find a better way of estimating longitudinal modulus of elasticity of glulam beams from laminae Young's modulus. However, as it was done in this study, tensile strain should be measured in the laminae to estimate the true Young's modulus. The tensile

strain used to estimate the longitudinal Young's modulus were measured only on one face of each lamina in this study. The author recommends measuring strains on both faces in future experiments, so that the elastic modulus could be computed from the average strain reading. It was shown that the shear modulus can be estimated by testing small glulam specimens in torsion. The method may be useful for measuring and studying the shear modulus of full-size beams.

Also, a better experimental test set-up should be developed to test glulam beams under combined bending and compression loads. Also, the beams should be subjected to uniformly distributed bending loads to simulate the stresses in a glulam element that is part of a glulam lattice dome.

BIBLIOGRAPHY

1. Allocca, A. J. and Stuart, A., *Transducers, Theory and Applications*, Reston Publishing Company, Virginia, 1984.
2. American Institute of Timber Construction, *Timber Construction Manual*, Third Edition, John Wiley & Sons, Inc., New York, 1985.
3. *American Society for Testing and Materials*, Annual Book of ASTM Standards, Part 22, Wood, Vol. 04.09, 1986.
4. Baran, N. M., *Finite Element Analysis on Microcomputers*, McGraw-Hill Book Company, N.Y., 1988.
5. Bender, D. A., Woeste, F. E., Schaffer, E. L., and Marx, C. M., 1985, "Reliability Formulation for the strength and Fire Endurance of glued-laminated beams," *USDA FPL Research Paper*, FPL 460, Madison, Wisconsin.
6. Biblis, E. J., 1965, "Analysis of Wood-Fiberglass Composite Beams Within and Beyond the Elastic Region," *Forest Products Journal*, February, pp 81-88.
7. Biblis, E. J., 1965, "Shear Deflection of Wood Beams," *Forest Products Journal*, November, pp. 492-498.
8. Bodig, J., 1975, "Current Developments in Properties of Wood," *Wood Structures--A Design Guide and Commentary*, Committee of Wood, ASCE Struc. Div., pp. 55-65.
9. Bodig, J. and Goodman, J. R., 1973, "Prediction of Elastic Parameters of Wood," *Wood Science*, Vol. 5(4), pp. 249-264.
10. Bodig, J., and Jayne, B. A., *Mechanics of Wood and Wood Composites*, VanNostrand Reinhold Co., New York, 1982.
11. Bohannon, B. and Moody, R. C., 1969, "Large Glued-Laminated Timber Beams With Two Grades of Tension Laminations," *U.S.D.A. Forest Service Research Paper*, FPL 113, Madison, Wis., pp. 1-43.

12. Boresi, A. P. and Sidebottom, O. M., *Advanced Mechanics of Materials*, 3rd Edition, John Wiley & Sons, N.Y., 1985.
13. Breyer, D. E., *Design of Wood Structures*, McGraw-Hill, N.Y., 1980.
14. Broker, F. W. and Schwab, E., 1988, "Torsionprüfung von Holz," *Holz als Roh-und Werkstoff*, vol. 46, pp. 47-52.
15. Conners, T. E., 1989, "Segmented models for stress-strain diagrams," *Wood Science Technology*, 23, pp. 65-73.
16. Cook, R. D. and Young, W. C., *Advanced Mechanics of Materials*, Macmillan Publishing Company, New York, 1985.
17. Davalos, F. J., "Background For Finite Element Analysis And Experimental Testing Of Glued-Laminated Space Beams," M.S. Thesis, 1987, Department of Civil Engineering, VPI&SU, Blacksburg, VA.
18. -----, "Geometrically Nonlinear Finite Element Analysis of a Glulam Timber Dome," PhD Dissertation, 1989, Department of Civil Engineering, VPI&SU, Blacksburg, VA.
19. -----, Loferski, J. R., and Holzer, S. M., 1988, "Verification of a 3-D Glulam Beam Finite Element," *Proceedings of the 1988 International Conference on Timber Engineering*, Vol. 2, FPRS, Madison, Wisconsin, pp. 194-204.
20. Ebrahimi, G. and Sliker, A., 1981, "Measurement of Shear Modulus in Wood by a Tension Test," *Wood Science*, Vol. 13, No. 3, January, pp. 171-176.
21. Filler, M. C., Hofstrand, A. D., and Howe, J. P., 1964 "Laminated Beam Design For Four Western Softwoods," *Forest Products Journal*, October, pp. 451-455
22. Fischer, S., Roman, I., Harel, H., Marom, G., and Wagner, H. D., 1981, "Simultaneous Determination of Shear and Young's Moduli in Composites," *Journal of Testing and Evaluation*, pp. 303-307.
23. Forest Products Laboratory, 1987, *Wood Handbook: Wood as an engineering material*, Agric. Handb. 72, Washington, DC: U.S. Department of Agriculture, Forest Service.
24. Foschi, R. O. and Barrett, J. D., 1980, "Glued-laminated beam Strength: A Model," *Journal of Structural Division*, ASCE, Vol.106, (No. ST 8), pp. 1735-1755.
25. Foschi, R. O., 1971, "Stresses in Curved Glued-Laminated Timber Beams: Experimental Study," *Forest Products Journal*, Vol. 21, No. 7, July, pp. 42-48.
26. Foschi, R. O. and Fox, P., 1970, "Radial Stresses in Curved Timber Beams," *Journal of Structural Engineering*, ASCE, ST 10, Oct., pp. 1997-2008.
27. Fox, S. P., 1978, "Development and Tests of 26f-E Hem-fir Glulam Beams," *Forest Products Journal*, Vol. 28, No. 6, pp. 48-55.
28. Gerhards, C. C., 1978, "Effect of Earlywood and Latewood on Stress-Wave Measurements Parallel to the Grain," *Wood Science*, Vol. 11, No. 2, October, pp. 69-72.
29. Goodman, J. R., and Bodig, J., 1970, "Orthotropic Elastic properties of Wood," *Journal of Structural Division*, ASCE, Vol. 96, (No. ST11), pp. 2301-2319.

30. Gunnerson, R. A., Goodman, J. R., and Bodig, J., 1973, "Plate Tests for Determination of Elastic Parameters of Wood," *Wood Science*, Vol. 5, No. 4, April, pp. 241-248.
31. Gurfinkel, G., *Wood Engineering*, Southern Forest Products Association, New Orleans, Louisiana, Upton Printing Co., 1973, pp. 1-20 & 58-79.
32. Gutkowski, R. M., Dewey, G. R., and Goodman, J. R., 1982, "Full-Scale Tests on Double-Tapered Glulam Beams," *Journal of the Structural Division*, ASCE, Vol. 108, No. ST10, October, pp. 2131- 2147.
33. Haan, C. T., *Statistical Methods in Hydrology*, Iowa State University Press, Ames, 1979.
34. Hibbitt, Karlson, and Sorensen, Inc., *ABAQUS*, 1984.
35. Holzer, S. M., *Computer Analysis of Structures: Matrix Structural Analysis, Structured Programming*, Elsevier, N.Y., 1985.
36. Holzer, M. Siegfried and Loferski, R. Joseph, "Analysis of Glued-laminated Timber Space Frames and Lattice Domes," Proposal, 1986, VPI&SU, Blacksburg, VA
37. Hoyle Jr., R. J. and Woeste, F. E., *Wood Technology in the Design of Structures*, Fifth Edition, Iowa State University Press, Ames, IA, 1989.
38. Jayne, B. A., *Theory and Design of Wood and Fiber Composite Materials*, Syracuse University Press, N.Y., 1972, pp. 1-48.
39. Johnson, J. W., 1971, "Design and Test of Large Glued-Laminated Beams Made of Nondestructively Tested Lumber," *Report T-27, Forest Research Laboratory*, School of Forestry, Oregon State University, Corvallis, Oregon.
40. Jones, M. Robert, *Mechanics of Composite Materials*, Hemisphere Publishing Corporation, New York, 1975.
41. Jorgensen, R. N., 1956, "Strength and Elastic Properties of Two-Species Laminated Wood Beams," *Forest Products Journal*, June, pp. 215-220.
42. Kline, D. E., Woeste, F. E., and Bendtsen, B. A., 1986, "Stochastic Model For Modulus of Elasticity of Lumber," *Wood and Fiber Science*, 18(2), pp. 228-238.
43. Koch, P., 1964, "Strength of beams with Laminae Located According to Stiffness," *Forest Products Journal*, October, pp. 456-460.
44. Koch, P., and Bohannon, B., 1965, "Beam Strength as Affected by Placement of Laminae," *Forest Products Journal*, July, pp. 289-295.
45. Leabo, A. Dick, *Basic Statistic*, Richard D. Irwin, Inc. Illinois, 1968, pp. 109-124.
46. Leahy, F. T., 1984, "The Delta-Element Reusable Strain Transducer," *Experimental Mechanics*, September, pp. 191-202.
47. Lekhnitskii, S. G., *Theory of Elasticity of an Anisotropic Body*, MIR Publishers, Moscow, 1981, pp. 263-313.
48. Livesley, R. K., *Matrix Methods of Structural Analysis*, 2nd Edition, Pergamon Press, Oxford, 1975.

49. Madsen, B. and Buchanan, A. H., 1986, "Size effect in timber explained by a modified weakest link theory," *Canadian Journal of Civil Engineering*, Vol. 13, pp. 218-232.
50. Mohler, K. and Hemmer, K., 1977, "Verformungs- und Festigkeitsverhalten von Nadelvoll- und Brettschichtholz bei Torsionbeanspruchung," *Holz als Roh- und Werkstoff*, Vol. 35, pp. 473-478.
51. Moody, R. C., 1970, "Glued-Laminated Timber Research At the Forest Products Laboratory," *Forest Products Journal*, Vol. 20, No. 9, pp. 81-86.
52. Moody, R. C., 1974, "Design Criteria For Large Structural Glued-Laminated Timber Beams Using Mixed Species of Visually Graded Lumber," *USDA Forest Service Res. Pap.*, FPL 236, Madison, Wisconsin.
53. National Forest Products Association, *National Design Specification for Wood Construction*, 1986 Edition, Washington, D.C..
54. Norton, N. H., *Handbook of Transducers for Electronic Measuring Systems*, Prentice-Hall, Inc., N.J., 1969.
55. Perry, C. C. and Lissner, H. R., *The Strain Gage Primer*, McGraw-Hill Book Company, New York, 1962.
56. Radcliffe, B. M., 1955, "A Method of Determining the Elastic Constants of Wood by Means of Electrical Resistance Strain Gages," *Forest Products Journal*, February, pp. 77-80.
57. Rockey, K. C., Evans, H. R., Griffiths, D. W., and Nethercot, D. A., *The Finite Element Method--A Basic Introduction*, Crosby Lockwood Staples, London, pp. 49-54 and pp 92-94.
58. Scharr, G., 1986, "Beitrag zur Torsionselastizitat von Holzern in Abhangigkeit von der Holztemperatur und der Belastungszeit," *Holz als Roh-und Werkstoff*, Vol. 44, pp. 57-60.
59. Semenov, P. I., 1966, "Determination of Shear Moduli of Orthotropic Materials From Torsion Tests," *Mekhanika Polimerov*, Vol. 2, No. 1, pp. 27-33.
60. Shuler, C. E., Grant, D. A., and Moody R. C., 1979, "Evaluation ion of Glued Laminated Beams of Eastern Spruce and Eastern Hemlock," *Forest Products Journal*, Vol. 29, No. 7, pp 23-28.
61. Sinclair, A. N. and Faschad, M., 1987, "A Comparison of Three Methods for Determining Elastic Constants of Wood," *Journal of Testing and Evaluation*, JTEVA, Vol. 15, No. 2, March, pp. 77-86.
62. Sliker, A., 1986, "Measuring Non-shear Compliances in the RT Plane of Wood," Forestry Department, Michigan State University, pp. 1-20.
63. Sliker, A., 1985, "Orthotropic strains in compression parallel to grain tests," *Forest Products Journal*, Vol. 35, No. 11/12, pp. 19-26.
64. Sliker, A., 1971, "Resistance Strain Gages and Adhesives for Wood," *Forest Products Journal*, Vol. 21, No. 12, December, pp. 40-43.
65. Stern, E. George, 1947, "Influence of Nonhomogeneity of Wood on its Strength Properties," *American Society for Testing Materials*, pp. 1-8.

66. Tang, R. C., Adams, S. F., and Mark, R. E., 1971, "Moduli of Rigidity and Torsional Strength of Scarlet Oak Related to Moisture Content," *Wood Science*, Vol. 3, No. 4, April, pp. 238-244.
67. Timoshenko, S., *Strength of Materials, Part I, Elementary Theory and Problems*, 3rd ed., Van Nostrand, New York, 1955.
68. -----, *Strength of Materials, Part II, Advanced Theory & Problems*, 3rd edition, Robert E. Krieger Publishing Company, Huntington, N.Y., 1976.
69. Trayer, G. W. and March, H. W., "The Torsion of Members Having Sections Common in Aircraft Construction," National Advisory Committee for Aeronautics, Report No. 334, 1930.
70. "Triax Domes, Glue-laminated Wood Structural Systems for Clear-Span Circular Buildings," Koppers Company, Inc., Glue Laminated Wood, 6, January 1975.
71. Trietley, L. H., *Transducers in Mechanical and Electronic Design*, Marcel Dekker, Inc., New York, 1986.
72. Vafai, A. V. and Pincus, G., 1973, "Torsional and Bending Behavior of Wood Beams," *Journal of the Structural Division*, ASCE, Vol. 99, No. ST6, June, pp. 1205-1221.
73. Van Wyk, W. J., and Gerischer, G. F. R., 1988, "A Method for Determining the G-Modulus of Wood," *Holzforschung*, Vol. 42, No. 3, pp. 191-194.
74. Wagner, H. D., Marom, G., and Roman, I., 1982, "Analysis of Several Loading Methods For Simultaneous Determination of Young's And Shear Moduli in Composites," *Fiber Science and Technology*, 16, pp. 61-65.
75. "Wood: A Modern Structural Material," A Comprehensive College Seminar Co-Sponsored By: American Institute of Timber Construction, American Plywood Association, Southern Forest Products

Appendix A. HP Data Acquisition Programs


```

10  !
20  ! AUGUST 1987
30  !
40  ! THE FOLLOWING PROGRAM ENABLES ONE TO CALIBRATE CLIP GAGES.
50  ! UPTO 10 CLIP GAGES CAN BE CONNECTED TO THE STRAIN GAGE CARD.
60  ! HOWEVER, THE FOLLOWING PROGRAM LETS YOU CALIBRATE ONE CLIP GAGE
70  ! AT A TIME. IT DOES NOT MATTER AS TO WHICH CHANNEL THE CLIP IS
80  ! CONNECTED TO.
90  !
100 ! THE PROGRAM WILL ASK YOU FOR A RANGE OF DELTA THAT YOU WILL INDUCE
110 ! USING THE EXTENSOMETER. IT CAN HANDLE VALUES IN TENSION AS WELL AS
120 ! IN COMPRESSION.
130 !
140 ! NOTE: ALWAYS GO IN TENSION FIRST AND THEN IN COMPRESSION.
150 !
160 OPTION BASE 1           !SPECIFIES THE DEFAULT LOWER BOUND OF ARRAYS
170 PRINTER IS CRT          !ADDRESS OF THE TERMINAL
180 OUTPUT KBD;"BK";        !CLEARS THE SCREEN
190 DIM Com$(100)
200 !
210 ! ASKING FOR THE NECESSARY INFORMATION
220 !
230 INPUT "ENTER THE DATE: ",Date$
240 INPUT "ENTER CLIP GAGE ID: ",Id$
250 INPUT "WHAT CHANNEL IS THE GAGE CONNECTED TO ? "%,%
260 INPUT "TIME BETWEEN READINGS IN SECONDS? ",S
270 INPUT "WHAT IS THE GAGE FACTOR? ",GF
280 PRINT "ENTER THE RANGE FOR DELTA TO CALIBRATE THE CLIP GAGES:"
290 PRINT
300 INPUT "ENTER THE LOWER LIMIT: ",Low
310 INPUT "ENTER THE UPPER LIMIT: ",High
320 INPUT "WHAT INCREMENTS YOU WANT TO CALIBRATE THE GAGE? ",Inc
330 INPUT "ENTER ANY COMMENTS YOU WOULD LIKE TO? ",Com$
340 N=(((High-Low)/Inc)*4)+1
350 OUTPUT KBD;"BK";
360 PRINT "YOU WILL BE TAKING",N," READINGS, STARTING FROM,"Low,"AND"
370 PRINT "ENDING WITH ",High
380 PRINT
390 PRINT "TO BEGIN CALIBRATING THE GAGE, PRESS CONT KEY"
400 PAUSE
410 ALLOCATE Ch(N,2)
420 !
430 ! CALCULATING THE DELTA VALUES TO PRINT LATER
440 !
450 Num=Low
460 FOR Row=1 TO N
470   Ch(Row,1)=Num
480   IF (Row)=((N-1)/4)+1 AND (Row<((N-INT(N/4)))) THEN
490     Num=Num-Inc
500   ELSE
510     Num=Num+Inc
520   END IF
530 NEXT Row
540 OUTPUT KBD;"BK";
550 !
560 ! TAKING THE EXCITATION VOLTAGE READING
570 !
580 PRINT "I AM READY TO TAKE THE VOLTAGE READING IF YOU ARE. PRESS CONT KEY"
590 PAUSE
600 CLEAR 709

```

```

610 CLEAR 722
620 OUTPUT 709;"SIAC30" !INITIALIZING THE SYSTEM & CLOSING CHANNEL 30
630 OUTPUT 722;"SOFIR4" !TELLING 3456 THAT IT IS DC VOLTAGE WITH 10 VOLT RANGE
640 ENTER 722;U !READING THE EXCITATION VOLTAGE
650 OUTPUT 709;"AR" !RESET THE CHANNELS OR OPENING ALL CLOSED ONES
660 !
670 ! TAKING THE INITIAL UNSTRAINED READINGS AND THE LATER STRAIN READINGS
680 ! FOR THE CHANNEL SPECIFIED
690 !
700 SELECT C
710 !
720 ! GAGE CONNECTED TO CHANNEL 0
730 !
740 CASE =1
750 DISP "TAKING THE INITIAL UNSTRAINED READINGS NOW"
780 OUTPUT 709;"AC20"
790 OUTPUT 722;"SOFIR4FL1Z1" !FL1 TURNS FILTER ON, Z1 TURNS AUTO ZERO ON
800 ENTER 722;A
810  $U_r = \text{SGN}(A/U) * \text{INT}(\text{ABS}((A/U) * 1.E+6) * .5)$  !INITIAL VOLTAGE RATIO
820 OUTPUT 709;"AR"
830 OUTPUT KBD;"BK";
840 FOR J=1 TO N
850 IF (J=1) THEN
860 PRINT "PRESS CONT KEY TO TAKE THE ZERO READINGS"
870 PAUSE
880 ELSE
890 PRINT "ADD STRAIN TO GAGES AND PRESS CONT KEY TO PROCEED"
900 PAUSE
910 END IF
920 WAIT 5
930 OUTPUT 709;"AC20"
940 OUTPUT 722;"SOFIR4FL1Z1"
950 ENTER 722;B
960  $T = \text{SGN}(B/U) * \text{INT}(\text{ABS}((B/U) * 1.E+6) * .5)$  !STRAINED VOLTAGE RATIO
970  $X = T - U_r$ 
980  $Ch(J,2) = -X/G_f$  !CALCULATING THE STRAIN
990 PRINT Ch(J,1);TAB(10);Ch(J,2)
1000 PRINT
1010 OUTPUT 709;"AR"
1020 NEXT J
1030 !
1040 ! GAGE CONNECTED TO CHANNEL 1
1050 !
1060 CASE =2
1070 DISP "TAKING THE INITIAL UNSTRAINED READINGS NOW"
1100 OUTPUT 709;"AC21"
1110 OUTPUT 722;"SOFIR4FL1Z1"
1120 ENTER 722;A
1130  $U_r = \text{SGN}(A/U) * \text{INT}(\text{ABS}((A/U) * 1.E+6) * .5)$ 
1140 OUTPUT 709;"AR"
1150 OUTPUT KBD;"BK";
1160 FOR J=1 TO N
1170 IF (J=1) THEN
1180 PRINT "PRESS CONT KEY TO TAKE THE ZERO READINGS"
1190 PAUSE
1200 ELSE
1210 PRINT "ADD STRAIN TO GAGES AND PRESS CONT KEY TO PROCEED"
1220 PAUSE
1230 END IF
1240 WAIT 5

```

```

1250     OUTPUT 709;"AC21"
1260     OUTPUT 722;"SOF1R4FL1Z1"
1270     ENTER 722;B
1280     T=SGN(B/U)*INT((ABS(B/U)+1.E+6)+.5)
1290     X=T-Ur
1300     Ch(J,2)=-X/Gf
1310     PRINT Ch(J,1);TAB(10);Ch(J,2)
1320     PRINT
1330     OUTPUT 709;"AR"
1340     NEXT J
1350     !
1360     ! GAGE CONNECTED TO CHANNEL 2
1370     !
1380     CASE =3
1410     DISP "TAKING THE INITIAL UNSTRAINED READINGS NOW"
1420     OUTPUT 709;"AC22"
1430     OUTPUT 722;"SOF1R4FL1Z1"
1440     ENTER 722;A
1450     Ur=SGN(A/U)*INT((ABS((A/U)+1.E+6)+.5)
1460     OUTPUT 709;"AR"
1470     OUTPUT KBD;"BK";
1480     FOR J=1 TO N
1490         IF (J=1) THEN
1500             PRINT "PRESS CONT KEY TO TAKE THE ZERO READINGS"
1510             PAUSE
1520         ELSE
1530             PRINT "ADD STRAIN TO GAGES AND PRESS CONT KEY TO PROCEED"
1540             PAUSE
1550         END IF
1560         WAIT S
1570         OUTPUT 709;"AC22"
1580         OUTPUT 722;"SOF1R4FL1Z1"
1590         ENTER 722;B
1600         T=SGN(B/U)*INT((ABS((B/U)+1.E+6)+.5)
1610         X=T-Ur
1620         Ch(J,2)=-X/Gf
1630         PRINT Ch(J,1);TAB(10);Ch(J,2)
1640         PRINT
1650         OUTPUT 709;"AR"
1660     NEXT J
1670     !
1680     ! GAGE CONNECTED TO CHANNEL 3
1690     !
1700     CASE =4
1710     DISP "TAKING THE INITIAL UNSTRAINED READINGS NOW"
1740     OUTPUT 709;"AC23"
1750     OUTPUT 722;"SOF1R4FL1Z1"
1760     ENTER 722;A
1770     Ur=SGN(A/U)*INT((ABS((A/U)+1.E+6)+.5)
1780     OUTPUT 709;"AR"
1790     OUTPUT KBD;"BK";
1800     FOR J=1 TO N
1810         IF (J=1) THEN
1820             PRINT "PRESS CONT KEY TO TAKE THE ZERO READINGS"
1830             PAUSE
1840         ELSE
1850             PRINT "ADD STRAIN TO GAGES AND PRESS CONT KEY TO PROCEED"
1860             PAUSE
1870         END IF
1880         WAIT S

```

```

1890     OUTPUT 709;"AC23"
1900     OUTPUT 722;"S0F1R4FL121"
1910     ENTER 722;B
1920     T=SGN(B/U)*INT(ABS((B/U)*1.E+6)+.5)
1930     X=T-Ur
1940     Ch(J,2)=-X/GF
1950     PRINT Ch(J,1);TAB(10),Ch(J,2)
1960     PRINT
1970     OUTPUT 709;"AR"
1980     NEXT J
1990     !
2000     ! GAGE CONNECTED TO CHANNEL 4
2010     !
2020     CASE =5
2050     DISP "TAKING THE INITIAL UNSTRAINED READINGS NOW"
2060     OUTPUT 709;"AC24"
2070     OUTPUT 722;"S0F1R4FL121"
2080     ENTER 722;A
2090     Ur=SGN(A/U)*INT(ABS((A/U)*1.E+6)+.5)
2100     OUTPUT 709;"AR"
2110     OUTPUT KBD;"BK";
2120     FOR J=1 TO N
2130         IF (J=1) THEN
2140             PRINT "PRESS CONT KEY TO TAKE THE ZERO READINGS"
2150             PAUSE
2160         ELSE
2170             PRINT "ADD STRAIN TO GAGES AND PRESS CONT KEY TO PROCEED"
2180             PAUSE
2190         END IF
2200         WAIT 5
2210         OUTPUT 709;"AC24"
2220         OUTPUT 722;"S0F1R4FL121"
2230         ENTER 722;B
2240         T=SGN(B/U)*INT(ABS((B/U)*1.E+6)+.5)
2250         X=T-Ur
2260         Ch(J,2)=-X/GF
2270         PRINT Ch(J,1);TAB(10),Ch(J,2)
2280         PRINT
2290         OUTPUT 709;"AR"
2300     NEXT J
2310     !
2320     ! GAGE CONNECTED TO CHANNEL 5
2330     !
2340     CASE =6
2350     DISP "TAKING THE INITIAL UNSTRAINED READINGS NOW"
2380     OUTPUT 709;"AC25"
2390     OUTPUT 722;"S0F1R4FL121"
2400     ENTER 722;A
2410     Ur=SGN(A/U)*INT(ABS((A/U)*1.E+6)+.5)
2420     OUTPUT 709;"AR"
2430     OUTPUT KBD;"BK"
2440     FOR J=1 TO N
2450         IF (J=1) THEN
2460             PRINT "PRESS CONT KEY TO TAKE THE ZERO READINGS"
2470             PAUSE
2480         ELSE
2490             PRINT "ADD STRAIN TO GAGES AND PRESS CONT KEY TO PROCEED"
2500             PAUSE
2510         END IF
2520         WAIT 5

```

```

2530      OUTPUT 709;"AC25"
2540      OUTPUT 722;"SOF1R4FL121"
2550      ENTER 722;B
2560      T=SGN(B/U)*INT(ABS((B/U)*1.E+6)+.5)
2570      X=T-Ur
2580      Ch(J,2)=-X/Gf
2590      PRINT Ch(J,1);TAB(10),Ch(J,2)
2600      PRINT
2610      OUTPUT 709;"AR"
2620  NEXT J
2630  !
2640  ! GAGE CONNECTED TO CHANNEL 6
2650  !
2660  CASE =7
2670  DISP "TAKING THE INITIAL UNSTRAINED READINGS NOW"
2700  OUTPUT 709;"AC26"
2710  OUTPUT 722;"SOF1R4FL121"
2720  ENTER 722;A
2730  Ur=SGN(A/U)*INT(ABS((A/U)*1.E+6)+.5)
2740  OUTPUT 709;"AR"
2750  OUTPUT KBD;"BK";
2760  FOR J=1 TO N
2770    IF (J=1) THEN
2780      PRINT "PRESS CONT KEY TO TAKE THE ZERO READINGS"
2790      PAUSE
2800    ELSE
2810      PRINT "ADD STRAIN TO GAGES AND PRESS CONT KEY TO PROCEED"
2820      PAUSE
2830    END IF
2840    WAIT 5
2850    OUTPUT 709;"AC26"
2860    OUTPUT 722;"SOF1R4FL121"
2870    ENTER 722;B
2880    T=SGN(B/U)*INT(ABS((B/U)*1.E+6)+.5)
2890    X=T-Ur
2900    Ch(J,2)=-X/Gf
2910    PRINT Ch(J,1);TAB(10),Ch(J,2)
2920    PRINT
2930    OUTPUT 709;"AR"
2940  NEXT J
2950  !
2960  ! GAGE CONNECTED TO CHANNEL 7
2970  !
2980  CASE =8
2990  DISP "TAKING THE INITIAL UNSTRAINED READINGS NOW"
3020  OUTPUT 709;"AC27"
3030  OUTPUT 722;"SOF1R4FL121"
3040  ENTER 722;A
3050  Ur=SGN(A/U)*INT(ABS((A/U)*1.E+6)+.5)
3060  OUTPUT 709;"AR"
3070  OUTPUT KBD;"BK";
3080  FOR J=1 TO N
3090    IF (J=1) THEN
3100      PRINT "PRESS CONT KEY TO TAKE THE ZERO READINGS"
3110      PAUSE
3120    ELSE
3130      PRINT "ADD STRAIN TO GAGES AND PRESS CONT KEY TO PROCEED"
3140      PAUSE
3150    END IF
3160    WAIT 5

```

```

3170     OUTPUT 709;"AC27"
3180     OUTPUT 722;"S0F1R4FL1Z1"
3190     ENTER 722;B
3200     T=SGN(B/U)*INT(ABS((B/U)*1.E+6)+.5)
3210     X=T-Ur
3220     Ch(J,2)=-X/Gf
3230     PRINT Ch(J,1);TAB(10),Ch(J,2)
3240     PRINT
3250     OUTPUT 709;"AR"
3260     NEXT J
3270     !
3280     ! GAGE CONNECTED TO CHANNEL 8
3290     !
3300     CASE =9
3310     DISP "TAKING THE INITIAL UNSTRAINED READINGS NOW"
3340     OUTPUT 709;"AC28"
3350     OUTPUT 722;"S0F1R4FL1Z1"
3360     ENTER 722;A
3370     Ur=SGN(A/U)*INT(ABS((A/U)*1.E+6)+.5)
3380     OUTPUT 709;"AR"
3390     OUTPUT KBD;"KK";
3400     FOR J=1 TO N
3410         IF (J=1) THEN
3420             PRINT "PRESS CONT KEY TO TAKE THE ZERO READINGS"
3430             PAUSE
3440         ELSE
3450             PRINT "ADD STRAIN TO GAGES AND PRESS CONT KEY TO PROCEED"
3460             PAUSE
3470         END IF
3480         WAIT S
3490         OUTPUT 709;"AC28"
3500         OUTPUT 722;"S0F1R4FL1Z1"
3510         ENTER 722;B
3520         T=SGN(B/U)*INT(ABS((B/U)*1.E+6)+.5)
3530         X=T-Ur
3540         Ch(J,2)=-X/Gf
3550         PRINT Ch(J,1);TAB(10),Ch(J,2)
3560         PRINT
3570         OUTPUT 709;"AR"
3580     NEXT J
3590     !
3600     ! GAGE CONNECTED TO CHANNEL 9
3610     !
3620     CASE =10
3630     DISP "TAKING THE INITIAL UNSTRAINED READINGS NOW"
3660     OUTPUT 709;"AC29"
3670     OUTPUT 722;"S0F1R4FL1Z1"
3680     ENTER 722;A
3690     Ur=SGN(A/U)*INT(ABS((A/U)*1.E+6)+.5)
3700     OUTPUT 709;"AR"
3710     OUTPUT KBD;"KK";
3720     FOR J=1 TO N
3730         IF (J=1) THEN
3740             PRINT "PRESS CONT KEY TO TAKE THE ZERO READINGS"
3750             PAUSE
3760         ELSE
3770             PRINT "ADD STRAIN TO GAGES AND PRESS CONT KEY TO PROCEED"
3780             PAUSE
3790         END IF
3800         WAIT S

```

```

3810     OUTPUT 709;"AC29"
3820     OUTPUT 722;"S0F1R4FL1Z1"
3830     ENTER 722;B
3840     T=SQN(B/U)*INT(ABS((B/U)*1.E+6)+.5)
3850     X=T-Ur
3860     Ch(J,2)=-X/Gf
3870     PRINT Ch(J,1);TAB(10);Ch(J,2)
3880     PRINT
3890     OUTPUT 709;"AR"
3900     NEXT J
3910 END SELECT
3920 !
3930 !   STORING THE READINGS ON HARD DISK IF ASKED FOR
3940 !
3950 INPUT "DO YOU WISH TO STORE THE DATA IN A FILE? ",Ans$
3960 IF Ans$="NO" THEN 4110
3970 INPUT "FILE YOU WISH TO STORE DATA UNDER? ",Name$
3980 PRINT "INSERT DATA DISK IN RIGHT DRIVE AND PRESS (CONT) "
3990 PAUSE
4000 CREATE BDATA Name$&":700,1",N
4010 ASSIGN @File TO Name$&":700,1"
4020 FOR K=1 TO N
4030   FOR L=1 TO C
4040     OUTPUT @File,K;Ch(K,L)
4050   NEXT L
4060 NEXT K
4070 ASSIGN @File TO *
4080 !
4090 !   PRINTING THE HARD COPY IF ASKED FOR
4100 !
4110 INPUT "WOULD YOU LIKE A HARD COPY?",Ans$
4120 IF Ans$="NO" THEN 4320
4130 PRINTER IS 701
4140 PRINT TAB(20),"STRAIN MEASUREMENTS"
4150 PRINT
4160 PRINT "DATE: ",Dates
4170 PRINT
4180 PRINT "CLIP GAGE ID: ",Ids
4190 PRINT
4200 PRINT "COMMENTS: ",Com$
4210 PRINT
4220 PRINT "   DELTA (INCHES)           STRAIN (MICROSTRAINS) "
4230 PRINT "   -----"           "-----"
4240 PRINT
4250 FOR J=1 TO N
4260   FOR K=1 TO 2
4270     PRINT USING "2X,0000.0000,15X,0";Ch(J,K)
4280   NEXT K
4290 PRINT
4300 NEXT J
4310 PRINTER IS CRT
4320 OUTPUT 709;"B"           ! CLEARING THE SYSTEM
4330 PRINT
4340 PRINT "THE TEST HAS BEEN COMPLETED"
4350 END

```

```

10  OPTION BASE 1
20  PRINTER IS CRT
30  OUTPUT KBD;"■K";
40  DIM Id$(15),Com$(80),Dates(15),D(50,11),Faces(5),Rnums(5)
50  Gf=2.00
60  INPUT "ENTER TODAY'S DATE: ",Dates
70  INPUT "ENTER RUN NUMBER: ",Rnums
80  C=10
90  INPUT "ENTER TIME BETWEEN READINGS: ",S
100 G1=2.180
110 INPUT "BEAM IDENTIFICATION: ",Ids
111 INPUT "ENTER THE BEAM FACE BEING TESTED?",Faces
150 OUTPUT KBD;"■K";
160 INPUT "HOW MANY OBSERVATIONS YOU WANT TO COLLECT? ",N
170 OUTPUT KBD;"■K";
180 INPUT "ENTER ANY COMMENTS: ",Coms
190 OUTPUT KBD;"■K";
200 ALLOCATE Ch(N,10),L(N)
210 DIM A(10),B(10),T(10),X(10),Ur(10),Cal(10)
220 !
230 ! TAKING READINGS BEFORE PUTTING STRAIN
240 !
250 Cal(1)=28.633
260 Cal(2)=31.028
270 Cal(3)=24.852
290 Cal(4)=25.666
290 Cal(5)=24.567
300 !Cal(6)=31.992
301 Cal(6)=28.339
310 Cal(7)=30.086
390 PRINT "PRESS CONT KEY TO TAKE THE EXCITATION VOLTAGE READING."
400 PAUSE
410 CLEAR 709
420 CLEAR 722
430 OUTPUT 709;"SIAC30"
440 OUTPUT 722;"S0F1R4"
450 ENTER 722;U
460 OUTPUT 709;"AR"
461 OUTPUT KBD;"■K";
470 PRINT "PRESS CONT KEY TO TAKE ZERO READINGS."
480 PAUSE
490 DISP "TAKING THE ZERO READINGS NOW"
500 OUTPUT 722;"S0F1R4Z01STI0.001STD"
510 OUTPUT 709;"AC1"
520 ENTER 722;Loint
530 OUTPUT 722;"S0F1DOT2Z0S01R21STI0.001STD"
540 OUTPUT 709;"AE1SD0AF20AL29AE2AC20"
550 FOR I=1 TO C
560     ENTER 722;A(I)
570 NEXT I
580 OUTPUT 709;"AR"
581 OUTPUT KBD;"■K";
583 PRINT "PRESS CONT KEY TO TAKE READINGS.  WHEN YOU WANT TO STOP THE TEST, P
RESS KO KEY."
584 PAUSE
590 OUTPUT KBD;"■K";
600 !
610 ! TAKING READINGS AFTER INDUCING STRAIN
620 !
621 PRINT "P(LBS)   G1      G2      G3      G4      G5      G6      G7      DEF1      DEF2
DEF3"
622 PRINT
630 FOR J=1 TO N
640     WAIT S
        !

```



```

560     OUTPUT 709;"AC1"
570     ENTER 722;Lvlat
580     OUTPUT 722;"S0F1DOT2Z0S01R21STI0.001STD"
590     OUTPUT 709;"AE1SD0AF20AL29AE2AC20"
600     FOR I=1 TO C
610         ENTER 722;B(I)
620     NEXT I
630     OUTPUT 709;"AR"
640     Lv=ABS(Lvlat-Lvint)
650     D(J,1)=-14.5149+2002.3474*Lv
660     PRINT USING "DDDDD,1X,*,",D(J,1)
670     FOR I=1 TO C
680         IF I<=7 THEN
690             Ur(I)=A(I)/U
700             T(I)=B(I)/U
710             X(I)=T(I)-Ur(I)
720             Ch(J,I)=-X(I)/Gf
730             Delta=Ch(J,I)*Cal(I)
740             D(J,I+1)=(Delta/G1)*10^6
750             PRINT USING "DDDDD,1X,*,",D(J,I+1)
760         ELSE
770             X(I)=A(I)-B(I)
780             IF I=8 THEN
790                 D(J,I+1)=X(I)/.00137
800             END IF
810             IF I=9 THEN
820                 D(J,I+1)=X(I)/.00137
830             END IF
840             IF I=10 THEN
850                 D(J,I+1)=X(I)/.00105
860             END IF
870             PRINT USING "DD.DDDD,1X,*,",D(J,I+1)
880         END IF
890     NEXT I
900     PRINT
910     ON KEY 0 LABEL "ABORT TEST" GOTO 890
920 NEXT J
930 OUTPUT 709;"AR"
940 N=J
950 INPUT "DO YOU WISH TO STORE THE DATA IN A FILE? ",Ans$
960 IF Ans$="NO" THEN 1100
970 INPUT "FILE YOU WISH TO STORE DATA UNDER? ",Names$
980 PRINT "INSERT DATA DISK IN RIGHT DRIVE AND PRESS (CONT) "
990 PAUSE
1000 CREATE BDAT Names$&":,700,1",50
1010 ASSIGN @File TO Names$&":,700,1"
1020 !FOR K=1 TO N-1
1030     !FOR Q=1 TO 11
1040         OUTPUT @File;D(*)
1050     !NEXT Q
1060 !NEXT K
1070 ASSIGN @File TO *
1080 INPUT "WOULD YOU LIKE A HARD COPY?",Ans$
1090 IF Ans$="NO" THEN 1300
1100 PRINTER IS 701
1110 PRINT TAB(30),"BEAM ID: ",Ids
1120 PRINT TAB(30),"-----"
1130 PRINT
1140 PRINT "DATE: ";Dates
1150 PRINT "RUN #: ";Rnum$
1160 PRINT "BEAM FACE TESTED: ";Faces$
1170 PRINT "COMMENTS: ";Com$
1180 PRINT
1190 PRINT "ALL STRAIN READINGS IN MICROSTRAINS"
1200 PRINT
1210

```

```

78 "
1220 PRINT "LOAD(LBS)  GAGE1      GAGE2      GAGE3      GAGE4      GAGE5      GAGE6      GAG
E7 "
1221 PRINT
1230 FOR J=1 TO N-1
1240   FOR K=1 TO 8
1250     PRINT USING "DDDDDD,3X,0,";D(J,K)
1260   NEXT K
1270   PRINT
1280 NEXT J
1281 PRINT
1282 PRINT "DEFLECTION READINGS"
1283 PRINT "DEF1(38IN)  DEF2(CL)      DEF3(76IN)  LOAD(LBS)"
1284 PRINT
1285 FOR J=1 TO N-1
1286   FOR K=9 TO 11
1287     PRINT USING "DD.DDDD,5X,0,";D(J,K)
1289   NEXT K
1290   PRINT USING "DDDDDD,5X,0,";D(J,1)
1292   PRINT
1293 NEXT J
1294 PRINTER IS CRT
1300 OUTPUT 709;"H"
1310 PRINT
1320 PRINT "THE TEST HAS BEEN COMPLETED"
1330 END

```

Appendix B. Fortran Code To Solve Lekhnitski's Orthotropic Torsion Solution

```

      REAL A1,B1,A2,B2,L1,L2,K1,K2,GTOL,GT,GR,BETA1,BETA2
      * ,GLT,GLR,C1,C2,D1,D2
      GTOL = 100.0
      GLT = 1.0
      GLR = 1.0
      GT = 0.0
      GR = 0.0
      A1 = 1.989
      A2 = 1.991
      B1 = 0.490
      B2 = 0.480
      K1 = 1033.0
      K2 = 778.00
      L1 = 12.00
      L2 = 12.00
      C1 = (A1/B1)*(SQRT(GLR/GLT))
      C2 = (A2/B2)*(SQRT(GLT/GLR))
      D1 = (K1*L1)/(A1*(B1**3.))
      D2 = (K2*L2)/(A2*(B2**3.))
      CALL BHETA1(C1,BETA1)
      CALL BHETA2(C2,BETA2)
      CALL GCAL(BETA1,BETA2,D1,D2,GLR,GLT)
10  IF((ABS(GLR-GR).GT.GTOL).OR.(ABS(GLT-GT).GT.GTOL)) THEN
      GR = GLR
      GT = GLT
      C1 = (A1/B1)*(SQRT(GLR/GLT))
      C2 = (A2/B2)*(SQRT(GLT/GLR))
      CALL BHETA1(C1,BETA1)
      CALL BHETA2(C2,BETA2)
      CALL GCAL(BETA1,BETA2,D1,D2,GLR,GLT)
      GOTO 10
    ENDIF
    WRITE(1,*) 'RECTANGULAR SAMPLES RN21 & RP21'
    WRITE(1,*) 'BETA1 = ',BETA1,'BETA2 = ',BETA2
    WRITE(1,*) 'GLR = ',GLR,'GLT = ',GLT
    STOP
  END
  *****
  *                               BHETA1                               *
  *****
  SUBROUTINE BHETA1(C1,BETA1)
  REAL BETA1,C1,SUM,PI
  PI = 3.141592654
  SUM = 0.0
  DO 10 K = 1,10,2
    SUM = (1/(K**4.))*(1-((2./(K*PI))*C1*TANH((K*PI)/2.))*
  $      (1./C1))) + SUM
10  CONTINUE
  BETA1 = (32./(PI**4.))*(C1**2.)*SUM
  RETURN
  END
  *****
  *                               BHETA2                               *
  *****
  SUBROUTINE BHETA2(C2,BETA2)

  REAL BETA2,C2,SUM,PI
  PI = 3.141592654
  SUM = 0.0
  DO 10 K = 1,10,2
    SUM = (1/(K**4.))*(1-((2./(K*PI))*C2*TANH((K*PI)/2.))*
  $      (1./C2))) + SUM
10  CONTINUE
  BETA2 = (32./(PI**4.))*(C2**2.)*SUM
  RETURN
  END
  *****
  *                               GCAL                               *
  *****
  SUBROUTINE GCAL(BETA1,BETA2,D1,D2,GLR,GLT)
  REAL BETA1,BETA2,GLR,GLT,D1,D2
  GLR = D2/BETA2
  GLT = D1/BETA1
  RETURN
  END

```

Vita

Vikram Yadama was born in Hyderabad, India. He graduated from Bangkok International School in 1982. He did his undergraduate at Iowa State University, Ames, Iowa. He majored in Forest Products. He graduated in 1986 and went to Virginia Tech to obtain MSc degree in Wood Engineering. Currently he is working at the Mississippi Forest Products Laboratory at Mississippi State University.

Vik Yadama